Geochronological and sedimentological constraints on the evolution of the lower Cuddapah Basin, India

Georgina Falster

Centre for Tectonics, Resources and Exploration

School of Earth and Environmental Sciences

The University of Adelaide, SA 5005

georgina.falster@student.adelaide.edu.au

ABSTRACT

The Palaeo- to Mesoproterozoic Cuddapah Supergroup was deposited in the Cuddapah Basin, which is one of a number of Proterozoic volcano-sedimentary basins that overlie the Indian Shield. On the south-western margin of the basin, the stratigraphic succession in the basal Papaghni and Chitravati groups is initially composed of gravelly fluvial deposits with dominant sediment input coming from the western foreland. These are succeeded by shallow-water stromatolitic dolomite and shale with a significantly reduced siliciclastic component, and finally by sub-tidal laminated silt and sand. A detailed facies analysis of these rocks suggests that deposition occurred initially in an active extensional setting which subsequently developed into a passive extensional setting. Stable isotope geochemistry of dolomites in the Vempalle Formation of the Papaghni Group indicates that deposition of the formation may initially have occurred in a restricted setting where $\delta^{13}C$ varied according to fractionation via environmental processes. Whether the Vempalle Formation was deposited in a shallow marine or lacustrine milieu is equivocal; $\delta^{13}C$ values may correlate with the conclusion of the global oceanic 'Lomagundi' positive $\delta^{13}C$ excursion around 2100 Ma, however, this inference requires the carbonates to have been precipitated in oceanic water, and have retained their primary isotopic signature during pervasive dolomitisation. U-Pb dating of detrital zircon grains from the Gandikota Formation – previously thought to be the uppermost formation of the Chitravati Group – yields a maximum depositional age of 1207 ± 22 Ma. This is significantly younger than intrusive igneous rocks within the Cuddapah Supergroup and it is therefore likely that the Gandikota Formation is part of the overlying Meso- to Neoproterozoic Kurnool Group. The detrital zircon age spectrum of the Gandikota Formation indicates significant sediment input from the east, which is likely to be a result of the thrusting of the Eastern Ghats Belt onto the Eastern Dharwar Craton and a reversal of the prevailing extensional regime in the Cuddapah Basin. A number of authors have proposed a genetic link between the Cuddapah Basin and several other Proterozoic basins of the Indian Shield. This study provides no reason to directly correlate the temporally and spatially distinct basins.

Keywords: Cuddapah Basin, Palaeo- Mesoproterozoic, detrital zircon geochronology, hafnium isotope analysis, provenance, stable isotopes, dolomite, basin evolution.

Contents

1 INTRODUCTION

The Indian Shield has an enigmatic history, involving several phases of extension and compression (Meert *et al.* 2010). Tectonic events in the shield during the Palaeo- to Mesoproterozoic eras are likely to have been affected by the amalgamation and rifting of several proposed continental reconstructions (e.g. Acharyya & Roy 2000; Zhao *et al.* 2003; Lu *et al.* 2008; Evans & Mitchell 2011). These periods of tectonic activity resulted in the development of a series of multiphase sedimentary basins which are widespread across the shield (Kailasam 1976; Naqvi & Rogers 1987) (see Figure 1a). These have been termed the 'Purana' basins, and display broadly similar sedimentary characteristics and geochronological constraints as well as an unusually low degree of deformation and metamorphism (Dhoundial 1987; Chaudhuri *et al.* 2002). On this basis alone, the basins are thought to be correlative (Dhoundial 1987; Kale & Phansalkar 1991). The widely accepted linking mechanism is that each of the basins developed in an area of pre-existing crustal weakness during intracontinental rifting (Sundaram *et al.* 1964).

The Cuddapah Basin is the second largest of the Purana basins, and features a thick package of well-preserved sediments (Manikyamba *et al.* 2008). The basin is separated into two major stratigraphic divisions - the basal Palaeo- to Mesoproterozoic Cuddapah Supergroup and the overlying Meso- to Neoproterozoic Kurnool Group - which are separated by a significant unconformity (King 1872). Basin evolution models proposed for the Cuddapah Basin are equivocal; the basin has variably been called a foreland basin (e.g. Singh & Mishra 2002; Mishra & Prajapati 2003), or the result of failed continental rifting (e.g. Chaudhuri *et al.* 2002; Zhao *et al.* 2004; Ravikant 2010). Despite the remarkable preservation of basin sediments which makes the successions ideal for palaeoenvironmental interpretation, little attempt has been made to assess the tectonic evolution of the basin using sedimentological evidence.

An integrated approach of sequence stratigraphy, stable isotope geochemistry and detrital zircon geochronology is used here to provide insight into the depositional environment of four key formations in the lowermost two groups of the Cuddapah Supergroup: the Gulcheru and Vempalle

Formations of the Papaghni Group, and the Tadpatri and Gandikota Formations of the Chitravati Group. This study has two aims:

1) to constrain the depositional setting and timing of deposition of these formations, and thus to provide support to either the foreland or rift basin initiation models, and

2) to assess the likelihood of a genetic linkage with the other Proterozoic Purana basins

Sedimentological observations are combined with analysis of stable isotope compositions of carbonate rocks to propose a palaeosedimentological model of basin evolution. U-Pb geochronology and hafnium isotope analysis of detrital zircon grains are used to constrain the timing of deposition and the likely provenance terranes of each formation. These constraints are used in conjunction to infer a plausible model of basin initiation.

2 GEOLOGICAL AND TECTONIC SETTING

2.1 Regional geology

The Indian Shield can be divided into two major cratonic blocks – the Northern Indian Block (NIB) and Southern Indian Block (SIB) (Radhakrishna & Naqvi 1986; Zhao *et al.* 2003), which are demarcated by a 1600 km long Proterozoic orogenic belt known as the Central Indian Tectonic zone (CITZ; see Figure 1b) (Acharyya 2003). The NIB is comprised of the Aravalli and Bundelkhand cratons, which amalgamated by *ca* 3300 Ma to form the stable Aravalli-Bundelkhand protocontinent (Mondal 2009). The SIB is subdivided into five major provinces, *viz*. the Dharwar, Bastar and Singhbhum cratons, the Eastern Ghats Belt (EGB) and the Southern Granulite Terrane (French *et al.* 2008; Meert *et al.* 2010). The two composite 'blocks' of India are separated by a complex network of suture zones, mobile belts and rifts (Meert *et al.* 2010). The Cuddapah Basin of the Dharwar Craton is one of a number of Proterozoic basins that lie unconformably on the cratonic basement of India (Figure 1a).

2.1.1 DHARWAR CRATON

The Dharwar Craton is divided into the Eastern Dharwar Craton (EDC) and the Western Dharwar Craton (WDC) based on major lithological and geochronological dissimilarities (Meert *et al.* 2010). The division between the EDC and WDC is poorly constrained to a 200 km wide lithological transitional zone from the basement gneisses of the WDC to the Closepet Granite on the western margin of the EDC (Meert *et al.* 2010), but a shear zone slightly to the west of the Closepet Granite is often cited as a more distinct boundary (e.g. Chadwick *et al.* 2000; Mishra & Prajapati 2003; Singh *et al.* 2004) (Figure 1b).

The WDC comprises a polyphase gneissic basement with four main units: a series of widespread undifferentiated Archaean gneisses known as the 'Peninsular Gneisses', several generations of granites, three major greenstone sequences, and younger metasedimentary and metaigneous rocks (Pitchamuthu & Srinivasam 1984; Naqvi & Rogers 1987; Naha *et al.* 1991; Rao *et al.* 1991; Meert *et al.* 2010).

The basement of the EDC consists of five major units: a series of Late Archaean plutonic belts known as the 'Dharwar Batholith', gneisses into which the batholith intruded, older undifferentiated TTG gneisses and greenstone belts, several greenstone and schist belts, and a widespread series of Proterozoic dyke swarms (Ramakrishnan & Vaidyanadhan 2008; Jayananda *et al.* 2009; Meert *et al.* 2010; Ahmad 2011). The Dharwar Batholith is the dominant lithology of the EDC, and comprises a calc-alkaline complex of juvenile and anatectic granitoids (Ramakrishnan & Vaidyanadhan 2008). A summary of age constraints in the Dharwar Craton based on U-Pb dating of zircon grains, and older, less reliable age constraints on these units are provided in Tables 1a and 1b, respectively.

2.1.2 EASTERN GHATS BELT

The EGB is a generally high-grade composite orogenic belt which extends for approximately 1000 km along the eastern margin of the Indian Shield (Simmat & Raith 2008; Meert *et al.* 2010) (Figure 1a). The EGB is comprised of four crustal units: the Late Archaean Jeypore and Rengali Provinces (northwest and northern domains, respectively), the Late Palaeoproterozoic Krishna Province

(southwest) and the Meso-Neoproterozoic Eastern Ghats Province (east) (Simmat & Raith 2008). Only the Krishna and Eastern Ghats Provinces are considered relevant to this study due to their spatial proximity to the Cuddapah Basin.

The Krishna Province abuts the Cuddapah Basin, and comprises the granulite facies Ongole Domain, and the low to medium grade Nellore Schist Belt (Dobmeier & Raith 2003). The Ongole Domain is predominantly formed of charnockitic granulites and metasedimentary rocks (Dobmeier & Raith 2003). The Nellore Schist Belt is divided into the Udayagiri Domain (a greenschist facies volcano-sedimentary sequence) and the Vinjamuru Domain (metasedimentary rocks with abundant felsic metavolcanic rocks), and also hosts what has been interpreted as a remnant ophiolite sequence (Vijaya Kumar *et al.* 2010). The contact between the Krishna Province and the basin is a tectonic melangé produced by imbricated thrusts and intense folding as well as several intrusive felsic plutons (Dobmeier & Raith 2003). Metamorphic zonation within the Krishna Province and Cuddapah basin suggests E-W oriented convergence during the late Palaeoproterozoic. This is supported by deep seismic sounding data (Kaila *et al.* 1987) and isotopic evidence for a tectonothermal event between 1640 and 1550 Ma; this collision has been termed the Krishna Orogen (Dobmeier & Raith 2003; Henderson 2011).

The Eastern Ghats Province is a highly deformed and metamorphosed assemblage of granulites with granitic and charnockitic intrusions (Dobmeier & Raith 2003). The province sits to the east of the Ongole Domain, and may have amalgamated with India *ca* 1100 Ma (Dobmeier & Raith 2003). A summary of age constraints on igneous and metamorphic activity in the EGB is provided in Tables 1a & 1b.

2.1.3 PURANA BASINS

The Indian Shield hosts a number of intra- and epicratonic Proterozoic volcano-sedimentary basins- the Purana basins- that have been thought to have initiated around 1800 Ma (Dhoundial 1987; Naqvi 2005). The Purana basins have a broad spatial distribution, and account for more than 20% of the exposure of Precambrian rocks on the Indian Shield (Kale & Phansalkar 1991). Each basin rests

unconformably on underlying Archaean basement (Murty 1968; Kale & Phansalkar 1991). Purana basin sequences occur in seven basins: the Vindhyan, Cuddapah, Chhattisgarh, Indravati, Pranhita-Godavari, Bhima and Kaladgi basins (Kale & Phansalkar 1991) (see Figure 1a).

A plausible explanation for the development of a number of broadly similar basins within Palaeo- to Mesoproterozoic India remains equivocal, especially if they share a genetic linkage (Deb 2004). Sedimentological and palaeobiological studies in the Purana basins have not revealed any palaeoclimatic or biostratigraphic marker which can be used for reliable interbasinal correlation (Chaudhuri *et al.* 1999; Kulkarni & Borkar 2002). However, various authors have attempted to correlate sediment packages based on lithological similarities, stromatolite assemblages and any available geochronological data (e.g. Raha 1987; Kale & Phansalkar 1991; Conrad *et al.* 2011). Authors who have conducted studies on the Kaladgi (Bose *et al.* 2008), Chhattisgarh (Deb 2004), Bhima (Nagarajan *et al.* 2011), Pranhita-Godavari (Rao 2000) and Vindhyan (Chakraborty 2006) basins have proposed that each of these may have developed as an extensional basin along pre-existing faults.

Several recent studies have provided maximum depositional ages for a number of the Purana Basins; these and all other available geochronological constraints on the timing of deposition in the Purana basins are summarised in Figure 2.

2.2 Study area

The northern, southern and western margins of the Cuddapah Basin unconformably overlie the EDC, whilst to the east the basin has been overthrust by the Krishna Province of the EGB. The Cuddapah Basin is the second largest of the Purana basins and is eastwardly concave in plan view and wedge-shaped in cross-section (thickening from the west to the east), with a length of *ca* 440 km, a maximum width of *ca* 200 km, a maximum depth of 12 km and an areal extent of around 44,500 km^2 (Kailasam 1976; Kalpana *et al.* 2010) (see Figure 1c).

2.2.1 STRATIGRAPHY

The Cuddapah Supergroup is divided into the unconformity-bounded Papaghni, Chitravati and Nallamalai Groups (Meijerink *et al.* 1984). The basal Papaghni Group consists of the Gulcheru and Vempalle Formations, which share a gradational contact. The Vempalle Formation is capped by a sequence of felsic pyroclastic rocks and lava flows (Anand *et al.* 2003). The Chitravati Group paraconformably overlies the Papaghni Group, and consists of the Pulivendla Formation and the Tadpatri Formation. The Gandikota Formation sits stratigraphically at the top of the Chitravati Group, where it has been variably said to conformably or unconformably overlie the Tadpatri Formation (e.g. Lakshminarayana & Bhattacharjee 2000; Dasgupta & Biswas 2006). However, descriptions of the Gandikota Formation and its upper/lower contacts are scarce in the literature and its position in the stratigraphy of the basin remains uncertain. The Nallamalai Group has been thrust over the Chitravati Group in the eastern side of the basin, and is composed of the Bairenkonda, Cumbum and Srisailam Formations (Saha & Chakraborty 2003). The stratigraphic position and estimated thickness of each formation, along with general sedimentary characteristics of and geochronological constraints on each formation are summarised in Figure 3.

The Kurnool Group is separated from the Cuddapah Supergroup by a net depositionary hiatus of around 500 - 600 myr (Mishra 2011). The Kurnool Group consists of the Banganapalle Formation (sandstones and conglomerates), the Narji Limestone, the Owk Shale, the Paniam Quartzite, the Kolikuntala Limestone and the Nandyal Shale (King 1872; Meijerink *et al.* 1984).

2.2.2 DEFORMATION AND IGNEOUS ACTIVITY

Sedimentary rocks in the western part of the basin are mostly undeformed, except for occasional minor faults (Saha 2002). Deformation is largely restricted to the easternmost arcuate Nallamalai Group, which has been intensely folded and thrusted to form the Nallamalai Fold Belt. This deformation is most likely a result of both the *ca* 1640 Ma convergence of the EGB with the EDC, and the amalgamation of the Indian shield into the supercontinent Gondwana approximately 510 Ma

(Alexander 2011). However, the timing and deformation history of the Nallamalai Group are poorly constrained (Saha 2002).

There are several significant igneous intrusions within the Cuddapah Supergroup. The upper Vempalle Formation is intruded by a series of basaltic sills, and is overlain by mafic and felsic volcanic rocks (Dasgupta & Biswas 2006). The Tadpatri Formation is intruded by a number of mafic to ultramafic sills which are present at varying stratigraphic levels, and have been dated at *ca* 1900 Ma (Anand *et al.* 2003). The Cumbum Formation was intruded by a lamproite at *ca* 1417 Ma (Chalapathi Rao *et al.* 1999), providing a minimum depositional age for the Cuddapah Supergroup (with the exception of the Srisailam Formation which is currently unconstrained).

2.2.3 BASIN EVOLUTION MODELS

There are two prevailing models for the initiation of subsidence to form the Cuddapah Basin. Singh & Mishra (2002; 2004) and Mishra & Prajapati (2003) propose a peripheral foreland basin origin for the Cuddapah Basin, describing it as a Proterozoic analogue to the present-day development of the Ganges Basin. In this scenario, the collision of the EGB with the EDC caused the development of accommodation space due to lithospheric flexure attributable to crustal loading by the EGB. This model was proposed following the delineation of deep basin-margin faults in a deep seismic sounding study by Kaila & Tewari (1985); this study showed an eastward-dipping crustal column beneath the eastern edge of the basin. Singh & Mishra (2002; 2004) and Mishra & Prajapati (2003) suggest that this is due to the subduction of the EDC under the EGB, and that subduction led to the formation of the basin on the passive margin block. They cite the apparent shallow marine shelf depositional environment as further support for this model.

Manikyamba *et al.* (2008) also propose a foreland basin model for the development of the Cuddapah Basin, but cite the Columbia reconstruction of Zhao *et al.* (2004) in which the eastern edge of the SIB was adjacent to the North China Craton. According to this model, the crustal components of Columbia assembled and accreted between 2100 and 1800 Ma, and the Cuddapah Basin developed as a foreland basin to the rising CITZ *ca* 1800 Ma.

In direct contrast to this, many authors advocate that the Cuddapah Basin developed as a failed continental rift basin (e.g. Chatterjee & Bhattacharji 2001; Chaudhuri *et al.* 2002; Anand *et al.* 2003; Hou *et al.* 2008). They base this proposal on the same deep basin-margin faults of Kaila & Tewari (1985), but suggest that apparent normal movement on the faults occurred during Proterozoic supercontinent fragmentation. Ravikant (2010) supports this hypothesis, and proposes that Palaeoproterozoic dyke swarms under the Cuddapah Basin are a result of the breakup of the supercontinent Columbia around 1900 Ma; the rifting of the south-eastern margin of the North China Craton from the EDC allowed an open seaway to form, leading to a marine incursion and sedimentation near the continental margin. The 'rift basin' model is also supported by Mohanty (2011), who suggests a supercontinent configuration involving the juxtaposition of southern India, Western Australia and the Napier Complex of Antarctica (the "SIWA" supercontinent), where the separation of south-eastern India from the Napier Complex *ca* 1950 Ma resulted in a rift basin which subsequently developed into a passive margin basin.

3 OUTLINE OF ANALYTICAL METHODS

3.1 Sedimentological analysis

Both field work and laboratory analysis were employed to infer the environment in which the sediments of the lower Cuddapah Basin were deposited. Five days were spent conducting field work in the state of Andhra Pradesh, south-east India. Lithostratigraphic logs were created for the Gulcheru, Vempalle and Tadpatri Formations, and samples were collected for analysis. The starting location and stratigraphic thickness of each section is summarised in Table 2. The location, resolution and length of each section were determined by the accessibility of outcrop and by time restrictions. In the absence of sufficient measureable exposure within the Gandikota Formation, detailed sedimentological observations were made near the base of the formation in order infer the palaeoenvironment during the initial stages of deposition of the formation, and hence a possible tectonic setting.

A series of samples of carbonate rocks were collected from the Vempalle Formation for analysis of their stable isotope (carbon and oxygen) composition. Analytical procedures for stable isotope analysis are outlined in Appendix I.

3.2 Isotopic analysis of detrital zircons

In order to propose a maximum depositional age for the four studied formations, U-Pb detrital zircon geochronology was conducted using a laser ablation inductively coupled plasma mass spectrometer (LA-ICP-MS) at Adelaide Microscopy, The University of Adelaide. Combined U-Pb dating and Hf isotope analysis of zircon grains is a useful tool for determining sediment provenance (Howard *et al.* 2009). The U-Pb analysis of zircon grains provides age spectra, and the Hf isotope composition allows comparison with the geochemical characteristics of possible source terranes. Accordingly, twenty concordant zircon grains from each sample were subsequently analysed for hafnium isotope composition using a laser ablation multi-element collector inductively coupled plasma mass spectrometer (LA-MC-ICP-MS); this method was applied in order to further constrain the provenance of the zircon grains, where the grains act as a proxy for sediment provenance of the rock. Analytical methods for U-Pb and Hf isotope analysis are provided in Appendix I.

4 SEQUENCE STRATIGRAPHY

4.1 Facies descriptions

On the basis of stratigraphic and sedimentological features, a number of discrete lithologies have been identified in each of the measured sections. A distilled description and interpretation of these lithologies is provided below; detailed sedimentary observations, interpretation of depositional processes and reasoning for facies assignations are outlined in Appendix II.

4.1.1 GULCHERU FORMATION

The basal Gulcheru Formation was logged in the Daditota Gorge near Parnapalle, where it disconformably overlies a highly weathered and weakly foliated granite, which is assumed to be the basement of the EDC (Figure 8a). Facies correspond to the stratigraphic log presented in Figure 4.

Clast-supported polymictic conglomerate (Facies 1), 100-290 cm

This facies is characterised by 6-30 cm rounded clasts supported by a matrix of smaller clasts, with a medium to coarse immature sandy matrix. Rocks of facies 1 display crude metre scale bedding and are generally overlain by facies St. The clasts are typically composed of microgranular quartzite (10-30 cm, ~ 40%), cherty/magnetic red and black laminated clasts termed 'banded ironstone' (BI; ~40% - Figure 8b) and milky white vein quartz (~20%). The proportion of BI clasts decreases up-section, as does the frequency of larger (20-30 cm) clasts. Large clasts are unidirectionally weakly to strongly imbricated, suggesting deposition from tractional transport under unimodal flow conditions. This facies also features occasional impersistent decimetre-scale lenticles of sand with centimetre- to decimetre-scale planar cross-bedding (Figure 8c). Given the poor sorting, imbricated clasts and crude bedding of this facies, it has been interpreted to represent bedload deposition from a high magnitude stream flood.

Trough cross-bedded granular sandstone (Facies 2), 10-50 cm

This facies is defined by compositionally mature decimetre-bedded medium to coarse sandstone with sub-angular to angular grains. Where this facies occurs immediately above facies 1, the contact is gradational. This facies grades from a basal granular conglomerate comprised of sub-angular vein quartz clasts (2-5 mm) to a medium sand. Beds are massive and tabular, and often contain trough cross-bedding. Sedimentary structures occurring in this facies include slump folding and small lenses of well sorted, well-rounded, more quartz-rich sand. Given the normally graded, trough cross-bedded nature of this facies, it has been interpreted to represent a waning flow deposit from sediment-laden flows following the deposition of facies 1 in a stream flood event.

Conglomeratic trough cross-stratified sandstone (Facies 3), 130-220 cm

This facies is characterised by horizontally discontinuous cross-stratified gravel layers interlayered with decimetre-bedded trough cross-stratified coarse, sub-rounded to sub-angular mature sand (Figure 8d). The gravel layers are clast-supported, and contain imbricated angular to sub-angular clasts of

quartzite, BI and vein quartz, often with centimetre to decimetre scale cross-stratification; these layers may represent intermittent high flow events. Occasionally, conglomerates are only one or two clasts thick, forming a pebble lag on the base of a scour. This facies typically contains small (up to 7 cm) lenses of well sorted, well rounded more quartz-rich sand as well as fining-up layers. Sedimentary structures occurring in this facies also include scour and fill structures and over-steepened foresets (Figure 8e). The size of the troughs increases up-section. The imbricated nature of the clasts in discontinuous beds interlayered with cross-stratified sand suggests bedload deposition in a pebbly braided stream setting with fluctuating discharge.

Laminated siltstone (Facies 4), 3-5 cm

This facies is defined by a fine grained siltstone. Beds are planar, and 0.5 – 1 cm in thickness. This facies only occurs overlying Facies 2, where it drapes the underlying sediments. This siltstone has been interpreted as having been deposited from suspension fall-out following a flood event.

Cross-stratified quartz arenite (Facies 5), 250-650 cm

Facies 5 is defined by decimetre-bedded medium to coarse grained trough and (rarely) planar cross-stratified quartz sandstone (Figures 8f & 8g). Grains are sub-rounded to rounded and are close to 100% quartz. Foresets are often steep (up to 40°) and occasionally internally laminated. Cross-bed sets vary from 5-50 cm in thickness, and increase in thickness up-section. Pebbles sometimes occur as lag deposits on the scour surfaces of trough cross-stratified beds (Figure 8h). The sand tends to fine up from coarse to medium sand within beds. Given the lack of any muddy intercalations with the cross-stratified sand beds, this facies is likely to represent deposition in a sandy braided stream setting, with fluctuating flow conditions within the lower flow regime.

No exposure zone, 470-870 cm

Zones of no exposure are marked by silty micaceous shale and fine sandstone lag, as well as a reduction in the gradient of the modern-day topography. Taking into account the prevailing fluvial

setting interpreted for this section, this zone is likely to represent a lithological transition to fine-grained floodplain sediment.

4.1.1.1 Palaeoflow

Palaeocurrent indicators were measured throughout the section, using a combination of tabular cross-stratification and strongly imbricated pebbles. Where imbricated pebbles were used as an indicator, the orientation of the clasts indicated flow from the west through to south-west (Figure 4). Where cross-stratification was used as an indicator of palaeoflow, they suggest broadly bimodal flow from the south-east and south-west, with no change throughout the section (Figure 4).

4.1.2 VEMPALLE FORMATION

In the interest of observing as much vertical distance as possible within a very limited timeframe, a slightly different logging methodology was adopted for the Vempalle Formation. Rather than defining facies, discrete lithological units were identified and described in the field, and then the vertical extent of the each unit was measured rather than the width of every individual bed (in the manner of Azerêdo *et al.* 2010). Several representative logs of lithological assemblages are provided where time and quality of outcrop allowed for detailed measurements to be made (Figure 6).

The Vempalle Formation conformably overlies the Gulcheru Formation with a gradational contact. The following lithological units correspond with the stratigraphic logs presented in Figures 5 & 6; the contact between the Gulcheru and Vempalle formations has been inferred to coincide with the first appearance of stromatolites in this log.

Interbedded fine sand and shale, ~5-35 m (LU1)

This lithological unit is defined by interbedded fine grained sandstone and shale. The sand is well sorted and well rounded, and compositionally mature. Sand beds are planar and range from one to twenty centimetres in thickness, and are interbedded with shale beds of up to five centimetres. Shale beds are variably grey-green or red, and frequently drape the troughs and crests of sandy ripples, or occur with lenticular bedding (Figure 9a). Herringbone cross-stratification in this unit indicates

bimodal flow, and the presence of both planar and trough cross-bedding reflects variable flow conditions. Shale beds often contain polygonal desiccation cracks, indicating periodic sub-aerial exposure (Figure 9b). Various loading structures occur, signifying rapid deposition of sand over unconsolidated mud (Figure 9c). Where sand beds overly mud beds with desiccation cracks, they occasionally contain rip-up clasts of the underlying shale, indicating that the deposition of the sand was a relatively high energy event (Figure 9d). This unit also features intermittent algal laminites, and stromatolites appear from around 36 metres in the measured section (Figure 9e). This unit is likely to represent deposition in a high energy, storm dominated environment with bimodal flow, which was punctuated by periods of quiet, stillwater deposition and sub-aerial exposure. This may alternately represent deposition in a muddy peritidal setting, or on a desiccated mud flat on a lake shore.

Dolomite with interbedded sand and mud, ~20 m (LU2)

This unit is defined by 10-20 cm stromatolitic dolomite beds alternating with centimetre-scale muddy beds. The sand content of the dolomite beds increases up-section, until sandy beds intercalate with the dolomite. Muddy beds contain polygonal desiccation cracks, and sandier beds occasionally contain a basal layer of rip-up clasts of the mud. Algal mat laminations occur in the lowermost few metres of the assemblage, and irregular fenestrae filled with black sulphides or sparry calcite occur within dolomite beds throughout the unit. This unit is likely to have been deposited predominantly in very shallow water, where precipitation of carbonate and growth of stromatolites occurred sub-aqueously, muddy beds were deposited from suspension during quiet periods, and the sand beds were deposited during high energy events. Exposure of the sediments occurred during periodic relative reductions in water level. This unit is likely to represent a series of shallowing-up events, with an increased input of siliciclastic material reflecting increasing energy up-section.

Thickly bedded dolomite with mixed sand, 100 m (LU3)

This lithological unit is characterised by thick laterally persistent stromatolitic dolomite beds with tabular to well-developed pinch and swell geometry. Dolomite beds contain sand, which occurs either mixed with the dolomite, or as thin discrete layers within dolomite beds, or occasional decimetre sand

beds (Figures 9f & 10a). Other sedimentary structures observed include scour and fill structures, low-angle domal stromatolites and very occasional clasts of the underlying dolomite within the base of sand beds. The dearth of sub-aerial exposure features implies deposition in a shallow-water setting which was affected by high energy storm events.

Stromatolitic dolomite, ~20-35 m (LU4)

This unit is characterised by 20-30 cm dolomite beds with occasional 5-10 cm muddy intervals. The dolomite beds contain columnar stromatolites and algal laminites as well as occasional low-angle symmetrical ripples. Bed thicknesses increase up-section, and the frequency and thickness of the muddy intervals decreases. The shale layers contain desiccation cracks, and dolomite beds near the base of the unit feature large irregularly distributed fenestrae, indicating periodic sub-aerial exposure. Other sedimentary features include prominent chert nodules and very occasional lensoid sand bodies. This unit records deposition in a very shallow water setting where fluctuating relative water level led to periodic exposure, and which was subject to rare inputs of coarser siliciclastic material.

Shale with interbedded sand, ~10 m (LU5)

This unit features thinly bedded red to brown shale which contains both desiccation cracks and internally zoned halite pseudomorphs (Figure 9g), indicating both saline water and extended periods of sub-aerial exposure. The shale is intercalated with thin impersistent beds of fine-grained quartz arenite, which occurs near the base of the section as lensoid scour and fill structures, or as lenticular bedding. The sand content increases upward through the section, and features cm-scale fining up sequences and planar cross-stratification, as well as straight crested or interference ripples. Planar cross-stratified sand beds contain basal rip-up clasts of shale. This unit is likely to have been deposited in a very shallow water environment where sand was deposited during relatively high energy events, which increase in frequency up-section. Deposition of sand was interspersed with depositional of sediment from suspension, and frequent periods of exposure – mostly likely a playa or sabkha-type setting.

Interbedded dolomite and mud, ~10-65 m (LU6)

This unit is defined by interbedded grey dolomite and pink to red mud in varying thicknesses. Dolomite beds are up to 60 cm in thickness, and are stromatolitic, or contain algal laminites. The dolomites occasionally contain a small proportion of sand, with rare current scouring and small symmetric ripples on the top of beds. Spheroidal chert nodules also occur within the dolomite. Dolomite beds are separated by thinly bedded cm-scale planar parallel mud beds. Very large micritic stromatolite mounds several metres in length and >2 metres in height occasionally occur; these are made up of decimetre-scale dolomite beds separated by shaley partings, and are draped with mud (Figure 10b). The growth of large stromatolite mounds indicates that this unit is likely to represent sub-aqueous deposition in a relatively deep water low energy milieu (Simonson *et al.* 1993), where the precipitation of dolomite alternated with the deposition of mud from suspension. Inputs of coarser siliciclastic material are likely to represent intermittent storm events.

Interbedded sandy dolomite and mud, with occasional sand beds, >45 m (LU7)

This lithological unit is characterised by intercalated dolomite and mud, with occasional sand beds. All dolomite beds contain stromatolites and/or algal laminites, and vary in colour from light to dark grey. Stromatolites often display ‘laterally linked hemispheroid’ morphology (Figure 9h). Dolomite beds contain varying amounts of sand, and occasionally exhibit symmetrically rippled bed tops. Sand beds contain trough cross-stratification, but further internal structures were not visible due to preferential shearing along the sand beds. Mud layers are fissile, and either brown or green in colour. Lenticular bedding and flame structures occasionally occur where sand and mud are interbedded. This assemblage was further divided into seven discrete lithologies, which are summarised in Figure 6 and Appendix II, along with their contact relationships. This unit is likely to represent a series of deepening-up sequences, where thick grey dolomite beds were deposited in relatively shallow water conditions, then mud beds were deposited in deeper water conditions. These sequences are likely to have been deposited in a fairly low energy setting, until further up in the section where sand beds appear and are rapidly deposited over shale.

4.1.3 TADPATRI FORMATION

The *ca* 4600 m thick Tadpatri Formation has previously been interpreted as a marine deposit, based on the identification of tidal bundles and flaser and lenticular bedding within the formation (Dasgupta & Biswas 2006). Considering the small vertical succession which was measured with no lateral comparison, and no strong evidence to the contrary, this marine interpretation is adopted in this study. The Tadpatri Formation unconformably overlies the Pulivendla Formation, which in turn nonconformably overlies the felsic volcanic rocks that cap the Vempalle Formation. The described section was measured within the uppermost Tadpatri Formation, and the facies outlined below correspond to the stratigraphic log presented in Figure 7.

Fine sand, 2-60 cm (F1)

This facies is defined as a very fine to medium grained purple arkosic sandstone. It typically occurs in beds of approximately two cm which are generally planar but occasionally wavy. Beds are often internally laminated (with planar mm-scale alternations of very fine and fine sand), or contain hummocky cross-stratification (Figure 11a). These fine sand beds occasionally occur with a scoured contact above shale, then fine up slightly to silt-sized grains; these may represent small turbidity currents generated by storms (Boggs 2001). Fining-up sequences also occur in sand beds without an erosive contact. This may indicate erosion of sediment from the beach during onshore storm events and subsequent injection of a plume of suspended fine sand into a deeper water setting, where progressively finer sediments settled out of suspension (Prothero & Schwab 1996). Fluid escape structures occur in places at the bottom of beds where the sand lies over shale, and some beds have loaded bases, indicating occasional rapid deposition of the sand. Small (2-3 cm) ball-and-pillow structures also occur where sand beds overlie shale (Figure 11b). The general predominance of fine-grained sediment and frequent planar lamination indicates that this facies is likely to have been deposited below the fair-weather base in a sub-tidal setting (Prothero & Schwab 1996). Where beds are only slightly wavy, this is likely to represent minor reworking by sluggish currents.

Highly convoluted fine sand with shale, 175 cm (F1a)

This facies occurs in one bed only; it is nominally composed of fine sand, however it is dominated by extensive syn-sedimentary deformation. This bed is deposited over shale, and the base of the sand contains large (dm-scale) flame structures. This bed also contains well developed ball (approx. 20 cm in diameter) and pillow structures, in which the sand that forms the balls is internally laminated, and the laminations have been curved to conform to the edge of the ball (Figures 11c & 11d). The interior of the sand balls is relatively massive. The planar-laminated nature of the sand which has been deformed indicates that the sand was not deposited unusually rapidly, but rather was deformed subsequent to deposition in a low energy setting. Accordingly, these sediments are likely to either have been deformed following a seismic event which caused the underlying mud to act thixotropically, or following the deposition of a large amount of sand over semi-consolidated mud *and* sand.

Interbedded shale and fine sand, 2-17 cm (F2)

This facies is defined by thinly interbedded to laminated very fine sand and purple shale. The shale is either reddish-purple or light grey-green. The facies typically occurs in 3-5 cm beds that may fine upward slightly, and there is occasional wavy bedding and or very low angle scour structures where sand overlies shale. Flame structures occur in places at the top of beds where this facies is deposited below sand. This facies is interpreted as having been deposited primarily from suspension in a low energy milieu, with occasional reworking of beds by weak currents, occasionally followed by rapid deposition of sand during slightly higher energy events. F2 often gradationally overlies F1, signifying a reduction in the energy of the depositional setting. Following the environmental interpretation proposed for F1, this may represent a reduced frequency and intensity of storm events affecting sub-tidal deposition.

Thinly bedded shale, 2-24 cm (L3)

This facies is characterised by light grey-green or purple shale. It occurs in 0.5-2 cm beds, and often has a gradational boundary with underlying sand. Bedding is generally parallel but occasionally is slightly wavy, and beds often contains millimetre-scale laminations. This facies is likely to reflect deposition in a very low energy setting with some slight reworking of sediment by weak currents. Where F3 gradationally overlies F2 or F1, this implies a reduction in the energy of the setting, and possibly a period of quiescence on the shoreline.

4.1.4 GANDIKOTA FORMATION

The Gandikota Formation overlies the Tadpatri Formation with an angular unconformity. The following observations were made in the Gandikota Gorge, near the base of the formation. Due to a lack of sufficient exposure, a stratigraphic log could not be created, nor could unit thicknesses or contact relationships be quantified. These rocks are described merely to provide a 'snapshot' of the sedimentary environment in the early stages of the deposition of this formation.

Cross-stratified sand

The observed lithology is characterised by sand beds of up to one metre interbedded with mud beds of approximately 10 cm. Muddy layers are highly weathered and internal structures are not apparent. The sand is fine to coarse grained and poorly sorted, and close to 100% quartz. The sandstone features planar parallel cross-stratified beds, hummocky cross-stratified beds and frequent climbing ripples (Figure 12a), which implies variable flow conditions. The sand also features large low-angle scour structures where finer sand has been scoured and filled by coarser sand. The sand is poorly sorted, and all foresets fine upward, resulting in prominent laminae. Bed tops occasionally feature slightly asymmetric ripples with broken crests, and rhomboidal interference ripples (Figure 12b), which indicates deposition in a very shallow wave-influenced environment. Small-scale synsedimentary detachment faulting occurs, in association with climbing ripples and flame structures (Figure 12c). This lithology implies rapid deposition of sediment from tractional transport, in a generally high energy wave-dominated setting. However, the lack of any visible contact relationships with under-

and overlying lithologies makes further constraint on the depositional setting of the Gandikota Formation implausible.

5 LA-ICP-MS U-Pb ZIRCON GEOCHRONOLOGY

One of the aims of this study is to constrain the maximum depositional age of formations of the lower Cuddapah Supergroup. Accordingly, one sample was selected from each of the Gulcheru (GF01), Vempalle (GF14), Tadpatri (GF09) and Gandikota (GF06) formations for preparation and imaging, then analysis using a LA-ICP-MS at Adelaide Microscopy.

Where metamorphic rims were identified in cathodoluminescence (CL) imagery, the cores of zircon grains were targeted to date the original crystallisation age of the grain. Discrete age populations were assigned on the basis of probability density diagrams produced using Isoplot/Ex 3.00 (Ludwig 2003).

5.1 Sample descriptions and results

Analytical LA-ICP-MS detrital zircon data are presented in Appendix Tables 1A-4C, and a summary of detrital populations within each sample is provided in Table 3. Graphical representations of results (conventional concordia and probability density plots) are presented in Figures 13 & 14, along with CL images of representative zircon grains. Zircon morphologies and internal characteristics are described in Table 4. The location of sample collection within each formation and a brief description of the bed from which each sample was collected are provided in Table 5. All ages presented are $^{207}Pb/^{206}Pb$ ages, and all age data which are discussed are within 10% of concordia.

5.1.1 GULCHERU FORMATION (GF01)

Sample GF01 from the Gulcheru Formation is a coarse-grained quartz arenite taken within Facies 1, approximately six metres up from the base of the Gulcheru section (Figure 4). Ninety-six analyses were performed on 93 zircon grains extracted from sample GF01, and 27 of these analyses were between 90 and 110% concordant. Concordant detrital zircon populations occur at *ca* 3426, 3368, 2985 and 2612 Ma. Single zircon grains record age populations at *ca* 3267, 3183 and 3123 Ma. The

youngest twelve grains give a mean weighted age of 2526 ± 13 Ma (MSWD = 1.3, zircon ages from *ca* 2563- 2490 Ma), which may be considered the maximum depositional age.

5.1.2 VEMPALLE FORMATION (GF14)

This sample is a coarse-grained quartz arenite taken from within the lithological association of interlayered sandy stromatolitic dolomite and mud which occurs from approximately 143-164 m in the Vempalle Formation section. Sample GF14 was obtained from approximately 162 m along the section (Figure 5). One hundred and eleven analyses were performed on 101 zircon crystals extracted from sample GF14 and of these analyses, 66 were less than 10% discordant. A dominant detrital population occurs at *ca* 2500 Ma (n = 42). Smaller peaks occur at 2584 and 2546 Ma. Further zircon populations are recorded by single grains at *ca* 2765 and 2422 Ma. A maximum depositional age for this sample is tentatively defined by the youngest single detrital zircon at 2422 ± 17 Ma (92% concordant), or may be more confidently defined by the dominant peak at 2500 ± 7 Ma (n = 42, MSWD = 1.8, zircon ages from *ca* 2532-2454 Ma).

5.1.3 TADPATRI FORMATION (GF09)

Sample GF09 was collected from a fine-grained muddy arkosic sandstone from within a chaotically bedded sandstone featuring prominent loading and water escape structures, which occurs at approximately five metres in the section through the upper Tadpatri Formation (Figure 7). Approximately 80 grains were extracted from the sample by Minsep Laboratories (W.A.) after no grains were extracted during in-house mineral separation. All zircon grains extracted were extremely small and generally fractured and grainy in CL, which is characteristic of zircons with a damaged crystal structure (Hay & Dempster 2009). Only 36 grains were analysed due to their highly discordant nature (concordance range of 1-67%), and many zircon grains contained a significant amount of common lead. Several grains were discounted due to an unacceptably high level of common lead (discarded analyses denoted with an asterisk in Appendix Table 3). Furthermore, many of the zircon grains in this sample had either anomalously high or low uranium counts, which signifies that the isotopic composition has been disrupted.

The most likely reason for an entire population of zircon grains which have not retained their isotopic information is that the grains were derived from a very fine grained sediment; very small zircon grains extracted from fine or muddy sediments are more likely to have a damaged crystal structure and reduced isotopic integrity (see explanation in Hay & Dempster 2009). These small, damaged grains are also inherently reactive, and are susceptible to post-depositional alteration. However, an approximate discordia can be drawn through a series of analyses to intercept the concordia at *ca* 2500 Ma, which implies that the zircons may have been derived from a *ca* 2500 Ma source.

5.1.4 GANDIKOTA FORMATION (GF06)

Sample GF06 from the Gandikota Formation is a texturally immature medium-grained clean quartz arenite. One hundred and forty analyses were performed on the 127 zircon grains extracted from sample GF06. Of these analyses, 52 were within 10% concordancy. The majority of concordant analyses form a detrital zircon peak which occurs at *ca* 2499 Ma (MSWD = 2.1, n = 29). Smaller peaks occur at *ca* 2635, 2569, 2196 and 1909 Ma. Discrete zircon populations represented by single grains occur at *ca* 3038, 2985, 1810, 1705, 1641, 1275 and 1207 Ma. The youngest zircon in this sample occurs at 1206.5 ± 22.08 Ma (98% concordant), which may be considered a maximum depositional age for the Gandikota Formation.

6 LA-MC-ICP-MS Hf ISOTOPE ANALYSIS

The zircon mounts prepared for U-Pb LA-ICP-MS analysis were also used for Lu/Hf isotopic analysis undertaken with a LA-MC-ICP-MS at The University of Adelaide (Waite Campus). Twenty grains each from samples GF01, GF14 and GF06 were chosen to analyse for Hf isotope composition. Grains were chosen to represent each of the identified detrital populations within each sample. Only grains with $^{207}Pb/^{206}Pb$ ages of greater than 95% concordance were analysed for Hf with the LA-MC-ICP-MS; no analyses from sample GF09 were of sufficiently high quality to warrant further analysis.

6.1 Results

From the three samples analysed for hafnium isotope composition, 55 analyses were conducted on 55 zircon grains. Initial hafnium values, ε_{HF} and $T_{(DM\text{-}crustal)}$ ages of these analyses were calculated at their $^{207}Pb/^{206}Pb$ age; results are displayed in Figure 15 and all isotopic data are provided in Appendix Table 5.

6.1.1 GULCHERU FORMATION

The zircon grains which are older than *ca* 3000 Ma have ε_{HF} values of -3.49 to 1.89, and $T_{(DM\text{-}crustal)}$ ages ranging from 3660-3450 Ma. The zircon grains which are around 2500 Ma yielded ε_{HF} values of -4.23 to 2.84, and $T_{(DM\text{-}crustal)}$ ages from 3660 to 3450 Ma.

6.1.2 VEMPALLE FORMATION

The *ca* 2500 Ma zircon grains have ε_{HF} values of -3.75 to 6.75, and $T_{(DM\text{-}crustal)}$ ages between 3220 and 2630 Ma. The *ca* 2767 Ma zircon yielded a ε_{HF} value -10.76, and $T_{(DM\text{-}crustal)}$ age of 3820 Ma.

6.1.3 GANDIKOTA FORMATION

The population of zircon grains at *ca* 2500 Ma display ε_{HF} values of between -4.42 and 3.96, and $T_{(DM\text{-}crustal)}$ ages between 3660 and 3450 Ma. The grains between approximately 1800 and 1700 Ma have ε_{HF} values between -6.45 and -0.83, and $T_{(DM\text{-}crustal)}$ ages between 2850 and 2430 Ma. The zircon grains of 1275-1207 Ma yielded ε_{HF} values of 3.52 to 2.92, and $T_{(DM\text{-}crustal)}$ ages of 1870 to 1780 Ma.

7 CARBON-OXYGEN STABLE ISOTOPE GEOCHEMISTRY

The excellent exposure of the Vempalle Formation facilitated the creation of continuous $\delta^{13}C_{dol}$ and $\delta^{18}O_{dol}$ profiles through the section. Following XRF-screening of samples, all were determined to be dolomitic. The carbon isotope ratios are reasonably consistent, displaying a transition from a relatively light composition for the first 150 m (between approximately 0 and -2‰) to a heavier composition around 250 m (around 1‰). The $\delta^{13}C_{dol}$ values subsequently fluctuate slightly for around 100 m, then remain fairly stable around 0‰ for the remainder of the measured section (Figure 16a). The oxygen isotope record is more scattered; $\delta^{18}O_{dol}$ values tend to fluctuate by approximately 3‰

around an average of -6.8‰. Overall, $\delta^{18}O_{dol}$ values display trend of becoming lighter with increased stratigraphic height (Figure 16a). The stable isotope composition ($\delta^{13}C_{dol}$ and $\delta^{18}O_{dol}$) of each sample is summarised in Appendix Table 6.

7.1 Alteration

In a geochemical analysis of sedimentary rocks, the effects of post-depositional alteration on primary isotopic compositions must be considered. In the case of rocks from the Palaeoproterozoic, $\delta^{18}O_{carb}$ values are more likely to become depleted during diagenesis than $\delta^{13}C_{carb}$ values (Bekker *et al.* 2001). Diagenetic alteration does not generally present a problem for carbon isotope data in the Palaeoproterozoic (Shields & Veizer 2002); the lack of terrestrial photosynthetic organisms during this time meant that meteoric water did not incorporate ^{13}C-depleted organic acids from the decay of these organisms. Hence, the assimilation of terrestrial fluids into pore water did not cause a reduction in $\delta^{13}C_{carb}$ of carbonate rocks during lithification, as can be the case in younger carbonates (Brand & Veizer 1981; Knauth & Kennedy 2009). The best evidence for alteration of carbon isotope composition is the presence of outlying data (Lindsay & Brasier 2002). The consistency of the $\delta^{13}C_{dol}$ values from the Vempalle Formation section may indicate that they have not been altered.

Oxygen isotope values are more susceptible to diagenetic alteration (Shields & Veizer 2002); depletion in ^{18}O may occur as meteoric water tends to be enriched in ^{16}O, depending on climate (Brand & Veizer 1981). $\delta^{18}O$ values of Precambrian carbonates are generally depleted with respect to most of the Phanerozoic (Shields & Veizer 2002), with average values around -7‰ (e.g. Veizer *et al.* 1990; Veizer *et al.* 1992), where dolomites record $\delta^{18}O$ values around 3 ± 2‰ heavier (Land 1980; Veizer *et al.* 1992). The values obtained from the Vempalle Formation dolomites have an average $\delta^{18}O$ value of -6.7‰, and are therefore only slightly lighter than the global average. If the rocks from the Vempalle Formation were precipitated from oceanic water, and if rocks used to calculate global marine averages through time represent an accurate record of the isotopic composition of the ocean through time, then it would appear from this comparison that the oxygen isotopic composition is unlikely to have been significantly altered.

7.1.1 DOLOMITISATION

The main indicator for alteration in the rocks of the Vempalle Formation is that each analysed sample from the >400 m section is dolomitic. Primary dolomite precipitates are generally metastable and non-stoichiometric, with a high degree of cation disorder and therefore higher free energy and greater solubility than dolomites which are closer to ideal stoichiometry of $CaMg(CO_3)_2$ (Hardie 1987). Therefore, primary dolomite has a propensity to undergo iterative dissolution and re-precipitation until a state of lower activity is reached (Land 1980; Warren 2000). During this progression toward a stable configuration, the isotopic record is likely to be reset several times as the crystal structure of the evolving dolomite comes into equilibrium with the chemical composition of the altering fluid (Land 1980; Sibley *et al.* 1994). Similarly, in order to dolomitise a typical limestone, hundreds or even thousands of pore volumes of Mg-bearing altering fluid must pass through the rock before it becomes pervasively dolomitised, depending on the origin and chemical characteristics of the fluid (Land 1985). The persistently dolomitic nature of the Vempalle Formation indicates that it was altered in an open system characterised by the passage of large volumes of pore fluid and possibly several episodes of dissolution and re-precipitation (Warren 2000). This is likely to have occurred during early diagenesis, as the porosity of dolomite decreases with increased burial, which significantly reduces the rate at which Mg-bearing fluids may move through the rock (Morrow 1982; Land 1985).

As most pore fluids contain abundant oxygen, the $\delta^{18}O$ values of the Vempalle Formation dolomites are likely to reflect the isotope composition of the altering fluids rather than any primary value (Brand & Veizer 1981). A wide range of fluids may act as dolomitising solutions, but from the data collected in this study it is not possible to determine the nature of the fluid which acted as a dolomitising fluid to the Vempalle Formation, and hence the environment or processes which the $\delta^{18}O$ values recorded in the rocks are likely to represent (Warren 2000).

In contrast to this, pore fluids typically have a low carbon content and the $\delta^{13}C$ value of a dolomite may therefore quite closely reflect the value of a precursor carbonate, if organic acids were not present in the pore fluids (Morrow 1982; Banner & Hanson 1990). Therefore, it remains possible that

the Vempalle Formation dolomites may have retained their original $^{13}C/^{12}C$ ratios, unless the altering fluid had a large amount of C or significantly different $^{13}C/^{12}C$ ratio to the original rock. However, as the composition of the altering fluid is unknown and the rocks are likely to have undergone several episodes of dissolution and recrystallisation, overprinting of the $\delta^{13}C$ values may not be ruled out. Thus it is that the consistency of the $\delta^{13}C$ values may reflect homogenisation by altering fluids.

7.2 Interpretation

Carbon and oxygen isotope compositions within the first 110 m of the section – corresponding with Lithological Unit 1 - show a strong positive correlation, where $\delta^{18}O$ and $\delta^{13}C$ trends appear co-variant (Figures 16b & 16c). This correlation may imply

1) fractionation via environmental processes, or

2) diagenetic alteration of the primary precipitate.

If the correlation were due to environmental processes, this may suggest that the precipitation of carbonate occurred in a restricted setting, where evaporation and consequent preferential transferral of ^{16}O into the vapour phase was coupled with an increase in $^{13}C/^{12}C$ as productivity in increasingly warm and nutrient-rich water rose, leading to an increased uptake of ^{12}C by algae and resultant enrichment of dissolved organic carbon in ^{13}C (Mayer & Schwark 1999).

However, given the dolomitic nature of the deposit, it is highly likely that the primary isotopic values of samples from the Vempalle Formation have been pervasively altered. The $\delta^{13}C$ values may retain some of their primary character and therefore the periodic reversal in trend (approximately every 10 m) may still represent a series of deepening and shallowing events in a restricted setting (Figure 16c). However, the $\delta^{18}O$ values are more likely to reflect the composition of dolomitising fluids. Fluctuations in isotopic values may also be a function of lithology; certain lithologies may have experienced a greater degree of alteration than others due to the timing of formation of cements or the relative porosity of the lithology. Varying degrees of alteration and therefore inconsistent dolomitisation may have caused the observed trends, where samples which have experienced a greater

degree of dolomitisation display relatively heavier $\delta^{18}O$ values due to differential isotopic fractionation of oxygen in limestones and dolomites (Land 1980).

Given this alteration, it is difficult to infer a depositional setting for the Vempalle Formation dolomites based on their stable isotope compositions. The rocks are likely to have undergone episodes of dissolution and re-precipitation, and hence may have adopted the isotopic character of dolomitising fluids (Land 1980). Several inferences may be made if the two-fold supposition is made that a) $\delta^{13}C$ values reflect the chemistry of the open ocean at the time of deposition of the rock, and b) that dolomitising fluids did not have a high carbon content or significantly different $^{13}C/^{12}C$ ratio to the primary precipitate, and hence that the original $\delta^{13}C$ values of the rock have been retained. These inferences are outlined below.

7.3 Global correlation

The Palaeoproterozoic oceanic carbon isotope record is marked by a strong positive $\delta^{13}C$ excursion which is thought to have lasted from around 2220-2000 Ma (Bekker *et al.* 2006; Melezhik *et al.* 2007). This has been termed the 'Lomagundi excursion', and has been recognised in marine deposits in North and South Africa, Russia, Australia, North and South America, India, Scotland, Brazil, Uruguay and the Fennoscandian Shield (summaries in Frauenstein *et al.* 2009; Maheshwari *et al.* 2010). This extensive distribution indicates that the Lomagundi excursion represents a global event. The end of the excursion is marked by a return to $\delta^{13}C$ values around 0‰. This is seen in the Mille Lacs group of the Lake Superior area, and the Nash Fork Formation of the Snowy Pass Supergroup, which are deposited above carbonates displaying the characteristic elevated $\delta^{13}C$ values of the Lomagundi excursion, and which (in the case of the Mille Lacs Group) must be younger than 2009 ± 7 Ma (Bekker *et al.* 2003; Holm *et al.* 2005; Bekker *et al.* 2006). Carbon isotopes from the Vempalle Formation display similar values to these uppermost rocks, and therefore – assuming a direct connection with the open ocean and retention of primary isotopic composition - may be correlatable with the termination of the Lomagundi excursion some time before 2000 Ma.

However, strong evidence for tidal influence on sedimentation in the Vempalle Formation section is lacking, and so a connection with the open ocean is not certain. Even assuming that the Vempalle Formation carbonates reflect the chemistry of the ocean at the time of deposition, the chemostratigraphy of the Vempalle section is most closely correlatable with the global average at approximately 2700 Ma (Shields & Veizer 2002) (Figure 17a) and less similar to the global mean at *ca* 2000 Ma. Carbonates of the Vempalle Formation indirectly overlie basement rocks of *ca* 2300 Ma, and therefore this comparison is not likely to be valid. The $\delta^{13}C$ values of rocks from the Vempalle Formation correlate quite well with the shift from -2 to 0‰ at around 2100 Ma on the composite carbon isotope curve created by Lindsay & Brasier (2002) (Figure 17b). However, this region of the curve comprises data from two different basins, both of which are poorly time constrained (Lindsay & Brasier 2002). The validity of this comparison is further questioned by the work of Frauenstein *et al.* (2009), who conclude that $\delta^{13}C$ values are more likely to reflect local or regional events and processes than global phenomena, and therefore that global correlations are only valid for comparison of very large anomalies. As the Vempalle Formation carbonates have $\delta^{13}C$ values around 0, this is not a significant enough deviation from the average global values through time to provide a valid correlation.

8 DISCUSSION

8.1 Depositional environments

8.1.1 GULCHERU FORMATION

The section logged through the base of the Gulcheru Formation is generally dominated by facies 1 and 3, with an increasing prevalence of facies 5 up-section. The basal coarse conglomerates interbedded with pebbly cross-bedded sands are strongly indicative of a fluvial setting that was subject to frequent high flow events. This, in conjunction with the small amount of fine floodplain sediment and highly variable discharge rate, indicates that the Gulcheru Formation was deposited in a braided stream setting (Miall 1992). This is supported by the work of Davies & Gibling (2010) who

propose that prior to the early Palaeozoic, the absence of both stabilising vegetation and a large amount of fine-grained sediment caused most if not all rivers to adopt a braided style.

Specific architectural elements formed by these facies could not be determined, as satisfactory definition of these elements requires tens of metres of lateral extent in outcrop (Miall 1985). As the observations in this study are limited to a vertical profile, the facies assemblage may be discussed in terms of a vertical profile model, but characteristics of these facies in absence of any lateral comparison may be non-diagnostic (Miall 1977, 1985).

In the absence of identifiable architectural elements, this assemblage may be said to represent a medium between two end-member facies models proposed by Miall (1978): the proximal, stream-flow dominated Scott-type gravelly stream, and the distal sand-dominated Donjek-type gravelly stream. This therefore suggests that the presented section through the Gulcheru Formation was deposited in a setting which was fairly close to a region of uplift, but not immediately adjacent. The environment was still subject to sporadic high flow events of sufficient energy to move boulders. The maturity of the sand suggests that this environment may have derived sediment from an old, chemically weathered terrane.

According to Miall (1992), gravelly rivers often occur as the distributaries of alluvial fans and fan deltas. Although it is impossible to determine from this study whether the logged section formed part of an alluvial fan, or series of fans, the small amount of stratigraphy seen at the base of the Gulcheru Formation section may indicate deposition in the middle reaches of a fan. This interpretation may be supported by the palaeocurrent indicators, which are consistently slightly divergent from the south-east through to the south-west (see rose diagrams in Figure 4), and may represent a radial drainage pattern.

8.1.2 VEMPALLE FORMATION

The interpretation of shallow water Precambrian carbonate assemblages is highly problematic due to the lack of faunal assemblages. The differentiation of ancient lacustrine and shallow marine settings may be attempted through a combination of faunal, chemical and physical characteristics; the absence

of marine and euryhaline lagoonal fauna or the presence of particular non-marine flora and fauna can be instrumental in determining the nature of an ancient carbonate deposit (Reading 1996). The absence of any fauna in these pre-1900 Ma deposits makes the determination of the depositional setting of the Vempalle Formation ambiguous, as physical processes recorded in ancient lake-formed sedimentary rocks are similar to those recorded in shallow marine deposits, and strong sedimentological evidence for tidal influence on the Vempalle Formation rocks (e.g. tidal bundles or clear shoaling cycles) were not seen in the field.

Accordingly, the Vempalle Formation may have been deposited in either a saline lacustrine setting, or a predominantly low energy shallow marine setting. The basal desiccated mud with rippled sand may represent deposition on an intertidal mud flat. However, the frequency with which sub-aerial exposure features occur throughout the entire section provides support for a lacustrine model; long-lasting equilibrium between water level and sedimentation rate is more likely to occur in a lacustrine than marine setting (Reading 1996).

The section through the Vempalle Formation shows an overall deepening-upward trend. Sub-aerial exposure features are prevalent within the stratigraphy for approximately the first 150 m of the section. The remainder of the section is dominated by shallow sub-aqueous deposition, where the relative water level eventually rose sufficiently high for large stromatolite mounds to develop. This progressive deepening was not a purely gradual process; the rise in water level appears to have been punctuated by several periods of sub-aerially exposed conditions and subsequent return to sub-aqueous deposition.

The abundance of stromatolitic dolomite and frequent occurrence of planar laminated muds implies that the Vempalle Formation was deposited in a fairly low energy environment. Occasional high energy events are recorded by the presence of discrete sand beds which often have erosive bases, and in sand which is mixed in with the dolomite in certain units.

In terms of providing support for a marine versus lacustrine depositional milieu for the Vempalle Formation, the stable isotope data are equivocal. The correlation between the $\delta^{13}C_{dol}$ and $\delta^{18}O_{dol}$ values

in the lowermost lithological unit is likely to represent diagenetic alteration rather than environmental fractionation, although the periodically fluctuating $\delta^{13}C_{dol}$ values may reflect a restricted evaporative setting.

However, the $\delta^{13}C_{dol}$ values are consistent with accepted global marine values in the mid-Palaeoproterozoic (Shields & Veizer 2002; Jaffrés *et al.* 2007); therefore, neither a shallow marine nor lacustrine depositional setting for the rocks of the Vempalle Formation may be discounted, pending further isotopic analysis of the formation.

8.1.3 TADPATRI FORMATION

The alternation of fine sand beds of varying thickness with planar laminated shale, combined with occasional evidence of higher energy events indicates that the section through the upper Tadpatri Formation may record deposition in a storm-dominated sub-tidal setting, which was affected by storms of varying magnitude (Boggs 2001). The frequency of fine grained planar laminated sediments and occasional storm signatures suggests deposition below the fair-weather wave base. The deposition of the upper Tadpatri Formation may have occurred concurrently with seismic activity.

8.1.4 GANDIKOTA FORMATION

Due to the lack of any visible contact relationships or a vertical succession of lithologies, it is not possible to determine a depositional setting for the Gandikota Formation. All that may plausibly be inferred is that during the initial stages of deposition of the Gandikota Formation, there was a large supply of sediment which was rapidly deposited in a generally high energy setting.

8.2 Geochronological framework of the lower Cuddapah Supergroup

There are several relevant published geochronological studies which can be used to constrain the timing of deposition of the Cuddapah Supergroup. The Pulivendla Sill which intrudes the lower Tadpatri Formation represents the oldest identified igneous intrusion within the sediments, and requires the both Papaghni and Chitravati Groups to have been deposited prior to 1899 ± 20 Ma (Anand *et al.* 2003). The western margin of the Cuddapah Basin is surrounded by a complex series of

widespread mafic dyke swarms, some of which terminate against the basin (Murty *et al.* 1987; Nagaraja Rao *et al.* 1987). One dyke which is directly overlain by the basin has been dated at 2366 Ma, and nearby dykes intruded the EDC around 2180 Ma (French & Heaman 2010). Therefore deposition of the sediments must post-date 2366 Ma, and may have initiated as late as post-2180 Ma.

Considering these prior age constraints for the timing of sedimentation, the $^{207}Pb/^{206}Pb$ detrital zircon ages obtained in this study do not place any further age constraints on the deposition of the Gulcheru, Vempalle or Tadpatri Formations (each sample yielded a maximum depositional age of *ca* 2500 Ma).

The *ca* 1207 Ma maximum depositional age obtained for the Gandikota Formation poses an interesting problem, as the formation is currently placed at the top of the >1900 Ma Chitravati Group. The Gandikota Formation has variably been reported as conformably (e.g. Lakshminarayana & Bhattacharjee 2000; Dasgupta *et al.* 2005; Saha & Tripathy 2011), or unconformably (e.g. Anand *et al.* 2003; Dasgupta & Biswas 2006) overlying the Tadpatri Formation, or is not mentioned in the stratigraphy of the basin at all (e.g. Meijerink *et al.* 1984; Naqvi 2005). Further confusing placement of the Gandikota Formation within the stratigraphy is the regional angular unconformity which separates the Cuddapah Supergroup and the Kurnool Group. This unconformity straddles the Gulcheru, Vempalle, Tadpatri and Gandikota formations (Kamal 1982; Saha & Tripathy 2011).

The lowermost formation of the Kurnool Group (in the north of the Cuddapah Basin) is the Banganapalle Formation, which consists of a basal conglomerate that fines up into cross-bedded sand (Kamal 1982; Ramakrishnan & Vaidyanadhan 2008). Where identified, the Banganapalle Formation unconformably overlies the Tadpatri Formation and is gradationally overlain by the Narji Limestone, and the Gandikota Formation is not present. However, the Banganapalle Formation has not been identified around the region where sample GF06 was collected, where the Gandikota Formation unconformably overlies the Tadpatri Formation, and is unconformably overlain by the Narji Limestone. This may indicate that the Gandikota Formation is a lateral equivalent of the Banganapalle Formation but lacks the basal conglomerate. Differential uplift in the west of the basin may have resulted in uplift and tilting of the Banganapalle/Gandikota Formation in the south of the basin, but

not have affected the formation in the north (*cf.* Dix & Nelson 2004). This may explain the conformable contact between the Banganapalle/Gandikota Formation in the north where the contact is unconformable in the south. Where authors have reported a gradational transition from the shale of the Tadpatri Formation to sandstone beds of the Gandikota Formation, it may be that the authors were documenting sandy beds at the top of the Tadpatri Formation. This model is speculative; confirmation or repudiation of this theory requires detailed analysis of the sedimentology and structure of the Gandikota and Banganapalle Formations and the Narji Limestone and their contact relationships.

Nevertheless, the isotopic age data presented in this study indicates that the Gandikota Formation should be re-assigned to the Kurnool Group. Previously, the best age constraint on the timing of deposition of the Kurnool Group was a lamproite which intrudes the underlying Nallamalai Group, and has been dated at 1417 ± 8.2 Ma (Chalapathi Rao *et al.* 1999). Considering the *ca* 1207 Ma zircon grain within sample GF06, the Kurnool Group must have been deposited later than *ca* 1207 Ma. This is the youngest direct maximum depositional age provided for the Kurnool Group.

8.3 Provenance of Cuddapah Supergroup sediments

In order to search for a source region for the basin sediments, both $^{207}Pb/^{206}Pb$ zircon ages and hafnium isotopes have been used to attempt to match potential sources terranes with the geochemical characteristics of zircon grains extracted from the basin sediments.

A number of considerations must be taken into account when interpreting the provenance of sediments from detrital zircon grains; a brief summary of restrictions on the use of detrital zircon isotope analysis in determining provenance is supplied in Appendix III. However, a major constraint when attempting a provenance study in the Cuddapah Basin is that provenance ascribed here is primarily dependent on which terranes have reliable geochronological constraints.

The hafnium isotope composition of zircon grains is a sensitive tracer for sediment provenance (Kinny & Maas 2003; Howard *et al.* 2009). Hafnium isotopes within zircons tend not to be affected by post-crystallisation thermal disturbances, so they provide an accurate record of whether the zircon

formed in a juvenile addition to the crust, or from reworked crust, or a combination of the two. There are no published studies in which authors present hafnium isotope data on zircon grains from the Dharwar Craton, precluding direct comparisons of hafnium composition of zircon grains from the Cuddapah Basin with possible source terranes. However, there are several studies in which authors have used whole rock Sm-Nd methods for geochronology. Lu-Hf and Sm-Nd systems tend to behave analogously, and as mantle and crustal processes do not generally result in any large-scale decoupling of the hafnium and neodymium systems, neodymium isotope data may be compared with hafnium data, with the use of a conversion factor of $\varepsilon_{HF} = 1.36\ \varepsilon_{Nd} + 2.95$ (Vervoort *et al.* 1999). All ε_{Nd} values used in comparison with obtained ε_{HF} have been processed using this equation.

8.3.1 PROVENANCE OF FORMATIONS

A combination of $^{207}Pb/^{206}Pb$ detrital zircon ages and hafnium isotope composition of zircon grains are compared here with available data from possible source regions. The ages and lithologies of all terranes mentioned and the source of these ages are outlined in Tables 1a and 1b; these tables also contain a summary of which terranes may have provided sediment to each formation.

Cuddapah Supergroup

Palaeoflow indicators in the vicinity of the sample taken from the Gulcheru Formation suggest flow from the south-east and south-west to west-south-west. Clear palaeoflow indicators were not seen within the rest of the remainder of the formations. Therefore $^{207}Pb/^{206}Pb$ detrital peaks from this study will be compared to terranes which lie to the southeast through to west of the basin.

The detrital zircon ages from the Cuddapah Supergroup show that the main source areas with high zircon fertility during the time of deposition (*ca* 2200 – 1900 Ma) were of latest NeoArchaean to earliest Palaeoproterozoic in age. The remaining populations are generally represented by one or two grains, and are likely to reflect terranes with relatively minor sediment input to the Cuddapah Supergroup. However it should be noted that these grains – and all other populations represented by a small number of grains- may represent a larger population due to the binomially distributed nature of detrital zircon datasets (Andersen 2005).

The vast majority of detrital zircon grains from the Cuddapah Supergroup yield $^{207}Pb/^{206}Pb$ ages between *ca* 2600 and 2400 Ma, and have been derived from a fairly juvenile source. The most likely sources for these zircon grains are the Dharwar Batholith, the Salem Block and various greenstone and schist belts of the EDC, given their extensive spatial distribution and location to the south and west of the basin (Table 1a, approximate location of the Salem Block is shown in Figure 1a). This is supported by the work of Chakrabarti *et al.* (2009) who cited the Dharwar Batholith and EDC schist belts as sources terranes for sediment of the Gulcheru Formation, based on provenance discrimination diagrams. Jayananda *et al.* (2000) obtained ε_{Nd} values between -7.93 and 7.0 for the Dharwar Batholith (calculated at 2540 Ma), which are in agreement with the obtained ε_{Hf} values of for 2500 Ma detritus of the Cuddapah Supergroup (-4.23 to 6.75). Several alternative possible sources are suggested in Tables 1a and 1b.

Sample GF01 from the Gulcheru Formation yielded several >2900 Ma detrital peaks which are absent in the other samples from the Cuddapah Supergroup. Some of these zircon grains may have been derived from the basement gneisses of the EDC or the volcano-sedimentary Sargur Group of the WDC (approximate location shown in Figure 1a). The ε_{Hf} values of the >3000 Ma zircon crystals (-3.49 and 1.89) are in slightly better agreement with ε_{Nd} values obtained for zircon grains of the Sargur Group (6 ± 7, calculated at 3352 Ma; Jayananda *et al.* 2008) than with those calculated for the EDC basement gneisses (-8 to -5, calculated at 2540 Ma; Jayananda *et al.* 2000). However, Jayananda *et al.* (2000) analysed only two grains, which is not sufficient evidence to discount the EDC gneisses as a possible source terrain.

Ascribing provenance to the remaining populations is problematic, due to the erratic nature of reliable geochronological constraints on older rocks in the Dharwar craton. Zircons >3200 Ma have only been reliably dated within the WDC, so in absence of any other comparisons, the oldest zircon populations identified within sample GF01 may be said to possibly have been derived from terranes of the WDC, pending further geochronological work in the Dharwar Craton.

Gandikota Formation

Given the unreliability of reports of the Gandikota Formation, and the small amount of outcropping rocks seen in the field, palaeoflow direction could not be determined with any degree of certainty. Therefore no terrain may be discounted due to spatial location. The Gandikota Formation was deposited following the proposed collision of the Krishna Province with the EDC in the *ca* 1640 Ma Krishna Orogen (Henderson 2011), and therefore may reflect sedimentation from an increased number of possible source terranes compared with the underlying rocks.

Similarly to the sediments of the Cuddapah Supergroup, the detrital zircon age spectrum is dominated by a peak at around 2500 Ma; this may have been derived from the source terranes discussed above, or from the underlying sediments. The isolated population at *ca* 2200 Ma is likely to represent sediment input from one of the *ca* 2200 Ma dyke swarms which transect the EDC around the western margin of the Cuddapah Basin.

All zircon populations younger than *ca* 2500 Ma may represent detrital input from the EGB, especially those younger than *ca* 2000 Ma, given the absence of dated terranes in the EDC bearing any similarity in age to many of the detrital populations represented in the sample from the Gandikota Formation. Recent geochronology performed on detrital zircon grains from metasedimentary rocks within the Ongole Domain has yielded a fairly continuous spread of zircons spanning the interval between *ca* 2598 and 1676 Ma. This represents a possible source for several detrital populations identified within the Gandikota Formation. The peaks between *ca* 2000 and 1600 Ma may have been derived from the three dated terranes within the EGB (Table 1a). It is also possible that zircon grains in this interval were derived from the Pulivendla Sill which intrudes the Tadpatri Formation. Zircon grains which grew as a result of metamorphism during the collision of the Krishna Province with the EDC *ca*1640 Ma (Henderson 2011) may also have formed part of the detritus contributing to the Gandikota Formation.

Several of these possible terranes have been analysed for Nd isotopic composition. The metasediments from the Ongole Domain have ε_{Hf} values between -12 and 4. The Tadpatri Sill has ε_{Nd}

values from -10 to 4 (calculated at 1900 Ma; Anand *et al.* 2003). Considering the number of grains analysed, both of these ranges are compatible with the ε_{Hf} values obtained from 2000-1600 Ma zircon grains from the Gandikota Formation, which range from -6.45 to -0.83.

The populations between 1300 and 1200 Ma may have been sourced from alkaline intrusions in the Krishna Province, or various terrains within the Eastern Ghats Province. The grains representing these populations yielded ε_{Hf} values between 2.92 and 3.52, which suggests that they formed in a relatively juvenile terrane; this may represent derivation of sediment from an active margin setting (Vervoort *et al.* 1999).

8.3.2 CHANGES IN PROVENANCE

There is a distinct difference in the age spectra yielded by the two samples from the lower Cuddapah Supergroup, despite that they share a gradational contact. The detrital zircon population from the Gulcheru Formation displays a polymodal age spectrum over a wide age range, attesting to numerous sediment sources draining into the basin. In contrast to this, the age population from the Vempalle Formation occurs over one broad peak straddling the Archaean-Proterozoic boundary, reflecting derivation from a lesser range of sources. This implies a transition from a tectonically active setting with shifting drainage patterns to a relatively quiet setting with comparatively stable fluvial systems transporting sediment from a restricted number of sources.

The detrital zircon age spectrum of the Gandikota Formation implies a major shift in provenance characteristics. Deposition subsequent to *ca* 1207 Ma appears to have included sediment input from the EGB as well as from the EDC. The polymodal age spectrum may be the result of reworking of the older Cuddapah Basin sediments along with sediment input from the EDC and EGB.

This shift from EDC-dominated sediment provenance to mixed EDC-EGB provenance is recorded in the Nallamalai Group, which sits stratigraphically between the Tadpatri Formation and the Gandikota Formation. Alexander (2011) and Gore (2011) report a mixed provenance for zircon grains of the Bairenkonda/Cumbum and Srisailam formations, respectively, where sediment is likely to have been derived from both the EGB and the EDC (Figure 18). This suggests that either the EGB only became

congruent with the EDC sometime between the deposition of the two formations (*ca* 1900 – 1660 Ma) or that some tectonic process led to alteration of the palaeoflow direction such that sediment was transported to the basin from the EGB only after 1900 Ma.

8.4 Basin Evolution

8.4.1 SEDIMENTARY EVOLUTION

Considering the very limited vertical and lateral extent of rocks seen in the field, it is implausible to attempt a robust palaeosedimentological model for the deposition of the Cuddapah Supergroup. However, the sedimentological and geochemical data presented in this study appear to suggest particular depositional settings, and the succession of these proposed environments is discussed below accordingly.

In the observed location on the western margin of the Cuddapah Basin, the basal Gulcheru Formation of the Cuddapah Supergroup appears to have been deposited sometime after 2366 Ma in a high energy fluvial environment fairly close to an uplifted area. The section through the Gulcheru Formation is likely to represent braided stream deposits that possibly formed part of an alluvial fan – or series of fans- that sourced sediment from a wide range of terranes. This terrestrial setting developed into a marginal to shallow sub-aqueous setting. This phase of basin evolution was characterised by frequent periods of sub-aerial exposure which alternated with deposition in a very shallow, then progressively deeper milieu, as evidenced by the gradual reduction of sub-aerial exposure features up-section, and appearance of large stromatolite mounds. Whether this was a lacustrine or intertidal to shallow marine setting remains ambiguous. This transition from the Gulcheru Formation to the Vempalle Formation was accompanied by a significant reduction in the energy of the depositional setting, which is reflected in both in the prolific growth of stromatolites and frequent deposition of fine grained sediment in the Vempalle Formation, and the apparently relatively stable drainage patterns supplying sediment to the basin from a reduced range of sources. The large >1500 m thickness of the Vempalle Formation implies that these conditions persisted for a significant period of time.

The unconformable transition from the Vempalle Formation to the deeper-water Tadpatri Formation represents a marine incursion on the basin, and deposition in a sub-tidal setting. Overall, the sedimentary rocks of the lower Cuddapah Supergroup appear to record a marine transgression with a gradual fining up from coarse clastics to carbonates with mixed sand, and ultimately to very fine-grained sub-tidal deposits.

The deposition of the Gandikota Formation at least 700 myr after the deposition of the Tadpatri Formation records a significant change in the depositional environment in the basin, where sediment input was rapid, and included detrital input from the EGB. Further analysis of the sedimentary rocks of the Gandikota Formation will be required to evaluate the depositional setting in the Cuddapah Basin post-1207 Ma.

8.4.2 TECTONIC IMPLICATIONS

Erosional base level falls may result in very thin braidplain or alluvial fan deposits, however these are unlikely to survive in Precambrian strata (Köykkä 2011). As a corollary of this, it is likely that the Gulcheru Formation– which reaches a maximum thickness of *ca* 250 m- was deposited as a result of a tectonic base level fall. This may conceivably have been the result of extensional tectonics; the presence of an extensive mafic dyke swarm which was emplaced into the EDC *ca* 2200 Ma has been interpreted as the result of intracontinental rifting (French & Heaman 2010), and several authors have cited re-activation of pre-existing basin-margin faults during rifting as a mechanism for basin initiation (e.g. Kaila & Tewari 1985; Chatterjee & Bhattacharji 2001). The data presented in this study appear to support a rift-basin model, where the basal Gulcheru Formation likely to have been deposited in an active setting close to an uplifted area. Whilst this may occur in a foreland or rift basin, palaeocurrent and provenance data strongly imply sediment transport from the southeast and southwest, both of which are located in the basin's foreland.

The transition from the fluvial-dominated setting of the Gulcheru Formation to a large (>1500 m) thickness of low energy carbonate deposits in the Vempalle Formation is likely to represent a change in the tectonic controls on basin evolution. The consistently shallow sub-aqueous to sub-aerially

exposed nature of the deposits indicates that the rate of subsidence was approximately in equilibrium with the rate of deposition for an extended period of time. This suggests either rapid sediment accumulation or a very slow reduction in base level. If the latter is the case, then the Vempalle Formation may represent deposition during thermal recovery and a passive extensional phase of basin development following the initial rifting phase.

The vertically extensive marine deposits of the Tadpatri Formation are likely to indicate the development of an open seaway. This implies further subsidence, and possibly an increased rate of subsidence, given that the rate of subsidence must have overtaken the rate of sedimentation. The suggestion of a protracted period of passive extension is supported by the work of French *et al.* (2008) and Anand *et al.* (2003) who propose that the sills which have intruded the Tadpatri Formation are the result of a prolonged passive extensional regime following intracratonic rifting.

The initiation of sediment input from the EGB following the accretion of the EGB onto the EDC in the *ca* 1640 Ma Krishna Orogen reflects a reversal of the initial extensional regime. The appearance of a significant EGB signature in the sedimentary rocks of the Nallamalai Group indicates that sediment was entering the basin from the eastwardly-adjacent EGB. If the palaeoflow directions and sediment provenance ascribed to the Papaghni and Chitravati Group rocks in this study are applicable basin-wide, this implies a major shift in the prevailing drainage patterns and the overall tectonic setting.

Compressional tectonics may have dominated the evolution of the basin for a significant time period, given that both the Nallamalai Group (deposited between 1660 and 1417 Ma) and the Gandikota Formation (deposited after 1207 Ma) both contain significant detrital input from the EGB. This is supported by the apparent increase in sediment input from the EGB relative to the EDC between the deposition of the Nallamalai Group and the Gandikota Formation, which implies increased relative palaeoflow from the east (hinterland) rather than the west (foreland).

8.5 Correlation with Purana basins

It is clear from the data summarised in Figure 2 that the Cuddapah Basin is unlikely to have formed contemporaneously with any of the other Purana Basins; excepting the Cuddapah Basin, the oldest basin with reliable depositional age constraints is the Vindhyan Basin. The Vindhyan Basin was deposited after 1854 ± 7 Ma (Deb *et al.* 2002), and the deposition of the Papaghni and Chitravati groups had already ceased by this time.

The palaeoenvironmental interpretations presented in this study support the model of basin initiation originally proposed by Sundaram *et al.* (1964), where the Purana basins developed along pre-existing areas of crustal weakness during intracontinental rifting. However, the significant difference in timing of basin initiation between the Cuddapah Basin and the other Purana basins requires several episodes of intracontinental rifting rather than one large-scale extensional event, if this model is to be applicable to each of the Purana basins.

9 CONCLUSIONS

Sedimentary successions within the Cuddapah Supergroup and Kurnool Group record a history of Palaeo- to Mesoproterozoic phases of extension and compression in the Cuddapah Basin. The following conclusions may be made from the study of these successions presented here:

1) In the logged section near Parnapalle, the basal Gulcheru Formation was deposited in a fluvial setting which was close but not immediately adjacent to a region of uplift. Palaeoflow was dominantly from the south-east and south-west, and sediment was sourced from the inland Dharwar Craton, which may reflect deposition in an extensional setting.

2) The overlying Vempalle Formation represents a transition to a long-lasting passive extensional regime, where the rate of sedimentation was in accord with the rate of subsidence for an extended period of time. The Tadpatri Formation reflects a continuation of the passive

extensional regime, but the appearance of deeper-water sedimentary rocks implies that rate of subsidence increased relative to the rate of sedimentation.

3) The depositional setting of the Vempalle Formation is equivocal; sedimentary features seen within the formation are not diagnostic of deposition in either a shallow marine or lacustrine setting, although the persistent presence of desiccation features is more indicative of a lacustrine deposit. The formation has been pervasively dolomitised and the $\delta^{18}O$ values are therefore more likely to reflect the isotopic composition of dolomitising fluids than the primary isotopic composition of the carbonates. If the $\delta^{13}C$ values have not been altered and the Vempalle Formation was deposited in an open shallow marine setting, then the deposition of the formation may be correlated with the termination of the 'Lomagundi' positive $\delta^{13}C$ excursion around 2100 Ma.

4) The Gandikota Formation, which was previously placed at the top of the Chitravati Group, must have been deposited after *ca* 1207 Ma, and is likely to be a lateral equivalent of the basal Banganapalle Formation of the Kurnool Group. The deposition of the Gandikota Formation also records a shift in provenance characteristics relative to the Gulcheru and Vempalle Formations; the latter two formations sourced sediment from the Dharwar Craton, but the Gandikota Formation received sediment from both the Dharwar Craton and the Eastern Ghats Belt. This reflects the reversal of the initial extensional setting in the basin following the Krishna Orogen *ca* 1640 Ma.

5) The data and interpretations presented in this study do not support a foreland basin origin for the Cuddapah Basin, as proposed by various authors. This model conflicts with both the age constraints on timing of deposition compared with the onset of the Krishna Orogen, and the palaeoflow and provenance data obtained in this study, which do not reflect any sediment input from the EGB until after the deposition of the Papaghni and Chitravati groups. Whilst the progradation of the EGB onto the EDC may have resulted in basin subsidence following the Krishna Orogen, several kilometres of sediment had already been deposited in the basin

before this time, and the combination of mafic intrusions into the sediments and the inferred palaeoenvironments are indicative of basin initiation in an extensional setting.

6) Whilst work presented in this study indicates that the Cuddapah Basin may plausibly have developed in a pre-existing area of crustal weakness during intracontinental rifting, the temporal disparity between the initiation of the Cuddapah Basin and the other Purana basins requires several episodes of intracontinental rifting if the linking mechanism of Sundaram *et al.* (1964) is to be valid.

9.1 Further work

Confirmation (or otherwise) of the 'alluvial fan' interpretation proposed in this study for the Gulcheru Formation requires a detailed, laterally and vertically extensive sedimentological study of the formation. In order to provide support for either a marine or lacustrine setting for the deposition of the Vempalle Formation, the transition from the Gulcheru Formation to the Vempalle Formation should be carefully detailed, and a thorough, high resolution geochemical investigation of the dolomites may be undertaken, along with analysis of fluid inclusions, trace element composition and diagenetic textures within the dolomites. A detailed sedimentological and structural study of the Gandikota and Banganapalle formations and their upper and lower contacts would help confirm the place of the Gandikota Formation within the stratigraphy of the Cuddapah Basin. The initiation of sedimentation in the basin may be more tightly constrained by dating of the felsic volcanic rocks which cap the Vempalle Formation.

10 ACKNOWLEDGEMENTS

Firstly I would like to thank my primary supervisor Alan Collins for all of his help in the field, and guidance throughout the year, and especially for introducing me to the deliciousness-in-a-cup which is Indian chai. Many thanks also to my secondary supervisor Martin Kennedy for encouraging me to think outside the square (read: sea) and for his assistance with all things sedimentary. I would like to acknowledge that this project was made possible by a research grant from the Australia-India

Strategic Research Fund; on that note I would like to extend many thanks to Sarbani Patranabis-Deb, Debapriya Chatterjee and Pratap Dhang from the Indian Statistical Institute for their company and assistance in the field and for providing Ryan and I with an ample supply of lunchtime bananas. Huge thanks to (almost) Dr.Katie Howard (B.Sc [Zircon Wizardry]) for happily sharing her exhaustive knowledge of detrital zircon geochronology as well as dispensing many general thesis-writing hints. The help and guidance provided by Angus Netting, Ben Wade, Ken Neubauer and Justin Payne in the various aspects of detrital zircon analysis is gratefully acknowledged. To Emma and Bonnie: thanks for being excellent field buddies and for sharing my enthusiasm for the devouring of curries and the purchasing of saris. And special thanks to Ryan for being a spectacularly fantastic field servant despite the occasional danger of rocks to the head and/or finger and/or monkey to the leg. Finally, thanks to my family for help and support through the year, and to Mab for emotional support through many cuddles and lots of purring.

11 REFERENCES

ACHARYYA S. K. 2003. The nature of Mesoproterozoic Central Indian Tectonic Zone with exhumed and reworked older granulites. *Gondwana Research* **6**, 197-214.

ACHARYYA S. K. & ROY A. 2000. Tectonothermal history of the Central Indian Tectonic Zone and reactivation of major faults/shear zones. *Journal of the Geological Society of India* **55**, 239-256.

AFTALION M., BOWES D. R., DASH B. & DEMPSTER T. J. 1988. Late Proterozoic charnockites in Orissa, India: U-Pb and Rb-Sr isotopic study. *Journal of Geology* **96**, 663-676.

AHMAD M. 2011. Enclaves in Granitoids of North of Jonnagiri Schist Belt, Kurnool District, Andhra Pradesh: Evidence of Magma Mixing and Mingling. *Journal of the Geological Society of India* **77**, 557-573.

ALEXANDER E. 2011. A geochronological and structural analysis of the Nallamalai Fold Belt, S. E. India. The University of Adelaide (unpubl.).

ANAND M., GIBSON S. A., SUBBARAO K. V., KELLEY S. P. & DICKIN A. P. 2003. Early Proterozoic melt generation processes beneath the intra-cratonic Cuddapah Basin, southern India. *Journal of Petrology* **44**, 2139-2171.

ANAND R. & BALAKRISHNAN S. 2010. Pb, Sr and Nd isotope systematics of metavolcanic rocks of the Hutti greenstone belt, Eastern Dharwar craton: Constraints on age, duration of volcanism and evolution of mantle sources during Late Archaean. *Journal of Asian Earth Sciences* **39**, 1-11.

ANAND R. & BALAKRISHNAN S. 2011. Geochemical and Sm-Nd isotopic study of titanite from granitoid rocks of the eastern Dharwar craton, southern India. *Journal of Earth System Science* **120**, 237-251.

ANDERSEN T. 2005. Detrital zircons as tracers of sedimentary provenance: limiting conditions from statistics and numerical simulation. *Chemical Geology* **216**, 249-270.

AZERÊDO A. C., SILVA R. L., DUARTE L. V. & CABRAL M. C. 2010. Subtidal stromatolites from the Sinemurian of the Lusitanian Basin (Portugal). *Facies* **56**, 211-230.

BALAKRISHNAN S., RAJAMANI V. & HANSON G. N. 1999. U-Pb ages for zircon and titanite from the Ramagiri area, southern India: Evidence for accretionary origin of the eastern Dharwar craton during the late Archaean. *Journal of Geology* **107**, 69-86.

BANNER J. L. & HANSON G. N. 1990. Calculation of simultaneous isotopic and trace element variations during water-rock interaction with applications to carbonate diagenesis. *Geochimica Et Cosmochimica Acta* **54**, 3123-3137.

BEKKER A., KARHU J. A., ERIKKSSON K. A. & KAUFMAN A. J. 2003. Chemostratigraphy of Paleoproterozoic carbonate successions of the Wyoming Craton: tectonic forcing of biogeochemical change? *Precambrian Research* **120**, 279-325.

BEKKER A., KARHU J. A. & KAUFMAN A. J. 2006. Carbon isotope record for the onset of the Lomagundi carbon isotope excursion in the Great Lakes area, North America. *Precambrian Research* **148**, 145-180.

BEKKER A., KAUFMAN A. J., KARHU J. A., BEUKES N. J., SWART Q. D., COETZEE L. L. & ERIKKSSON K. A. 2001. Chemostratigraphy of the Paleoproterozoic Duitschland Formation, South Africa: Implications for coupled climate change and carbon cycling. *American Journal of Science* **301**, 261-285.

BOGGS S. 2001. *Principles of Sedimentology and Stratigraphy* (Third edition). Prentice Hall, New Jersey.

BOSE P. K., SARKAR S., MUKHOPADHYAY S., SAHA B. & ERIKKSSON P. 2008. Precambrian basin-margin fan deposits: Mesoproterozoic Bagalkot Group, India. *Precambrian Research* **162**, 264-283.

BRAND U. & VEIZER J. 1981. Chemical diagenesis of a multicomponent carbonate system 2: Stable isotopes. *Journal of Sedimentary Petrology* **51**, 987-997.

CHADWICK B., VASUDEV V. N. & HEGDE G. V. 1997. The Dharwar craton, southern India, and its Late Archaean plate tectonic setting: current interpretations and controversies. *Proceedings of the Indian Academy of Sciences-Earth and Planetary Sciences* **106**, 249-258.

CHADWICK B., VASUDEV V. N. & HEGDE G. V. 2000. The Dharwar craton, southern India, interpreted as the result of Late Archaean oblique convergence. *Precambrian Research* **99**, 91-111.

CHAKRABARTI G., SHOME D., BAULUZ B. & SINHA S. 2009. Provenance and weathering history of Mesoproterozoic clastic sedimentary rocks from the basal Gulcheru Formation, Cuddapah Basin. *Journal of the Geological Society of India* **74**, 119-130.

CHAKRABORTY C. 2006. Proterozoic intracontinental basin: The Vindhyan example. *Journal of Earth System Science* **115**, 3-22.

CHAKRABORTY P. P., DEY S. & MOHANTY S. P. 2010. Proterozoic platform sequences of Peninsular India: Implications towards basin evolution and supercontinent assembly. *Journal of Asian Earth Sciences* **39**, 589-607.

CHALAPATHI RAO N. V., MILLER J. A., GIBSON S. A., PYLE D. M. & MADHAVAN V. 1999. Precise ^{40}Ar-^{39}Ar age determinations of the Kotakonda kimberlite and Chelima lamproite, India: implication to the timing of mafic dyke swarm emplacement in the Eastern Dharwar Craton. *Journal of the Geological Society of India* **53**, 425-432.

CHATTERJEE N. & BHATTACHARJI S. 2001. Petrology, geochemistry and tectonic settings of the mafic dykes and sills associated with the evolution of the Proterozoic Cuddapah basin of south India. *Earth and Planetary Sciences* **110**, 433-453.

CHAUDHURI A. K. & HOWARD J. D. 1985. Ramgundam Sandstone: A Middle-Proterozoic shoal bar sequence. *Journal of Sedimentary Petrology* **55**, 392-397.

CHAUDHURI A. K., MUKHOPADHYAY J., PATRANABIS-DEB S. & CHANDA S. K. 1999. The Neoproterozoic Cratonic Successions of Peninsular India. *Gondwana Research* **2**, 213-225.

CHAUDHURI A. K., SAHA D., DEB G. K., DEB S. P., MUKHERJEE M. K. & GHOSH G. 2002. The Purana basins of southern cratonic province of India - A case for mesoproterozoic fossil rifts. *Gondwana Research* **5**, 23-33.

CLARK C., COLLINS A. S., TIMMS N. E., KINNY P. D., CHETTY T. R. K. & SANTOSH M. 2009. SHRIMP U-Pb age constraints on magmatism and high-grade metamorphism in the Salem Block, southern India. *Gondwana Research* **16**, 27-36.

CONRAD J. E., HEIN J. R., CHAUDHURI A. K., PATRANABIS-DEB S., MUKHOPADHYAY J., KUMAR DEB G. & BEUKES N. J. 2011. Constraints on the development of Proterozoic basins in central India from $^{40}Ar/^{39}Ar$ analysis of authigenic glauconitic minerals. *Geological Society of America Bulletin* **123**, 158-167.

CRAWFORD A. R. & COMPSTON W. 1973. The age of the Cuddapah and Kurnool systems, southern India. *Journal of the Geological Society of Australia* **19**, 453-464.

CROWE W. A. 2003. Age constraints for magmatism and deformation in the northern Eastern Ghats Belt, India: tectonic implications for the development of East Gondwanaland. *Precambrian Research* **in press**.

DAS K., YOKOYAMA K., CHAKRABORTY P. P. & SARKAR A. 2009. Basal tuffs and Contemporaneity of the Chattisgarh and Khariar Basins Based on New Dates and Geochemistry. *The Journal of Geology* **117**, 88-102.

DASGUPTA P. K. & BISWAS A. 2006. *Rhythms In Proterozoic Sedimentation: An Example From Peninsular India*. Satish Serial Publishing House, Delhi.

DASGUPTA P. K., BISWAS A. & MUKHERJEE R. 2005. Cyclicity in Paleoproterozoic to Neoproterozoic Cuddapah Supergroup and its significance in basinal evolution. *In:* Mabesoone J. M. & Neumann V. H. eds., *Cyclic Development of Sedimentary Basins*, Elsevier.

DAVIES N. S. & GIBLING M. R. 2010. Cambrian to Devonian evolution of alluvial systems: The sedimentological impact of the earliest land plants. *Earth-Science Reviews* **98**, 171-200.

DEB M., THORPE R. & KRSTIC D. 2002. Hindoli Group of Rocks in the Eastern Fringe of the Aravalli-Delhi Orogenic Belt-Archaean Secondary Greenstone Belt of Proterozoic Supracrustals? *Gondwana Research (Gondwana Newsletter Section)* **5**, 879-883.

DEB S. P. 2004. Lithostratigraphy of the Neoproterozoic Chattisgarh Sequence and its bearing on the tectonics and palaeogeography. *Gondwana Research* **7**, 323-337.

DHOUNDIAL D. P. 1987. Purana Basins of Peninsular India. *In:* Radhakrishna B. P. ed., *Purana Basins of Peninsular India (Middle to Late Proterozoic)*, Geological Society of India, Bangalore.

DIX G. R. & NELSON C. S. 2004. The role of tectonism in sequence development and facies distribution of Upper Oligocene cool-water carbonates: Coromandel Peninsula, New Zealand. *Sedimentology* **51**, 231-251.

DOBMEIER C. J. & RAITH M. M. 2003. Crustal architecture and evolution of the Eastern Ghats Belt and adjacent regions of India. *In:* Yoshida M., Windley B. F. & Dasgupta S. eds., *Proterozoic East Gondwana: Supercontinent Assembly and Breakup*, Vol. 206, pp 145-169, The Geological Society of London, London.

EVANS D. A. D. & MITCHELL R. N. 2011. Assembly and breakup of the core of Paleoproterozoic-Mesoproterozoic supercontinent Nuna. *Geology* **39**, 443-446.

FRAUENSTEIN F., VEIZER J., BEUKES N. J., VAN NIEKERK H. S. & COETZEE L. L. 2009. Transvaal Supergroup carbonates: Implications for Paleoproterozoic $\delta^{18}O$ and $\delta^{13}C$ records. *Precambrian Research* **175**, 149-160.

FRENCH J. E. & HEAMAN L. M. 2010. Precise U-Pb dating of Paleoproterozoic mafic dyke swarms of the Dharwar craton, India: Implications for the existence of the Neoarchaean supercraton Sclavia. *Precambrian Research* **183**, 416-441.

FRENCH J. E., HEAMAN L. M., CHACKO T. & RIVARD B. 2004. Global mafic magmatism and continental breakup at 2.2 Ga.: evidence from the Dharwar craton, India. *Geological Society of America Annual Meeting, Program Abstracts 36*, 340.

FRENCH J. E., HEAMAN L. M., CHACKO T. & SRIVASTAVA R. K. 2008. 1891-1883 Ma Southern Bastar-Cuddapah mafic igneous events, India: A newly recognized large igneous province. *Precambrian Research* **160**, 308-322.

FRIEND C. R. L. & NUTMAN A. P. 1991. SHRIMP U-Pb Geochronology of the Closepet Granite and Peninsular Gneiss, Karnataka, South India. *Journal of the Geological Society of India* **38**, 357-368.

GORE R. 2011. Geochronological and sedimentological constraints of the Srisailam Formation, S. E. India. The University of Adelaide (unpubl.).

GSI 1981. *Geological and Mineral Map of the Cuddapah Basin* (2nd edition). Geological Survey of India, Calcutta.

HALLS H. C., KUMAR A., SRINIVASAN R. & HAMILTON M. A. 2007. Paleomagnetism and U/Pb geochronology of easterly trending dykes in the Dharwar Craton, India; feldspar clouding, radiating dyke swarms and the position of India at 2.37 Ga. *Precambrian Research* **155**, 47-68.

HARDIE L. A. 1987. Dolomitization; a critical view of some current views. *Journal of Sedimentary Petrology* **57**, 166-183.

HAY D. C. & DEMPSTER T. J. 2009. Zircon alteration, formation and preservation in sandstones. *Sedimentology* **56**, 2175-2191.

HENDERSON B. 2011. The tectonic evolution of the Ongole Domain, India: A geochronological and metamorphic approach. The University of Adelaide (unpubl.).

HOLM D. K., VAN SCHMUS W. R., MACNEILL L. C., MBOERBOOM T. J., SCHWEITZER D. & SCHNEIDER D. A. 2005. U-Pb geochronology of Paleoproterozoic plutons from the northern midcontinent, USA: evidence for subduction flip and continued convergence after geon 18 Penokean orogenesis. *Geological Society of America Bulletin* **117**, 259-275.

HOU G. T., SANTOSH M., QIAN X. L., LISTER G. S. & LI J. H. 2008. Configuration of the Late Paleoproterozoic supercontinent Columbia: Insights from radiating mafic dyke swarms. *Gondwana Research* **14**, 395-409.

HOWARD K. E., HAND M., BAROVICH K. A., REID A., WADE B. P. & BELOUSOVA E. 2009. Detrital zircon ages: Improving interpretation via Nd and Hf isotopic data. *Chemical Geology* **262**, 277-292.

JAFFRÉS J. B. D., SHIELDS G. & WALLMAN K. 2007. The oxygen isotope evolution of seawater: A critical review of a long-standing controversy and an improved geological water cycle model for the past 3.4 billion years. *Earth-Science Reviews* **83**, 83-122.

JAYANANDA M., KANO T., PEUCAT J. & CHANNABASAPPA S. 2008. 3.35 Ga komatiite volcanism in the western Dharwar craton, southern India: constraints from Nd isotopes and whole-rock geochemistry. *Precambrian Research* **162**, 160-179.

JAYANANDA M., MIYAZAKI T., GIREESH R. V., MAHESHA N. & KANO T. 2009. Synplutonic dykes from Late Archaean Granitoids in the Eastern Dharwar Craton, Southern India. *Journal of the Geological Society of India* **73**, 117-130.

JAYANANDA M., MOYEN J.-F., MARTIN H., PEUCAT J., AUVRAY B. & MAHABALESWAR B. 2000. Late Archaean (2550-2520 Ma) juvenile magmatism in the Eastern Dharwar craton, southern India: constraints from geochronology, Nd-Sr isotopes and whole rock geochemistry. *Precambrian Research* **99**, 225-254.

KAILA K. L. & TEWARI H. C. 1985. Structural trends in the Cuddapah Basin from deep seismic soundings (DSS) and their tectonic implications. *Tectonophysics* **115**, 69-86.

KAILA K. L., TEWARI H. C., CHOWDHURY K. R., RAO V. K., SRIDHAR A. R. & MALL D. M. 1987. Crustal structure of the northern part of the Proterozoic Cuddapah basin of India from deep seismic soundings and gravity data. *140*, 1-12.

KAILASAM L. N. 1976. Geophysical studies of major sedimentary basins of the Indian Craton, their deep structural features and evolution. *Tectonophysics* **36**, 225-245.

KALE V. S. & PHANSALKAR V. G. 1991. Peninsular basins of peninsular India: a review. *Basin Research* **3**, 1-36.

KALPANA G., MADHAVI T., PATIL D. J., DAYAL A. M. & RAJU S. V. 2010. Light gaseous hydrocarbon anomalies in the near surface soils of Proterozoic Cuddapah Basin: Implications for hydrocarbon prospects. *Journal of Petroleum Science and Engineering* **73**, 161-170.

KAMAL M. 1982. Intraformational conglomerate of the Banganapalle Formation, Kurnool Group. *Current Science (Bangalore)* **51**, 196.

KING M. 1872. Kadaph and Karnul formations in the Madras Presidency. *Memoirs of the Geological Survey of India* **8**.

KINNY P. D. & MAAS R. 2003. Lu-Hf and Sm-Nd isotope systems in zircon. *In:* Hanchar J. M. & Hoskin P. W. O. eds., *Zircon*, Vol. 53, pp 327-341, Reviews in Mineralogy and Geochemistry.

KNAUTH L. P. & KENNEDY M. J. 2009. The late Precambrian greening of the Earth. *Nature* **460**, 728-732.

KOVACH V. P., SIMMAT R., RICKERS K., BEREZHNAYA N. G., SALNIKOVA E. B., DOBMEIER C. J., RAITH M. M., YAKOVLEVA S. Z. & KOTOV A. B. 2001. The Western Charnockite Zone of the Eastern Ghats Belt, India - An Independent Crustal Province of Late Archaean (2.8 Ga) and Palaeoproterozoic (1.7-1.6 Ga) Terrains. *Gondwana Research* **4**, 666-667.

KÖYKKÄ J. 2011. Precambrian alluvial fan and braidplain sedimentation patterns: Example from the Mesoproterozoic Rjukan Rift Basin, southern Norway. *Sedimentary Geology* **234**, 89-108.

KROGSTAD E. J., HANSON G. N. & RAJAMANI V. 1991. U-Pb ages of zircon and sphene for two gneiss terrances adjacent to the Kolar Schist Belt, South India: Evidence for separate crustal evolution histories. *The Journal of Geology* **99**, 801-815.

KROGSTAD E. J., HANSON G. N. & RAJAMANI V. 1995. Sources of continental magmatism adjacent to the late Archaean Kolar suture zone, South India; distinct isotopic and elemental signatures of two late Archaean magmatic series. *Contributions to Mineralogy and Petrology* **122**, 159-173.

KULKARNI K. G. & BORKAR V. D. 2002. Trace fossils and pseudofossils from the Proterozoic Cuddapah Supergroup. *Journal of the Geological Society of India* **59**, 531-536.

LAKSHMINARAYANA G. & BHATTACHARJEE S. 2000. Shallow marine siliciclastic sedimentation in the middle proterozoic Gandikota Formation, Cuddapah Basin, Andhra Pradesh. *Journal of the Geological Society of India* **55**, 65-76.

LAND L. S. 1980. The isotopic and trace element geochemistry of dolomite: the state of the art. *In:* Zenger D. H., Dunham J. B. & Ethington L. eds., *Concepts and models of dolomitization*, Vol. 28, pp 87-110, SEPM Special Publication.

LAND L. S. 1985. The origin of massive dolomite. *Journal of Geological Education* **33**, 112-125.

LINDSAY J. F. & BRASIER M. D. 2002. Did global tectonics drive early biosphere evolution? Carbon isotope record from 2.6 to 1.9 Ga carbonates of Western Australian basins. *Precambrian Research* **114**, 1-34.

LU S., ZHAO G., WANG H. & HAO G. 2008. Precambrian metamorphic basement and sedimentary cover of the North China Craton: A review. *Precambrian Research* **160**, 77-93.

LUDWIG K. R. 2003. Isoplot/Ex, rev. 3.00: a geochronological toolkit for Microsoft Excel. *Berkeley Geochronology Centre Special Publication 4*, 71.

MACKINTOSH J. 2010. Age and Basin Evolution of the Cuddapah Supergroup, India. The University of Adelaide (unpubl.).

MAHESHWARI A., SIAL A. N., GAUCHER C., BOSSI J., BEKKER A., FERREIRA V. P. & ROMANO A. W. 2010. Global nature of the Paleoproterozoic Lomagundi carbon isotope excursion: A review of occurences in Brazil, India and Uruguay. *Precambrian Research* **182**, 274-299.

MAHESHWARI A., SIAL A. N., GUHEY R. & FERREIRA V. P. 2005. C-isotope Composition of Carbonates from Indravati Basin, India: Implications for Regional Stratigraphic Correlation. *Gondwana Research* **8**, 603-610.

MALL D. M., REDDY P. R. & MOONEY W. D. 2008. Collision tectonics of the Central Indian Suture zone as inferred from a deep seismic sounding study. *Tectonophysics* **460**, 116-123.

MANIKYAMBA C., KERRICH R., GONZALEZ-ALVAREZ I., MATHUR R. & KHANNA T. C. 2008. Geochemistry of Paleoproterozoic black shales from the Intracontinental Cuddapah basin, India: implications for provenance, tectonic setting, and weathering intensity. *Precambrian Research* **162**, 424-440.

MAYER B. & SCHWARK L. 1999. A 15,000-year stable isotope record from sediments of Lake Steisslingen, Southwest Germany. *Chemical Geology* **161**, 315-337.

MAZUMDER R., BOSE P. K. & SARKAR S. 2000. A commentary on the tectono-sedimentary record of the pre-2.0 Ga continental growth of India vis-a-vis a possible pre-Gondwana Afro-Indian supercontinent. *Journal of African Earth Sciences* **30**, 201-217.

MEERT J. G., PANDIT M. K., PRADHAN V. R., BANKS J., SIRIANNI R., STROUD M., NEWSTEAD B. & GIFFORD J. 2010. Precambrian crustal evolution of Peninsular India: A 3.0 billion year odyssey. *Journal of Asian Earth Sciences* **39**, 483-515.

MEIJERINK A. M. J., RAO D. P. & RUPKE J. 1984. Stratigraphic and structural development of the Precambrian Cuddapah Basin, SE India. *Precambrian Research* **26**, 57-&.

MELEZHIK V., HUHMA H., CONDON D. J., FALLICK A. E. & WHITEHOUSE M. J. 2007. Temporal constraints on the Paleoproterozoic Lomagundi-Jatuli carbon istotopic event. *Geology* **35**, 655-658.

MIALL A. D. 1977. A review of the Braided-River Deposition Environment. *Earth-Science Reviews* **13**, 1-62.

MIALL A. D. 1985. Architectural-Element Analysis: A New Methof of Facies Analysis Applied to Fluvial Deposits. *Earth-Science Reviews* **22**, 261-308.

MIALL A. D. 1992. Alluvial Deposits. *In:* Walker R. G. & James N. P. eds., *Facies Models: Reponse to sea level change*, Geological Association of Canada.

MISHRA D. C. 2011. Long hiatus in Proterozoic Sedimentation in India: Vindhyan, Cuddapah and Pakhal Basins - A Plate Tectonic Model. *Journal of the Geological Society of India* **77**, 17-25.

MISHRA D. C. & PRAJAPATI S. K. 2003. A plausible model for evolution of schist belts and granite plutons of Dharwar Craton, India and Madagascar during 3.0-2.5 Ga: Insight from gravity modelling constrained in part from seismic studies. *Gondwana Research* **6**, 501-512.

MOHANTY S. 2011. Palaeoproterozoic assembly of the Napier Complex, Southern India and Western Australia: Implications for the evolution of the Cuddapah Basin. *Gondwana Research* **20**, 344-361.

MONDAL M. E. A. 2009. Was Bundelkhand-Aravalli nucleus part of Ur supercontinent? *Current Science* **96**, 33-35.

MORROW D. W. 1982. Diagenesis 2; Dolomite: Part 2. Dolomitization models and ancient dolostones. *Geosciences Canada* **9**, 95-107.

MURTY T. V. 1968. Eparchaean unconformity and Archaean-Purana boundary. *Current Science (Bangalore)* **37**, 186.

MURTY Y. G. K., BABU RAO V., GUPTASARMA D., RAO J. M., RAO M. N. & BHATTACHARJI S. 1987. Tectonic, petrochemical and geophysical studies of mafic dyke swarms around the Proterozoic Cuddapah basin, South India. *In:* Halls H. C. & Fahrig W. F. eds., *Mafic Dyke Swarms. Geological Association of Canada Special Paper*, Vol. 34, pp 303-316.

NAGARAJA RAO B. K., RAJAUKAR S. T., RAMALINGASWAMY G. & RAVINDRA BABU B. 1987. Stratigraphy, structure and evolution of the Cuddapah Basin. *Memoirs of the Geological Society of India* **6**.

NAGARAJAN R., MADHAVARAJU J., ARMSTRONG-ALTRIN J. S. & NAGENDRA R. 2011. Geochemistry of Neoproterozoic limestones of the Shahabad Formation, Bhima Basin, Karnataka, southern India. *Geosciences Journal* **15**, 9-25.

NAHA K., SRINIVASAN R. & JAYARAM S. 1991. Sedimentological, structural and migmatitic history of the Archaean Dharwar tectonic province, southern India. *Proceedings of the Indian Academy of Sciences (Earth and Planetary Science)* **100**, 413-433.

NAQVI S. M. 2005. *Geology and Evolution of the Indian Plate*. Capital Publishing Company, New Delhi.

NAQVI S. M. & ROGERS J. W. 1987. *Precambrian Geology of India*. Clarendon-Oxford University Press, New York.

NUTMAN A. P., CHADWICK B., RAO B. K. & VASUDEV V. N. 1996. SHRIMP U/Pb zircon ages of acid volcanic rocks in the Chitradurga and Sandur groups, and granites adjacent to the Sandur schist belt, Karnataka. *Journal of the Geological Society of India* **47**, 153-164.

NUTMAN A. P. & EHLERS K. 1998. Evidence for multiple Palaeoproterozoic thermal events and magmatism adjacent to the Broken Hill Pb-Zn-Ag orebody, Australia. *Precambrian Research* **90**, 203-238.

PATRANABIS-DEB S., BICKFORD M. E., HILL B., CHAUDHURI A. K. & BASU A. 2007. SHRIMP Ages of Zircon in the Uppermost Tuff in Chattisgarh Basin in Central India Require ~500-Ma Adjustment in Indian Proterozoic Stratigraphy. *The Journal of Geology* **115**, 407-415.

PAUL D. K., BARMAN T., MCNAUGHTON N. J., FLECTHER I. R., POTTS P. J., RAMKRISHNAN M. & AUGUSTINE P. F. 1990. Archaean Proterozoic evolution of Indian charnockites - isotope and geochemical evidence from granulites of the Eastern Ghat belt. *Journal of Geology* **98**, 253-263.

PITCHAMUTHU C. S. & SRINIVASAM R. 1984. The Dharwar Craton. Perspective Report Series 7. *Indian National Science Academy*, 3-34.

PRADHAN V. R., MEERT J. G., PANDIT M. K., KAMENOV G., GREGORY L. C. & MALONE S. 2010. India's changin place in global Proterozoic reconstructions: new geochronologic constraints on key paleomagnetic poles from the Dharwar and Aravalli/Bundelkhand Cratons. *Journal of Geodynamics*.

PROTHERO D. R. & SCHWAB F. 1996. *Sedimentary Geology*. W. H. Freeman and Company, New York.

RADHAKRISHNA B. P. & NAQVI S. M. 1986. Precambrian continental crust of India and its evolution *Journal of Geology* **94**, 145-166.

RAHA P. K. 1987. Stromatolites and Correlation of the Purana (Middle to Late Proterozoic) Basins of Peninsular of India. *In:* Radhakrishna B. P. ed., *Purana Basins of Peninsular India*, Geological Society of India, Bangalore.

RAMAKRISHNAN M. & VAIDYANADHAN R. 2008. *Geology of India* (Vol. 1). Geological Society of India, Bangalore.

RAO G. N. 2000. Sedimentation, stratigraphy and petroleum potential of Krishna-Godavari basin, East Coast of India. *AAPG Bulletin* **85**, 1623-1643.

RAO Y. J. B., NAHA K., SRINIVASAN R. & GOPALAN K. 1991. Geology, geochemistry and geochronology of the Archaean Peninsular Gneiss around Gorur, Hassan District, Karnataka, India. *Indian Academy of Science (Earth and Planetary Sciences) Proceedings* **100**, 399-412.

RAVIKANT V. 2010. Palaeoproterozoic (~ 1.9 Ga) extension and breakup along the eastern margin of the Eastern Dharwar Craton, SE India: New Sm-Nd isochron age constraints from anorogenic mafic magmatism in the NeoArchaean Nellore greenstone belt. *Journal of Asian Earth Sciences* **37**, 67-81.

RAY J. S., MARTIN M. W., VEIZER J. & BOWRING S. A. 2002. U-Pb zircon dating and Sr isotope systematics of the Vindhyan Supergroup, India. *Geology* **30**, 131-134.

READING H. G. (Editor) 1996. *Sedimentary Envrironments: Processes, Facies and Stratigraphy* (Third edition). Blackwell Publishing, Oxford.

ROGERS A. J., KOLB J., MEYER F. M. & ARMSTRONG R. A. 2007. Tectono-magmatic evolution of Hutti-Maski greenstone belt, India: constrained using geochemical and geochronological data. *Journal of Asian Earth Sciences* **31**, 55-70.

SAHA D. 2002. Multi-stage Deformation in the Nallamalai Fold Belt, Cuddapah Basin, South India - Implications for Mesoproterozoic Tectonism Along Southeastern Margin of India. *Gondwana Research* **5**, 701-719.

SAHA D. & CHAKRABORTY S. 2003. Deformation pattern in the Kurnool and Nallamalai groups in the northeastern part (Palnad area) of the Cuddapah basin, South India and its implication on Rodinia/Gondwana tectonics. *Gondwana Research* **6**, 573-583.

SAHA D. & TRIPATHY V. 2011. Paleoproterozoic Sedimentation in the Cuddapah Basin, south India and Regional Tectonics - a Review. *in review*.

SARANGI S., GOPALAN K. & SRINIVASAN R. 2007. Small scale sampling for Pb-Pb dating of marbles: Example from the Sargur supracrustal rocks, Dharwar Craton, South India. *Precambrian Research* **152**, 83-91.

SARKAR A. & PAUL D. K. 1998. Geochronology of the Eastern Ghats Precambrian Mobile Belt - a review. *Geological Survey of India Special Publications* **44**, 51-86.

SHIELDS G. & VEIZER J. 2002. Precambrian marine carbonate isotope database: Version 1.1. *Geochemistry Geophysics Geosystems* **3**, 1-12.

SIBLEY D. F., NORDENG S. H. & BORKOWSKI M. L. 1994. Dolomitization kinetics in hydrothermal bombs and natural settings. *Journal of Sedimentary Research Section A* **64**, 630-637.

SIMMAT R. & RAITH M. M. 2008. U-Th-Pb monazite geochemistry of the Eastern Ghats Belt, India: Timing and spatial disposition of poly-metamorphism. *Precambrian Research* **162**, 16-39.

SIMONSON B. M., SCHUBEL K. A. & HASSLER S. W. 1993. Carbonate sedimentology of the early Precambrian Hamersley Group of Western Australia. *Precambrian Research* **60**, 287-335.

SINGH A. P. & MISHRA D. C. 2002. Tectonosedimentary evolution of Cuddapah basin and Eastern Ghats mobile belt (India) as Proterozoic collision: gravity, seismic and geodynamic constraints. *Journal of Geodynamics* **33**, 249-267.

SINGH A. P., MISHRA D. C., GUPTA S. B. & RAO M. R. K. P. 2004. Crustal structure and domain tectonics of the Dharwar Craton (India): insight from new gravity data. *Journal of Asian Earth Sciences* **23**, 141-152.

SUNDARAM R. K., SWAMINATH J. & VENKATESH V. 1964. Tectonics of Peninsular India. *International Geological Congress,* New Delhi, pp. 539-556.

UPADHYAY D., GERDES A. & RAITH M. M. 2009. Unraveling Sedimentary Provenance and Tectonothermal History of High-Temperature Metapelites, Using Zircon and Monazite Chemistry: A Case Study from the Eastern Ghats Belt, India. *Journal of Geology* **117**, 665-683.

VASUDEVAN D., KROENER A., WENDT I. & TOBSCHALL H. 2005. Geochemistry, petrogenesis and age of felsic to intermediate metavolcanic rocks from the Palaeoproterozoic Nellore Schist Belt, Vinjamur, Andhra Pradesh, India. *Journal of Asian Earth Sciences*, in review.

VEIZER J., CLAYTON R. N., HINTON R. W., VON BRUNN V., MASON T. R., BUCK S., G. & HOEFS J. 1990. Geochemistry of Precambrian carbonates: 30shelf seas and non-marine environments of the Archaean. *Geochimica Et Cosmochimica Acta* **54**, 2717-2729.

VEIZER J., PLUMB K. A., CLAYTON R. N., HINTON R. W. & GROTZINGER J. P. 1992. Geochemistry of Precambrian carbonates: V. Late Paleoproterozoic seawater. *Geochimica Et Cosmochimica Acta* **56**, 2487-2501.

VERVOORT J. D., PATCHETT P. J., BLICHERT-TOFT J. & ALBARÈDE F. 1999. Relationships between Lu-Hf and Sm-Nd isotopic systems in the global sedimentary system. *Earth and Planetary Science Letters* **168**, 79-99.

VIJAYA KUMAR K., ERNST W. G., LEELANANDAM C., WOODEN J. L. & GROVE M. J. 2010. First Paleoproterozoic ophiolite from Gondwana: Geochronologic-geochemical documentation of ancient oceanic crust from Kandra, SE India. *Tectonophysics* **487**, 22-32.

WARREN J. 2000. Dolomite: occurence, evolution and economically important associations. *Earth-Science Reviews* **52**, 1-81.

ZHAO G., SUN M. & WILDE S. A. 2003. Correlations between the Eastern Block of the North China Craton and the South Indian Block of the Indian Shield: an Archaean to Palaeoproterozoic link. *Precambrian Research* **122**, 201-233.

ZHAO G., SUN M., WILDE S. A. & LI S. 2004. A Paleo-Mesoproterozoic superconinent: assembly, growth and breakup. *Earth-Science Reviews* **67**, 91-123.

12 FIGURE CAPTIONS AND LIST OF TABLES

12.1 Figure captions

Figure 1. (a) Selective geological map of India, modified after French *et al.* (2008) and Dobmeier & Raith (2003). **Archaean cratons** - A: Aravalli craton; B: Bastar craton; Bu: Bundelkhand craton; EDC: Eastern Dharwar craton; S: Singhbhum craton; WDC: Western Dharwar craton. **Proposed Purana basins** – Bh: Bhima basin; C: Cuddapah basin; Ch: Chhatisgarh basin; I: Indravati basin; K: Kaladgi basin; PG: Pranhita-Godavari basin; V: Vindhyan basin. **Provinces of the Eastern Ghats Belt** – NSB: Nellore Schist Belt; OD: Ongole Domain; EGP: Eastern Ghats Province. The broad study area is highlighted by the pale box. Very approximate locations of the Sargur Group (SG) and Salem Block (SB) are shown by the black stars (Sarangi *et al.* 2007; Clark *et al.* 2009); (b) Tectonic map of India, after Mall *et al.* (2008) and Mazumder *et al.* (2000) (c) Geological map of the Cuddapah basin, modified after Anand *et al.* (2003) and (Dasgupta *et al.* 2005). The approximate location of each fieldwork area is shown.

Figure 2. Summary of current geochronological constraints in the Purana basins. Basins are arranged from north to south, and then westward from the Cuddapah Basin. References are as follows: a) U-Pb dating of a kimberlite (Pradhan *et al.* 2010); b) U-Pb dating of a felsic tuff (Ray *et al.* 2002); c) U-Pb dating of a felsic tuff (Deb *et al.* 2002); d) U-Pb zircon dating of a tuff (Patranabis-Deb *et al.* 2007); e) U-Pb dating of basal tuff (Das *et al.* 2009); f) inferred correlation with Upper Vindhyan carbonates (Maheshwari *et al.* 2005); g) inferred age of a lamproite (Chaudhuri *et al.* 1999); h) K-Ar dating of sandstone (Chaudhuri & Howard 1985); i) dating of authigenic glauconite minerals (Conrad *et al.* 2011); j) unspecified inference (Mishra 2011); k) U-Pb zircon dating, this study; l) whole rock geochronology on a granitic intrusion (Crawford & Compston 1973); m) Ar-Ar dating of a mafic sill (Anand *et al.* 2003); n) U-Pb dating of mafic dykes (French *et al.* 2004); o) unspecified inference(Chakraborty *et al.* 2010); p) stratigraphic correlation of carbonates (Chakraborty *et al.* 2010); q) stromatolite analysis (Ramakrishnan & Vaidyanadhan 2008).

Figure 3. Stratigraphic column of the Cuddapah Supergroup, after Anand (2003). The full range of reported thicknesses of each unit are given (GSI 1981; Nagaraja Rao *et al.* 1987; Dasgupta & Biswas 2006). Age determinations are as follows: a. Maximum depositional ages (LA-ICP-MS U/Pb geochronology on detrital zircons; this study) b. Age of emplacement of a mafic-ultramafic sill in the lower Tadpatri Formation; minimum depositional age (^{40}Ar-^{39}Ar laser-fusion data on phlogopite separates; Anand *et al.* 2003) c. Maximum depositional ages (LA-ICP-MS U/Pb geochronology on detrital zircons; Mackintosh 2010) d. Age of emplacement of a lamproite; minimum depositional age (^{40}Ar-^{39}Ar geochronology on micas; Chalapathi Rao *et al.* 1999) e. Maximum depositional age (LA-ICP-MS U/Pb geochronology on detrital zircons; Gore 2011) f. Age of intrusion of the Penukonda dyke (U/Pb dating on baddeleyite; French & Heaman 2010)

Figure 4. Stratigraphic log of the section through the base of the Gulcheru Formation. A brief facies description is given in the key, but expanded facies descriptions are provided in the body of the text and Appendix II (this applies for each subsequent stratigraphic log). Grain size notations and sedimentary structures are also applicable for each ensuing log. The position in the section where sample GF01was collected is shown by the concentric red circles. The black star denotes the bed which was logged in greater detail, and which is shown in the last column. Note that the key does *not* apply to subsequent logs.

Figure 5. Stratigraphic log of the section through the uppermost Gulcheru Formation and lower Vempalle Formation. The contact between the formations has been inferred at approximately 40 m in the section. $\delta^{13}C_{dol}$ and $\delta^{18}O_{dol}$ are plotted in ‰ relative to VPDB. The position in the log where sample GF14 was collected is indicated by the concentric red circles. Lithological units which have been logged in greater detail are denoted with a black star; the corresponding higher-resolution logs are provided in Figure 6. Lithological units correspond to those outlined in Appendix II.

Figure 6. Supplementary logs to the stratigraphic log through the Vempalle Formation: **a**) Expanded log of the first occurrence of LU6 (description provided in the body of the text). Stratigraphic height corresponds to that of Figure 5. **b**) Representative log through a section within LU3. Note the scale,

which is not related to that of Figure 5, but is intended to show relationships between lithologies within the unit. This log corresponds to Figure 10**a**. **c**) Expanded log of LU7 (description provided in the body of the text). L1-L7 in this log correspond to the lithologies described in Appendix II. Stratigraphic height corresponds to that of Figure 5.

Figure 7. Stratigraphic log of the section through the uppermost Tadpatri Formation. Brief facies descriptions are provided in the key, but these correspond to more detailed descriptions in the body of the text, and Appendix II. The concentric red circles represent the position where sample GF09 was collected. The beginning of the log was denoted zero metres as the actual position of the section within the basin stratigraphy could not be determined.

Figure 8. Photographs of sedimentary structures in rocks of the Gulcheru Formation: (a) unconformable contact of the base of the Gulcheru Formation with weathered granite interpreted as the EDC; (b) a banded ironstone clast from within facies Gm; (c) imbricated clasts and a sandy bar within facies Gm; (d) interlayered cross-stratified gravel with cross-stratified sand in facies St-Gt; (e) overturned foreset within facies St-Gt; (f) planar foresets within facies St-Sp; (g) trough cross-bedded sand in facies St-Sp; (h) trough cross-bedded sand with a basal pebble lag on scour surface in facies St-Sp.

*Figure 9.*Photographs of sedimentary structures in rocks of the Vempalle Formation: (a) lenticular bedding within LU1; (b) desiccation cracks in mud beds in LU1 (interbedded fine sand and mud); (c) ball and pillow structures (load casts) in LU1; (d) basal rip-up clasts of mud in a sandy bed in LU1; (e) a stromatolite within LU1; (f) thin sand beds at the base of dolomite beds in LU3; (g) halite pseudomorphs from within LU5 (shale with interbedded sand); (h) laterally linked hemispheroid stromatolites from within the dark grey dolomite in LU7 (interbedded sandy dolomite and mud, with occasional sand beds).

Figure 10. Photographs of sedimentary structures seen in the Vempalle Formation: (a) interbedded sand and dolomite in LU3 (thickly bedded dolomite with mixed sand) – this photo corresponds with

Section 6**c**; (b) a large stromatolite mound from within LU6 (interbedded dolomite and mud) – notebook indicated by the blue arrow is 20 cm high.

Figure 11. Photographs of sedimentary structures in the Tadpatri Formation: (a) hummocky cross-stratification from within the 'fine sand' facies of the Tadpatri Formation; (b) small ball and pillow structures from within the 'fine sand' facies of the Tadpatri Formation; (c) sand ball from within the 'highly convoluted fine sand with shale' facies of the Tadpatri Formation – note laminated exterior of the sand ball; (d) ball and pillow structure from within the 'highly convoluted fine sand with shale' facies of the Tadpatri Formation.

Figure 12. Photographs of sedimentary structures in the Gandikota Formation: (a) climbing ripples; (b) rhomboidal interferences ripples; (c) small syn-sedimentary detachment fault with associated flame structures. Black arrows indicate movement of sediment.

Figure 13. Graphical representations of geochronological data from samples GF01 (Gulcheru Formation) and GF14 (Vempalle Formation): a_1) conventional concordia plot showing all acquired zircon data from sample GF01; a_2) probability density plot for data of <90% concordancy (light grey) and ≥90% concordancy (dark grey) from sample GF01. Mean weighted average $^{207}Pb/^{206}Pb$ ages are shown above each peak, and uncertainties are quoted at 1σ. A representative zircon is shown in the top right corner; b_1) conventional concordia plot showing all acquired zircon data from samples GF14. Inset shows a close-up of the main population at 2600-2000 Ma; b_2) probability density plot for data of <90% concordancy (light grey) and ≥90% concordancy (dark grey) from sample GF14. Mean weighted average $^{207}Pb/^{206}Pb$ ages are shown above each peak, and uncertainties are quoted at 1σ. A representative zircon is shown in the top right corner.

Figure 14. Graphical representations of geochronological data from samples GF06 (Gandikota Formation) and GF09 (Tadpatri Formation): a_1) conventional concordia plot showing all acquired zircon data from sample GF06. Inset shows a close-up of the populations between 2300 Ma and 1200 Ma; a_2) probability density plot for data of <90% concordancy (light grey) and ≥90% concordancy

(dark grey) from sample GF06. Mean weighted average $^{207}Pb/^{206}Pb$ ages are shown above each peak, and uncertainties are quoted at 1σ. A representative zircon is shown in the top left corner; b) conventional concordia plot showing analyses from sample GF09 excluding those which were discounted due to an unacceptably high level of common lead. A rough discordia has been included, indicating modern day lead loss from zircon grains of approximately 2500 Ma. As no concordant analyses were obtained, no probability density plot is presented. A representative zircon grain is shown in the bottom right corner.

Figure 15. Graphical representation of hafnium isotope data from samples GF01, GF14 and GF06: a) plot of the $^{207}Pb/^{206}Pb$ age of detrital zircons against their initial $^{176}Hf/^{177}Hf$ composition. The blue line represents the isotopic evolution of the depleted mantle, and the green line represents the evolution of the chondritic uniform reservoir (CHUR). Inferred inputs of juvenile material are indicated by the black arrows. Points which plot close to the depleted mantle line are likely to have a fairly juvenile composition, and points which plot close to the CHUR line are likely to be the result of reworking of pre-existing crust. All points may represent a combination of juvenile input and reworking of crust; b) plot of the $^{207}Pb/^{206}Pb$ age of detrital zircons against their ε_{Hf} values. Blue and green lines are as in Figure 15a. Points which plot above the CHUR line are likely to represent some incorporation of juvenile material into the melt, and points which plot below the CHUR line are likely to represent dominant re-working of pre-existing crust.

Figure 16. Graphical representations of stable isotope geochemistry of dolomites from the Vempalle Formation: a) plot of $\delta^{18}O_{dol}$ (light grey diamonds) and $\delta^{13}C_{dol}$ (dark grey circles) against stratigraphic height (this corresponds to the log presented in Fig. 9). The lowermost 12 analyses for correspond to the well-correlated data presented in Figures 16b & 16c; b) Cross-plot of $\delta^{18}O_{dol}$ against $\delta^{13}C_{dol}$. Light blue diamonds represent a series of analyses which have an R^2 value of 0.96 for a linear correlation. Light green diamonds represent analyses with anomalously heavy $\delta^{18}O_{dol}$ values; c) plot of $\delta^{18}O_{dol}$ (light blue/green diamonds) and $\delta^{13}C_{dol}$ (dark blue/green circles) against stratigraphic height (this

corresponds to the log presented in Fig. 9). Blue points coincide with well correlated data presented in Figure 16b, and apparent trends in isotopic composition have been inferred.

Figure 17. Comparison of $\delta^{13}C$ values obtained from dolomites of the Vempalle Formation with proposed global $\delta^{13}C$ oceanic reference curves: a) Carbon isotopic evolution of marine carbonates through time based on published analyses of various carbonate minerals (after Shields & Veizer 2002). Poorly time-constrained samples (greater than ± 50 Ma) are shown as open circles, and the blue line represents a running mean. $\delta^{13}C$ values obtained from the Vempalle Formation are shown as green points, and have been compared with the two most likely time intervals in terms of global mean ocean values. Inset box shows the average global oceanic values through time: note that the values are close to zero through time; b) Composite $\delta^{13}C_{PDB}$ curve based on values from a series of basins in Western Australia (after Lindsay & Brasier 2002). Dashed lines indicate time periods with no available chemostratigraphic data from the analysed series of basins. $\delta^{13}C$ values obtained from the Vempalle Formation are shown as green points, and overlap regions of the composite curve where $\delta^{13}C_{PDB}$ values have been obtained from the Ashburton (older) and Earaheedy (younger) basins.

Figure 18. Comparison of detrital age populations from the Papaghni, Nallamalai and Kurnool Groups: a) probability density plot showing ≥90% concordant $^{207}Pb/^{206}Pb$ ages obtained from the Gulcheru and Vempalle Formations of the basal Papaghni Group; b) probability density plot showing ≥90% concordant $^{207}Pb/^{206}Pb$ ages obtained from the Bairenkonda/Cumbum and Srisailam Formations of the Nallamalai Group; c) probability density plot showing ≥90% concordant $^{207}Pb/^{206}Pb$ ages obtained from the Gandikota Formation of the Kurnool Group. The grey rectangles indicate peaks which are common to two or more of the groups.

12.2 List of tables

Table 1. Table detailing geochronological constraints on rocks within the Dharwar Craton. Table a: Only ages which were derived from accurate U-Pb zircon methods are included. References are as follows: a) Meert *et al.* (2010) b) Nutman *et al.* (1996) c) Nutman & Ehlers (1998) d) Rogers *et al.* (2007) e) Anand & Balakrishnan (2011) f) Balakrishnan *et al.* (1999) g) Friend & Nutman (1991) h)

Krogstad *et al.* (1995) i) Ramakrishnan & Vaidyanadhan (2008) j) Chadwick *et al.* (1997) k) French & Heaman (2010) l) Halls *et al.* (2007) m) French *et al.* (2004) n) French *et al.* (2008) o) Vasudevan *et al.* (2005) p) Kovach *et al.* (2001) q) Upadhyay *et al.* (2009) r) Sarkar & Paul (1998) s) Aftalion *et al.* (1988) t) Paul *et al.* (1990) u) Crowe (2003) v) Henderson (2011) w) Pitchamuthu & Srinivasam (1984) x) Naha *et al.* (1991) y) Rao *et al.* (1991) z) Naqvi & Rogers (1987) aa) Krogstad *et al.* (1991) bb) Ahmad (2011) cc) Jayananda *et al.* (2009) dd) Jayananda *et al.* (2000) ee) Vajaya Kumar *et al.* (2010) ff) Anand & Balakrishnan (2010) gg) Clark *et al.* (2009). The formations to which each terrane may have supplied sediment are GF (Gulcheru Formation), VF (Vempalle Formation), GaF (Gandikota Formation. Table b: This table outlines further geochronological constraints on rocks within the Dharwar Craton. Ages included in this table are supplementary to the ages in Table 1a, but are derived from unreliable or out-dated geochronological methods, or were unsubstantiated ages with no supporting data. References are as for Table 1a.

Table 2. Starting location of each logged section, and approximate stratigraphic thickness of each section.

Table 3. Summary of detrital age populations from the Gulcheru (GF01), Vempalle (GF14) and Gandikota (GF06) formations. Age populations have been calculated using Isoplot/Ex.3, and where the population is represented by more than one zircon grain, the age of the population is a mean weighted average of all included analyses.

Table 4. Summary of average physical characteristics of zircon grains, according to detrital populations.

Table 5. Location of each sample collected for geochronological analysis, with a brief summary of the depositional environment

13 TABLES

a.

Locality	Unit	Rock type	Dating method	Age (Ma)	Possible source terrane?	References
WDC	Protolith to Sargur Group	-	SHRIMP U/Pb zircon	~3600		a.
WDC	Peninsular Gneiss	TTG gneiss	U/Pb zircon (unspecified)	3600-3500		a.
WDC	Sargur Group	volcano-sedimentary greenstone granite	Pb-Pb evaporation detrital zircons, SHRIMP U/Pb zircon	~3300-3100	GF	a.
EDC	Unspecified	cratonic gniess	Pb-Pb single zircon grain evaporation	~3100-3150	GF	dd.
West of the Cuddapah Basin	assorted	greenstone/schist belts	SHRIMP U/Pb zircon	2757-2523	GF, VF, GaF	b., c., d., e.. Ff.
West of the Cuddapah Basin	Ramagiri Schist Belt	felsic volcanics	U/Pb zircon	2707 ± 18		f.
Widespread through EDC	Dharwar Batholith	granitic intrusives	SHRIMP U/Pb zircon	2700-2500	GF, VF, GaF	g., h., b., c., e., dd.
Northern end of Closepet Granite	Sandur Schist Belt	schist belt	SHRIMP U/Pb zircon	2658 -2500	GF, VF	b., i.
WDC	Dharwar Supergroup	schist belt	SIMS U/Pb zircon	~2610	GF, VF	j.
Krishna Province	Ongole Domain	metasediment	LAICPMS U/Pb zircon (cores)	~2598-1676	GaF	v.
Southern EDC	Salem Block	charnockite	SHRIMP U/Pb zircon	2560-2360	GF, VF, GaF	gg.
Western border of EDC	Closepet Granite	granite	SHRIMP U/Pb zircon	2513 ± 5	GF, VF	g., h., b., c., e.
EDC, west of the Cuddapah Basin	Bangalore dyke swarm	mafic dyke swarm	IDTIMS U/Pb zircon and baddeleyite	2369-2365		k., l.
EDC, widespread	Dyke swarm	mafic dyke swarm	IDTIMS U/Pb zircon and baddeleyite	2209-2221	GaF	k.
EDC, west of the Cuddapah Basin	Mahbubnagar dyke swarm	mafic dyke swarm	IDTIMS U/Pb zircon and baddeleyite	2181-2177		k., m.
Nelllore Schist Belt	Kandra ophiolite complex	gabbro	SHRIMP U/Pb zircon	1850	GaF	ee.
Western Cuddapah Basin	Pulivendla Sill	mafic intrusion	IDTIMS U/Pb zircon	1885.4 ± 3.1	GaF	n.
Krishna Province	Vinjamuru Domain	felsic magmatism	Pb-Pb single zircon grain evaporation	1870-1770	GaF	o.
Krishna Province	Ongole Domain	enderbite-charnockite	U/Pb zircon (unspecified)	1720-1700	GaF	p.
Eastern Ghats Province	Vijayawada metapelite	metapelite	LAICPMS U/Pb zircon (cores)	1640	GaF	q.
Eastern Ghats Province	Vijayawada metapelite	metapelite	LAICPMS U/Pb zircon (cores)	1200	GaF	q.
Eastern Ghats Province	Angul and Phulbani Domains	felsic magmatism	U/Pb zircon data (asstd)	1200-1150	GaF	s., t., u.

b.

Locality	Unit	Rock type	Dating method	Age (Ma)	References
WDC	Peninsular Gneiss	TTG gneiss	whole rock Rb-Sr and Pb-Pb	3400-3300	a., b., c.
WDC	Peninsular Gneiss	migmatitic gneiss	not specified	3300-3000	d.
WDC	-	granitoid suite	not specified	2600-2500	e.
WDC	-	supracrustal belts	not specified	3000-2600	f.
EDC	-	gneisses hosting Dharwar Batholith	not specified	2900-2700	e., g.
EDC	-	TTG gneisses and greenstone belts	not specified	>3000	h., i.
Northern margin of Krishna Province	Kunavaram Alkaline Complex	alkaline intrusion	Rb-Sr whole rock	1265 ± 58	r.

Table 1.

	Start location		Stratigraphic thickness
Formation	Latitude	Longitude	
Gulcheru	14°35.069'N	77°56.147'E	45 m
Vempalle	14°33.057'N	77°58.023'E	440 m
Tadpatri	14°48.530'N	77°14.174'E	9.5 m

Table 2.

Sample	Peak age (Ma)	1σ error (Ma)	n	MSWD	Probability
GF01	3426	22	2	0.47	0.49
	3368	170	2	1.5	0.23
	3267.7	16.31	1	-	-
	3182.9	15.81	1	-	-
	3123	15.89	1	-	-
	2985	17	4	0.78	0.51
	2612	17	4	1.12	0.34
	2526	13	12	1.3	0.2
GF14	2765	16.22	1	-	-
	2584	14	12	1.6	0.095
	2546	11	10	0.36	0.95
	2500	7.3	42	1.8	0.001
	2422.1	17.3	1	-	-
GF06	3038.4	17.75	1	-	-
	2985.2	16.41	1	-	-
	2635	79	3	2.3	0.1
	2569	14	8	0.56	0.79
	2499	10	29	2.1	0.001
	2195	33	2	0.72	0.4
	1909	26	3	0.86	0.42
	1810.1	26.8	1	-	-
	1705.7	24.62	1	-	-
	1641.7	27.12	1	-	-
	1275.1	23.63	1	-	-
	1206.5	22.08	1	-	-

Table 3.

Sample	Formation	Age population (Ma)	Size (μm)	Aspect ratio	Colour	Morphology	CL description	Description based on # zircons
GF01	Gulcheru	2526 ± 13	90-200	1:1.8	Yellow, orange, pink or pale pale pink	Stubby to subrounded oblate	Vary between fine oscillatory zoning and no zoning	12
		2612 ± 17	90-140	1:1.4		Stubby or acicular	No zoning, with occasional strongly luminescent zones	4
		2985 ± 17	90-120	1:1.6		acicular to subrounded oblate	Faint thick oscillatory zoning	4
		3123 ± 16	100	1:1.9		Subrounded oblate	Osciallatory zoning	1
		3183 ± 16	180	1:1.5		Subrounded oblate	Featureless	1
		3268 ± 16	180	1:1.5		Stubby	Featureless	1
		3368 ± 170	120	1:1		Rounded, equant	Faint oscillatroy zoning, with strongly luminescent zones	2
		3426 ± 22	90-110	1:1		Rounded, equant to slightly oblate	Thick oscillatory zoning	2
GF14	Vempalle	2765 ± 16	120	1:1.8	Clear, pale pink, pale orange, pink or orange	Stubby	Strongly luminescent oscillatory zoned core, thin rim	1
		2584 ± 14	90-130	1:1.6		Stubby to ovoid	Varies between fine and thick oscillatroy zoning	42
		2546 ± 11	70-90	1:1.8		Stubby	Vary between fine oscillatory zoning and no zoning, occasionally with convoluted zones	10
		2500 ± 7	80-160	1:1.7		Stubby to elongate and prismatic	Vary between fine oscillatory zoning and no zoning, or thick convoluted zones	12
		2422 ± 17	100	1:1.4		Stubby	Thick oscillatory zoning	1
GF09	Tadpatri	n/a	30-60	1:1.7	Clear to very pale pink	Stubby, prismatic or acicular	Vary from fine oscillatory zoning to no zoning, often with metamict cores and thin	2
GF06	Gandikota	1207 ± 22	100	1:1.6	Clear, pale pink, pale yellow or light grey	Stubby	Thick oscillatory zoning, stongly luminescent zoning	1
		1275 ± 24	grain broken				Thick oscillatory zoning, stongly luminescent zoning	1
		1642 ± 27	150	1:1.8		Stubby	Strongly luminescent oscillatory zoned core, very thin rim	1
		1706 ± 25	150	1:1.8		Stubby	Strongly luminescent oscillatory zoned core, very thin rim	1
		1810 ± 27	100	1:1.6		Subrounded oblate	Strongly luminescent, some faint oscillatory zoning	1
		1909 ± 26	100	1:1.8		Stubby to prismatic	Fine scale oscillatory zoning, stronly luminescent	3
		2195 ± 33	60-80	1:1.5		Stubby to rounded and equant	No zoning, with strongly luminescent zones	2
		2499 ± 10	50-120	1:1.8		Stubby or prismatic	Vary from fine oscillatory zoning to no zoning, a few thin rims	29
		2569 ± 14	50-80	1:1.7		Stubby to subrounded oblate or equant	Vary from no zoning to faint or thick oscillatory zoning, with occasional rims	8
		2635 ± 79	50-70	1:1.4		Prismatic or rounded equant	Vary from no zoning to oscillatory zoning	3
		2985 ± 16	70	1:1.5		Stubby	No zoning	1
		3038 ± 18	grain broken				Fine scale oscillatory zoning	1

Table 4.

Sample Name	Formation	Location	Bed width	Lithology	Environment
GF01	Gulcheru	14°35'5.34"N 77°56'10.20"E	290 cm	Polymictic conglomerate with large scale bar cross bedding	Bedload deposit from high energy stream flow
GF14	Vempalle	14°33'20.82"N 77°58'32.22"E	~30 cm	Coarse quartz arenite with symmetric ripples, underlain by mud	Deposition by a high energy event in a dominantly quiet setting
GF09	Tadpatri	14°48'30.60"N 78°14'10.80"E	175 cm	Fine sandstone with extensive soft-sediment convolution	Deposition in a storm-dominated sub-tidal setting
GF01	Gandikota	14°45'3.42"N 78°17'51.12"E	-	Clean cross bedded quartz arenite	-

Table 5.

14 FIGURES

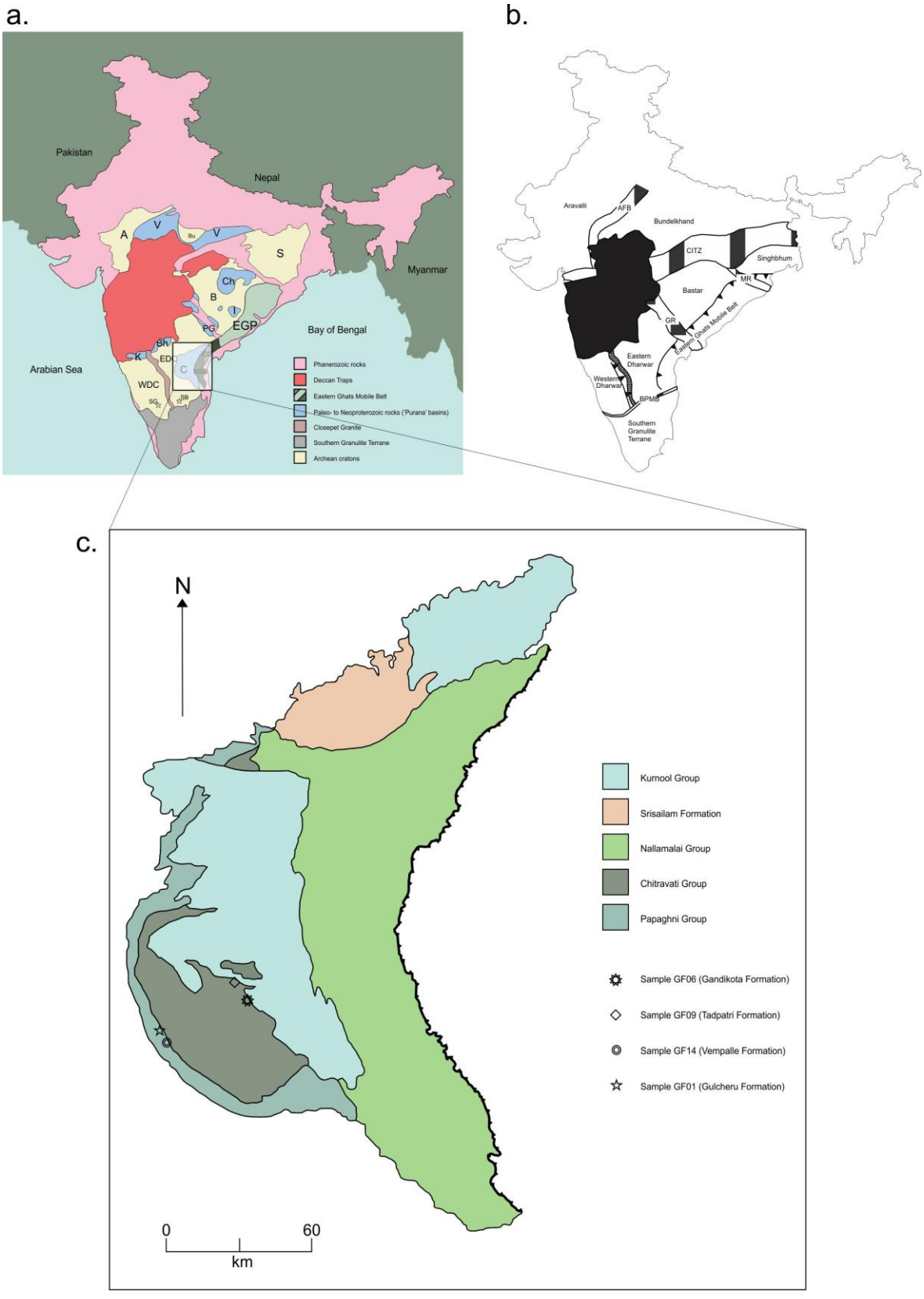

Figure 1.

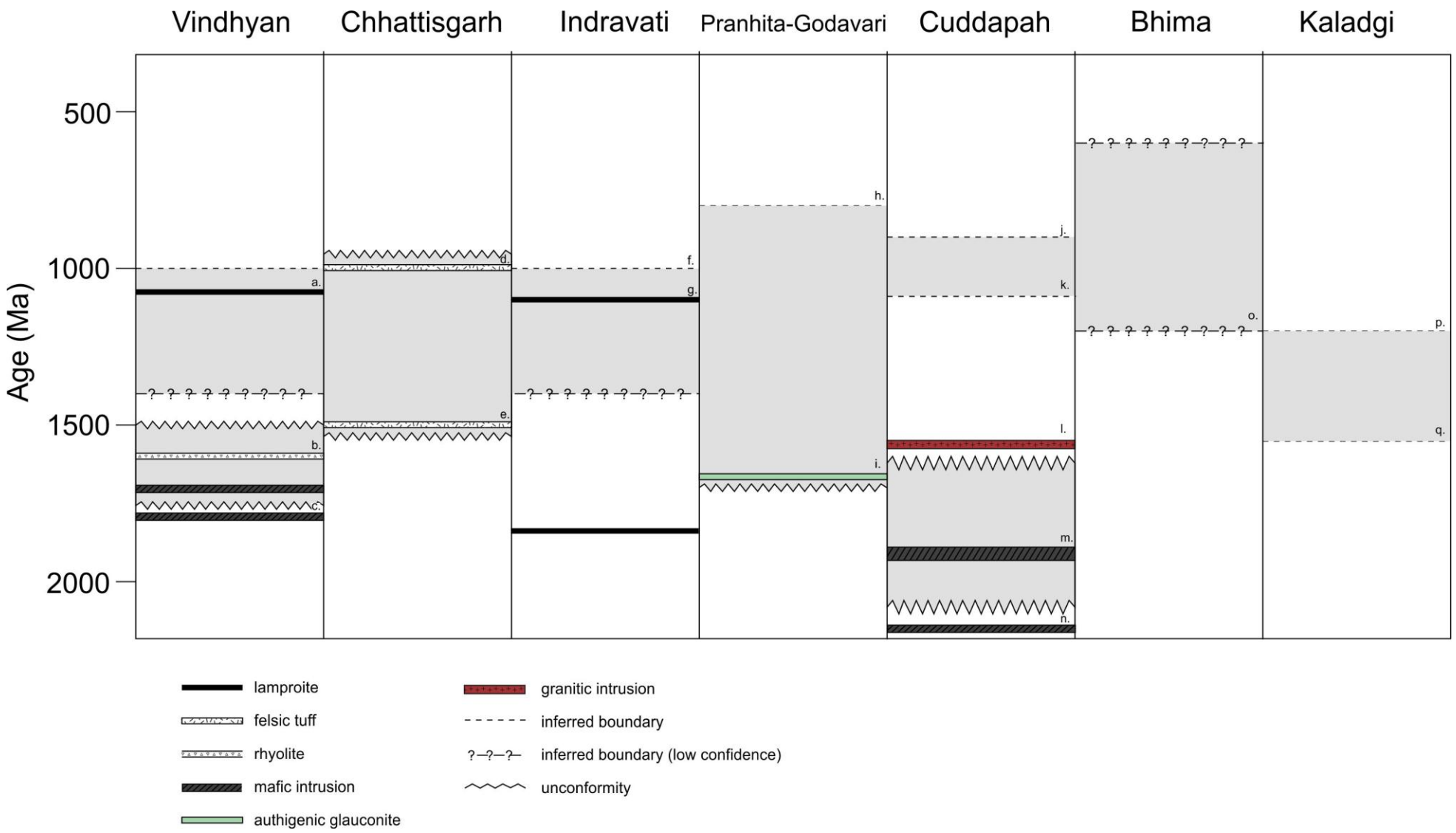
Vindhyan
Chhattisgarh
Indravati
Pranhita-Godavari
Cuddapah
Bhima
Kaladgi
Age (Ma)
500
1000
1500
2000
a.
b.
c.
d.
e.
f.
g.
h.
i.
j.
k.
l.
m.
n.
o.
p.
q.
lamproite
felsic tuff
rhyolite
mafic intrusion
authigenic glauconite
granitic intrusion
inferred boundary
inferred boundary (low confidence)
unconformity

Figure 2.

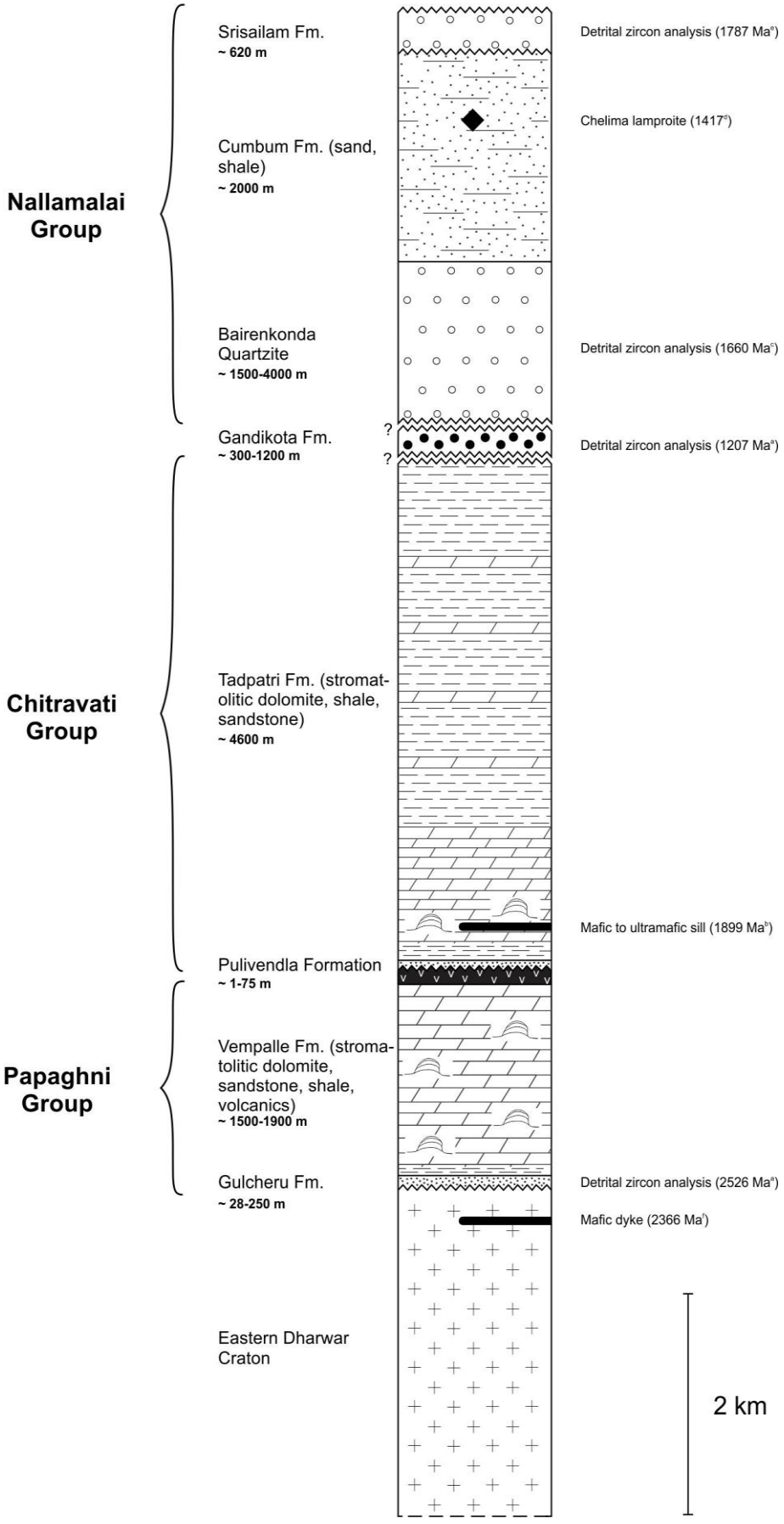
Nallamalai Group
Srisailam Fm.
~ 620 m
Cumbum Fm. (sand, shale)
~ 2000 m
Bairenkonda Quartzite
~ 1500-4000 m
Gandikota Fm.
~ 300-1200 m
Chitravati Group
Tadpatri Fm. (stromatolitic dolomite, shale, sandstone)
~ 4600 m
Pulivendla Formation
~ 1-75 m
Papaghni Group
Vempalle Fm. (stromatolitic dolomite, sandstone, shale, volcanics)
~ 1500-1900 m
Gulcheru Fm.
~ 28-250 m
Eastern Dharwar Craton
Detrital zircon analysis (1787 Ma[e])
Chelima lamproite (1417[e])
Detrital zircon analysis (1660 Ma[c])
Detrital zircon analysis (1207 Ma[e])
Mafic to ultramafic sill (1899 Ma[b])
Detrital zircon analysis (2526 Ma[e])
Mafic dyke (2366 Ma[f])
2 km

Figure 3.

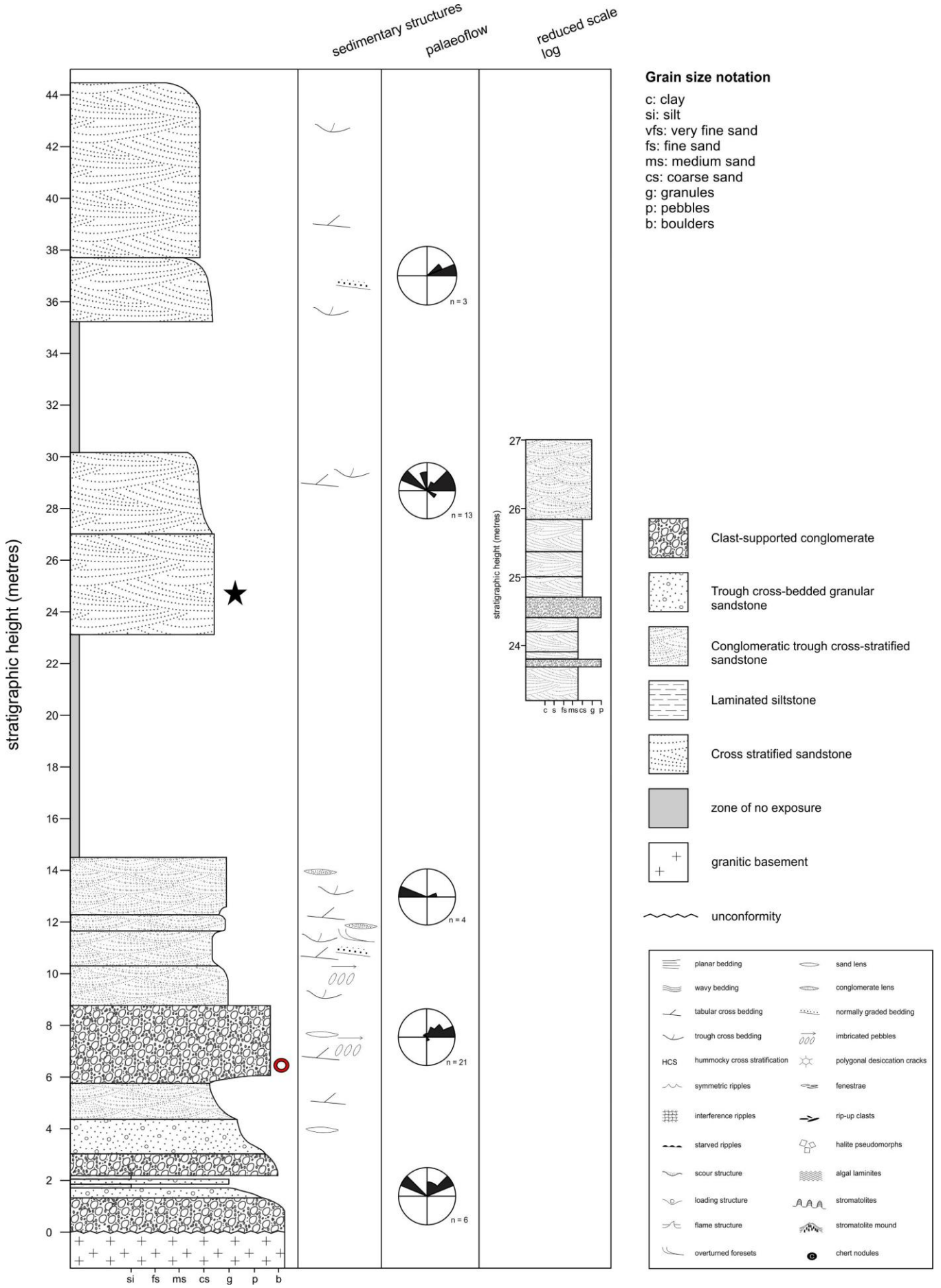
sedimentary structures
palaeoflow
reduced scale log
stratigraphic height (metres)
si fs ms cs g p b
n = 3
n = 13
n = 4
n = 21
n = 6
Grain size notation
c: clay
si: silt
vfs: very fine sand
fs: fine sand
ms: medium sand
cs: coarse sand
g: granules
p: pebbles
b: boulders
Clast-supported conglomerate
Trough cross-bedded granular sandstone
Conglomeratic trough cross-stratified sandstone
Laminated siltstone
Cross stratified sandstone
zone of no exposure
granitic basement
unconformity
planar bedding
wavy bedding
tabular cross bedding
trough cross bedding
HCS
hummocky cross stratification
symmetric ripples
interference ripples
starved ripples
scour structure
loading structure
flame structure
overturned foresets
sand lens
conglomerate lens
normally graded bedding
imbricated pebbles
polygonal desiccation cracks
fenestrae
rip-up clasts
halite pseudomorphs
algal laminites
stromatolites
stromatolite mound
chert nodules

Figure 4.

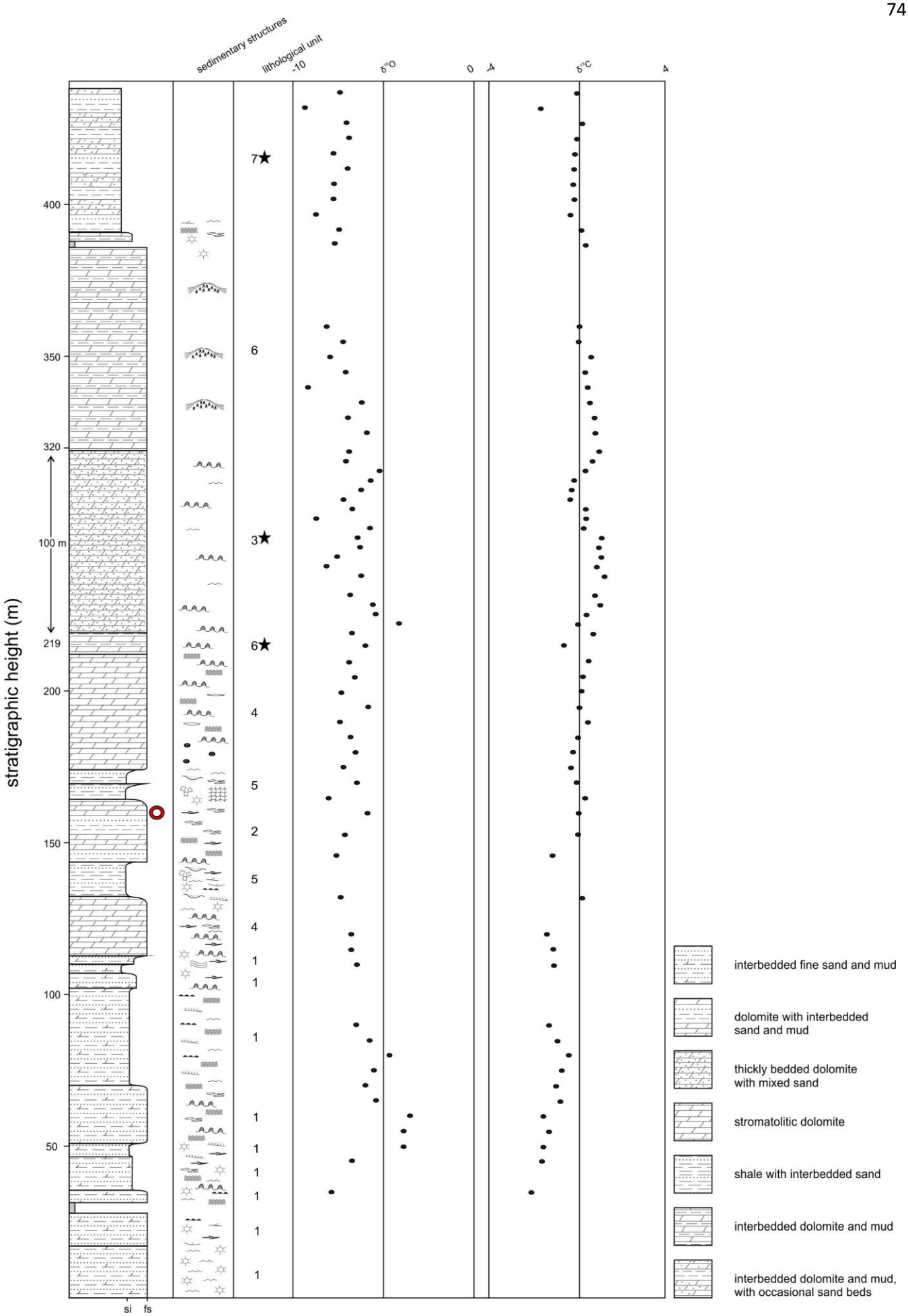
sedimentary structures
lithological unit
-10
δ18O
0
-4
δ13C
4
stratigraphic height (m)
400
350
320
100 m
219
200
150
100
50
7★
6
3★
6★
4
5
2
5
4
1
1
1
1
1
1
1
1
1
si
fs
interbedded fine sand and mud
dolomite with interbedded sand and mud
thickly bedded dolomite with mixed sand
stromatolitic dolomite
shale with interbedded sand
interbedded dolomite and mud
interbedded dolomite and mud, with occasional sand beds

Figure 5.

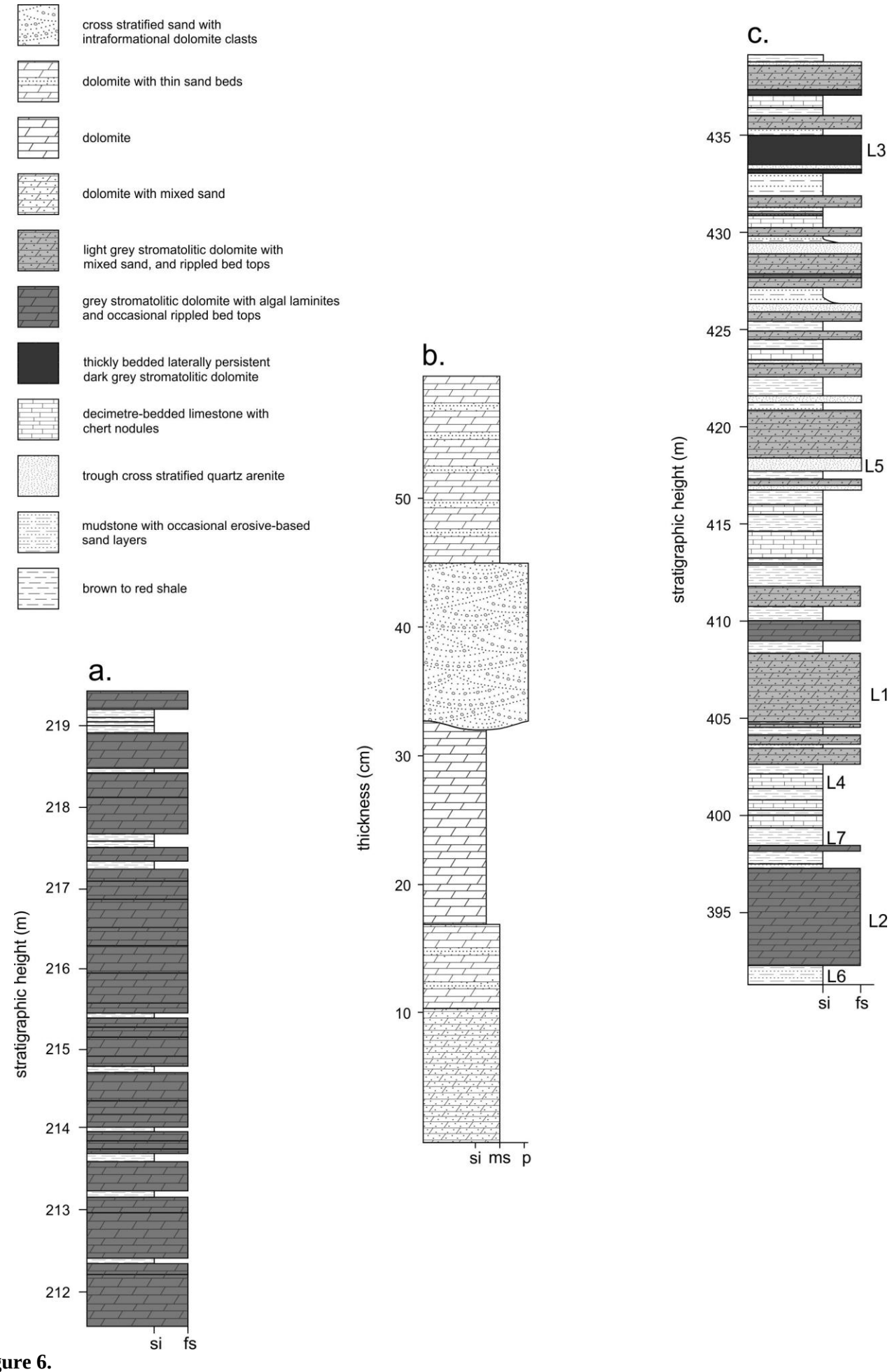
cross stratified sand with intraformational dolomite clasts
dolomite with thin sand beds
dolomite
dolomite with mixed sand
light grey stromatolitic dolomite with mixed sand, and rippled bed tops
grey stromatolitic dolomite with algal laminites and occasional rippled bed tops
thickly bedded laterally persistent dark grey stromatolitic dolomite
decimetre-bedded limestone with chert nodules
trough cross stratified quartz arenite
mudstone with occasional erosive-based sand layers
brown to red shale
a.
stratigraphic height (m)
219
218
217
216
215
214
213
212
si
fs
b.
thickness (cm)
50
40
30
20
10
si
ms
p
c.
stratigraphic height (m)
435
430
425
420
415
410
405
400
395
L3
L5
L1
L4
L7
L2
L6
si
fs

Figure 6.

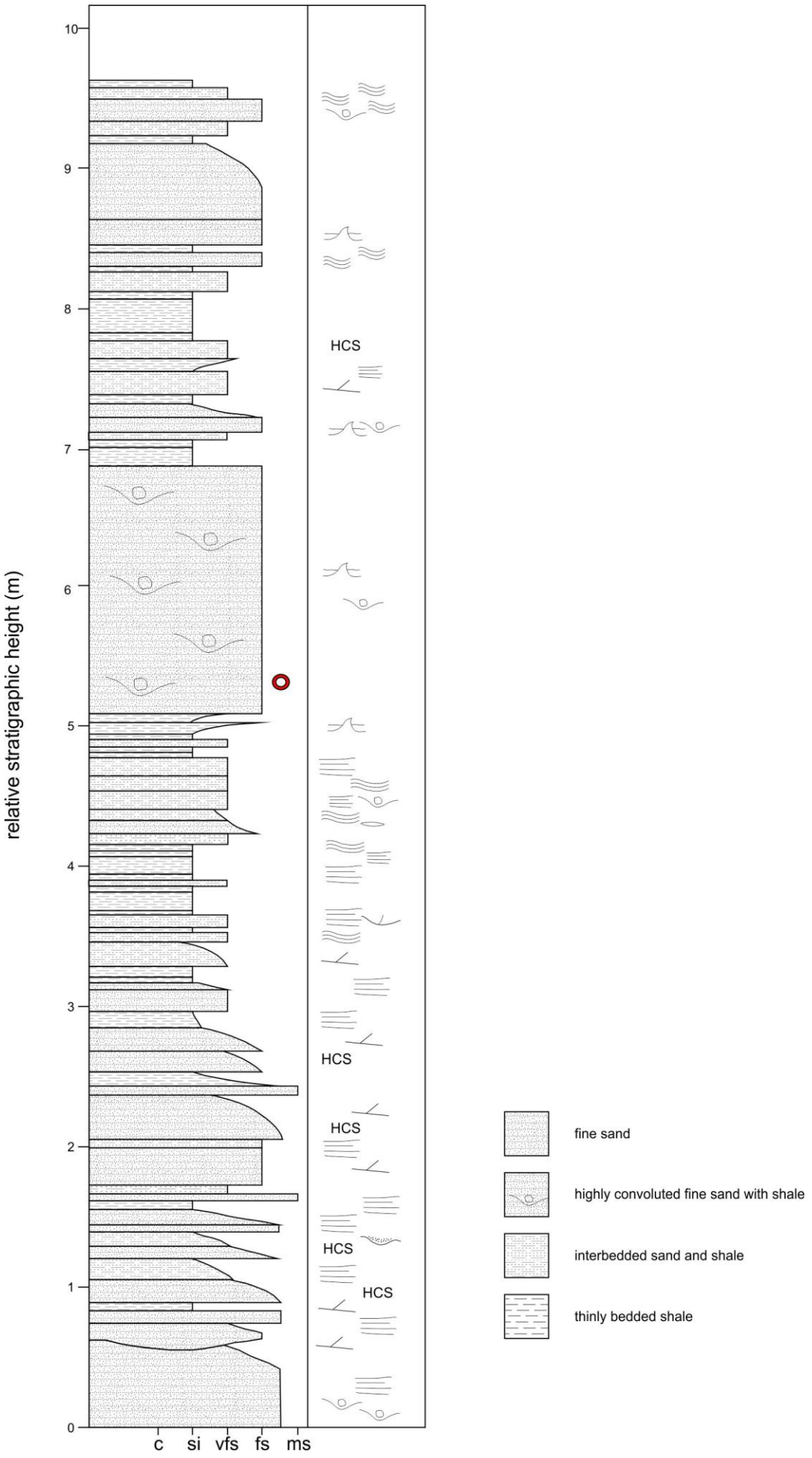
relative stratigraphic height (m)
0
1
2
3
4
5
6
7
8
9
10
c
si
vfs
fs
ms
HCS
HCS
HCS
HCS
HCS
fine sand
highly convoluted fine sand with shale
interbedded sand and shale
thinly bedded shale

Figure 7.

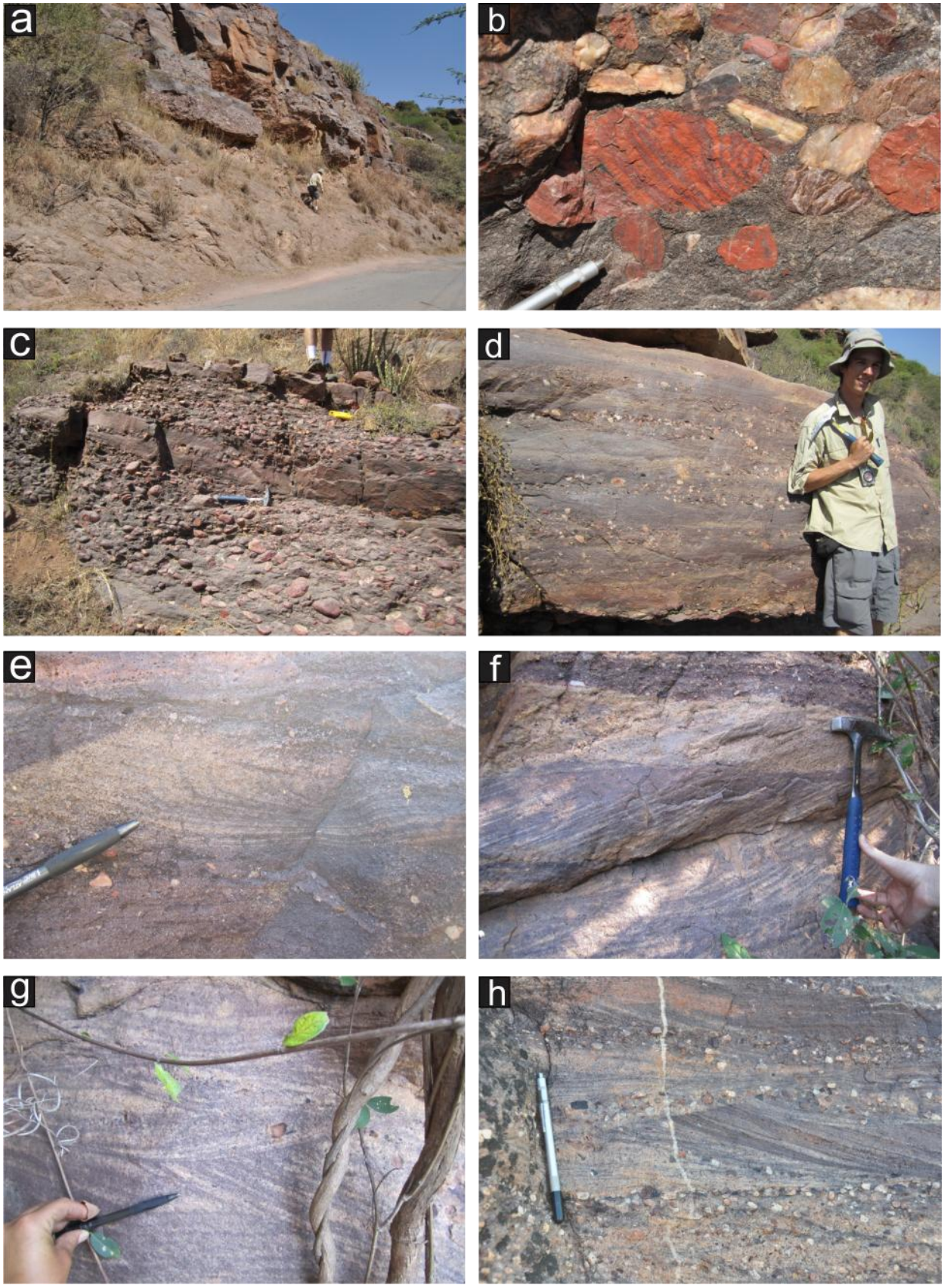

Figure 8.

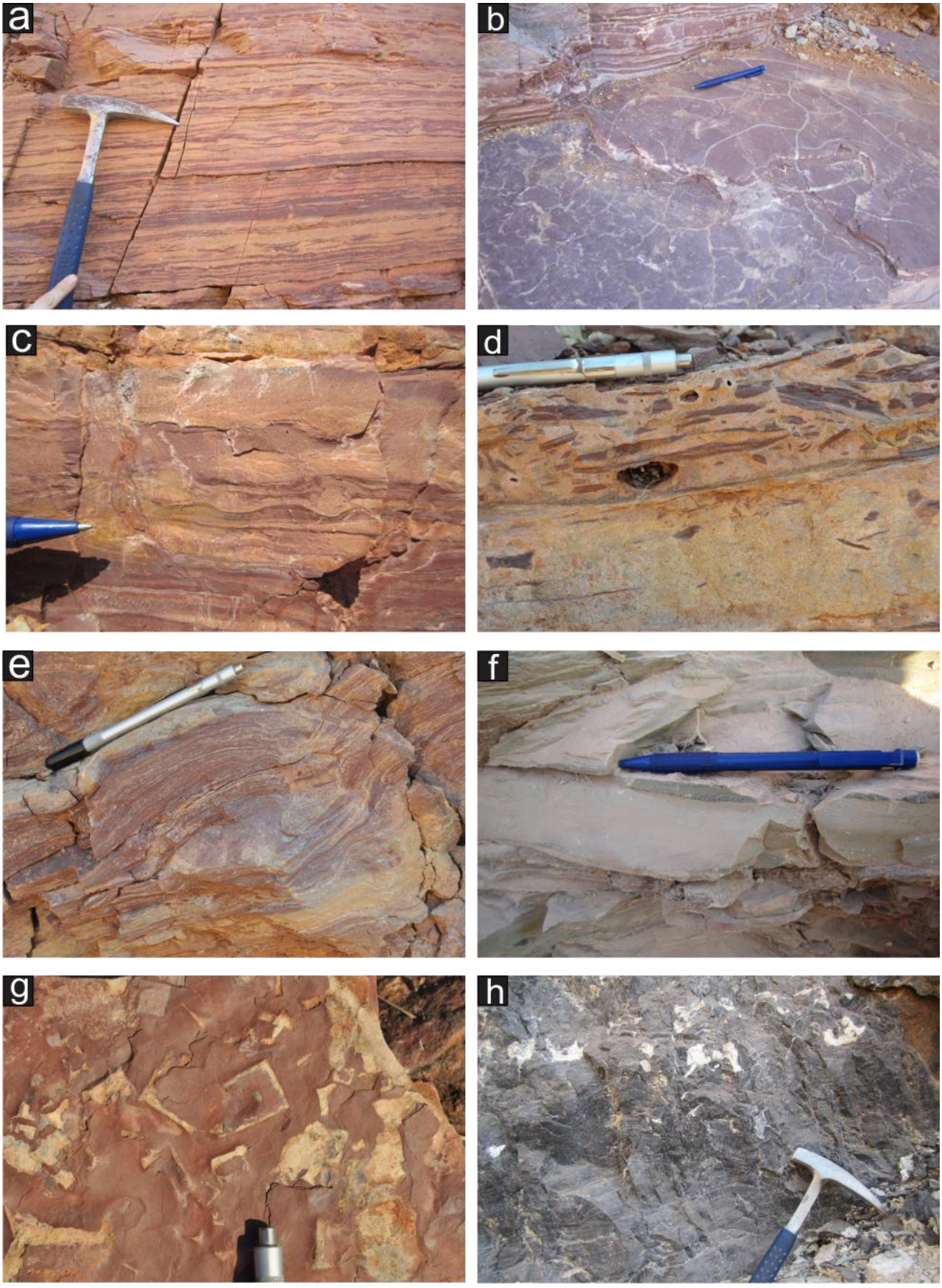

Figure 9.

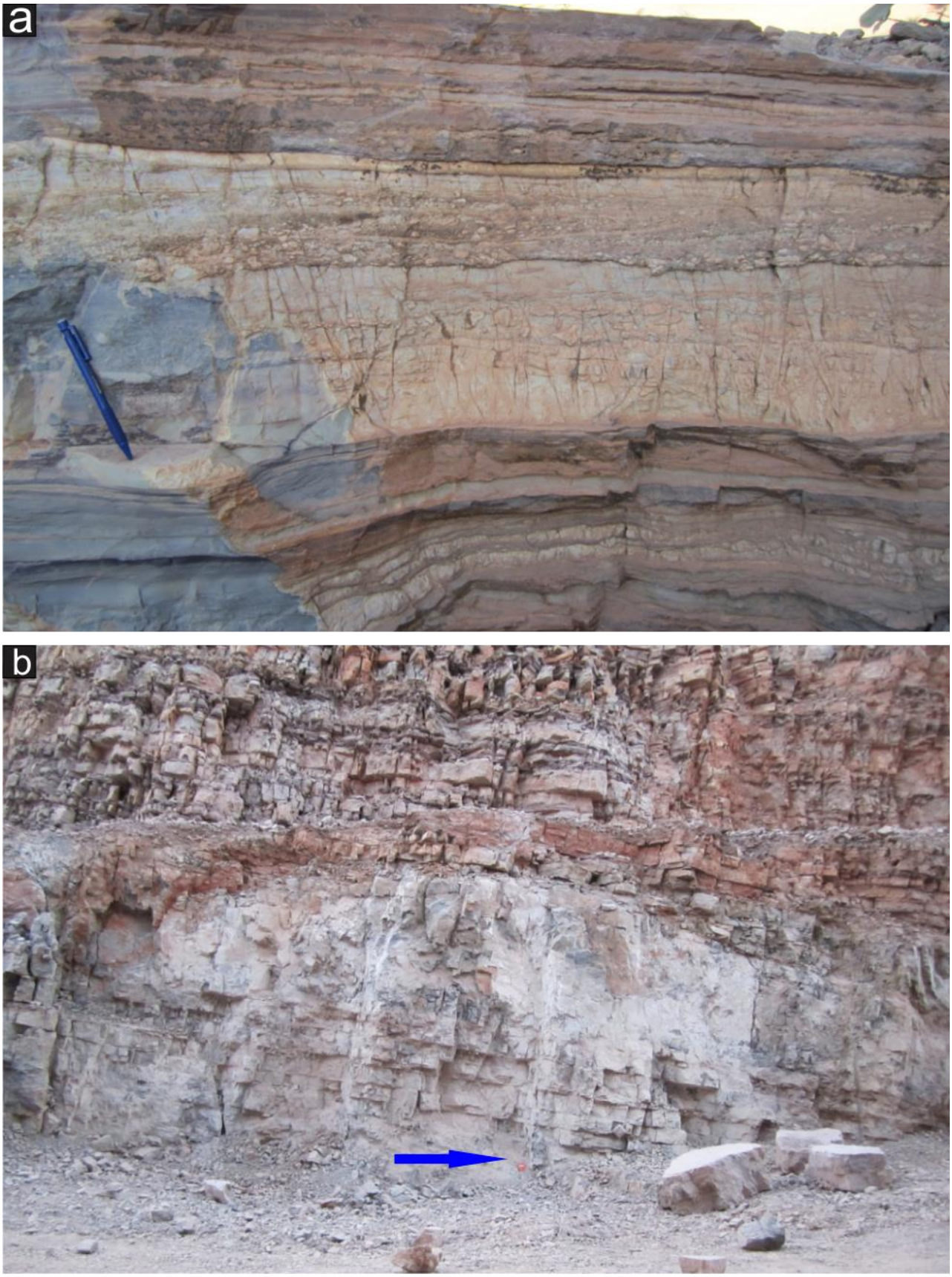

Figure 10.

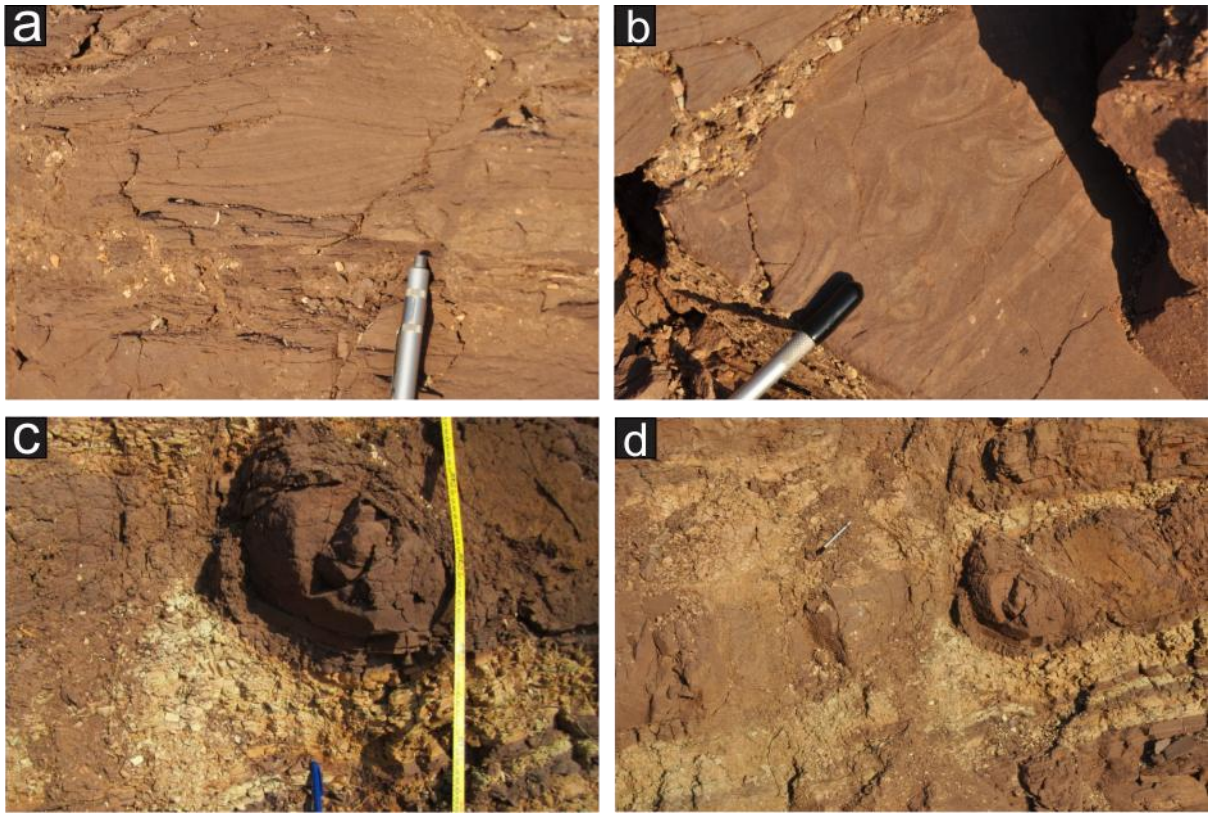

Figure 11.

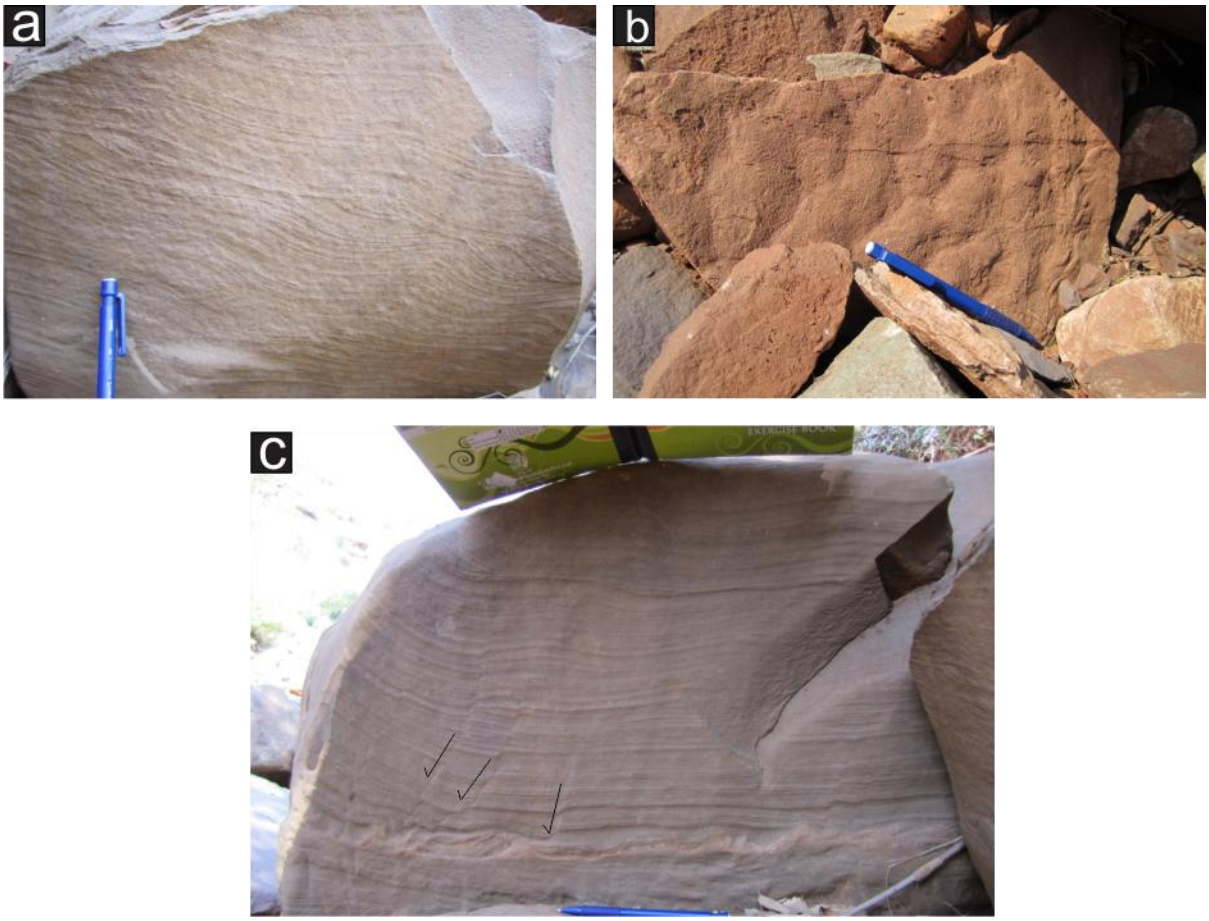

Figure 12.

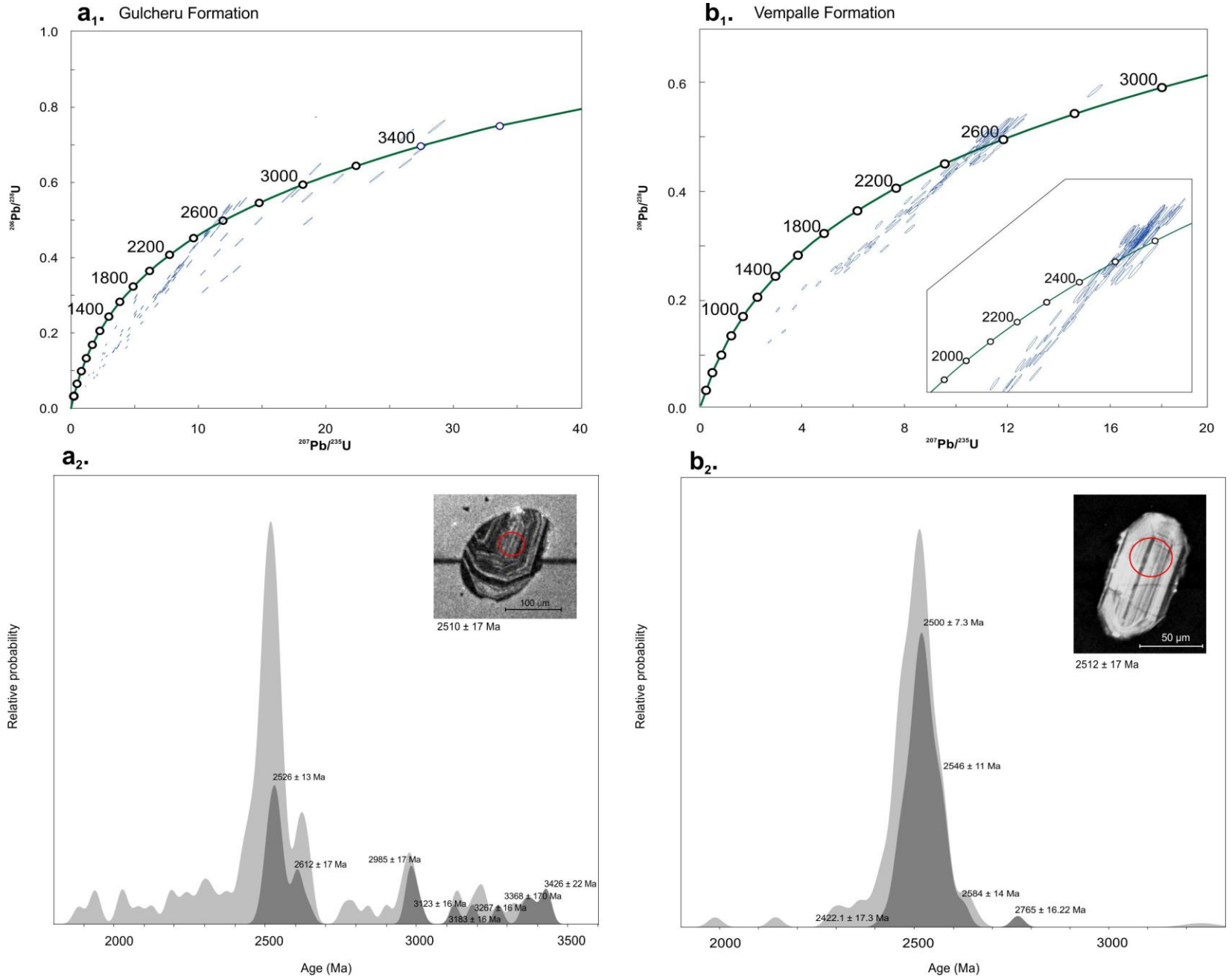
a1. Gulcheru Formation
b1. Vempalle Formation
a2.
b2.
Relative probability
Age (Ma)
2510 ± 17 Ma
2526 ± 13 Ma
2612 ± 17 Ma
2985 ± 17 Ma
3123 ± 16 Ma
3267 ± 16 Ma
3183 ± 16 Ma
3368 ± 17.0 Ma
3426 ± 22 Ma
2500 ± 7.3 Ma
2546 ± 11 Ma
2584 ± 14 Ma
2422.1 ± 17.3 Ma
2765 ± 16.22 Ma
2512 ± 17 Ma
100 µm
50 µm

Figure 13.

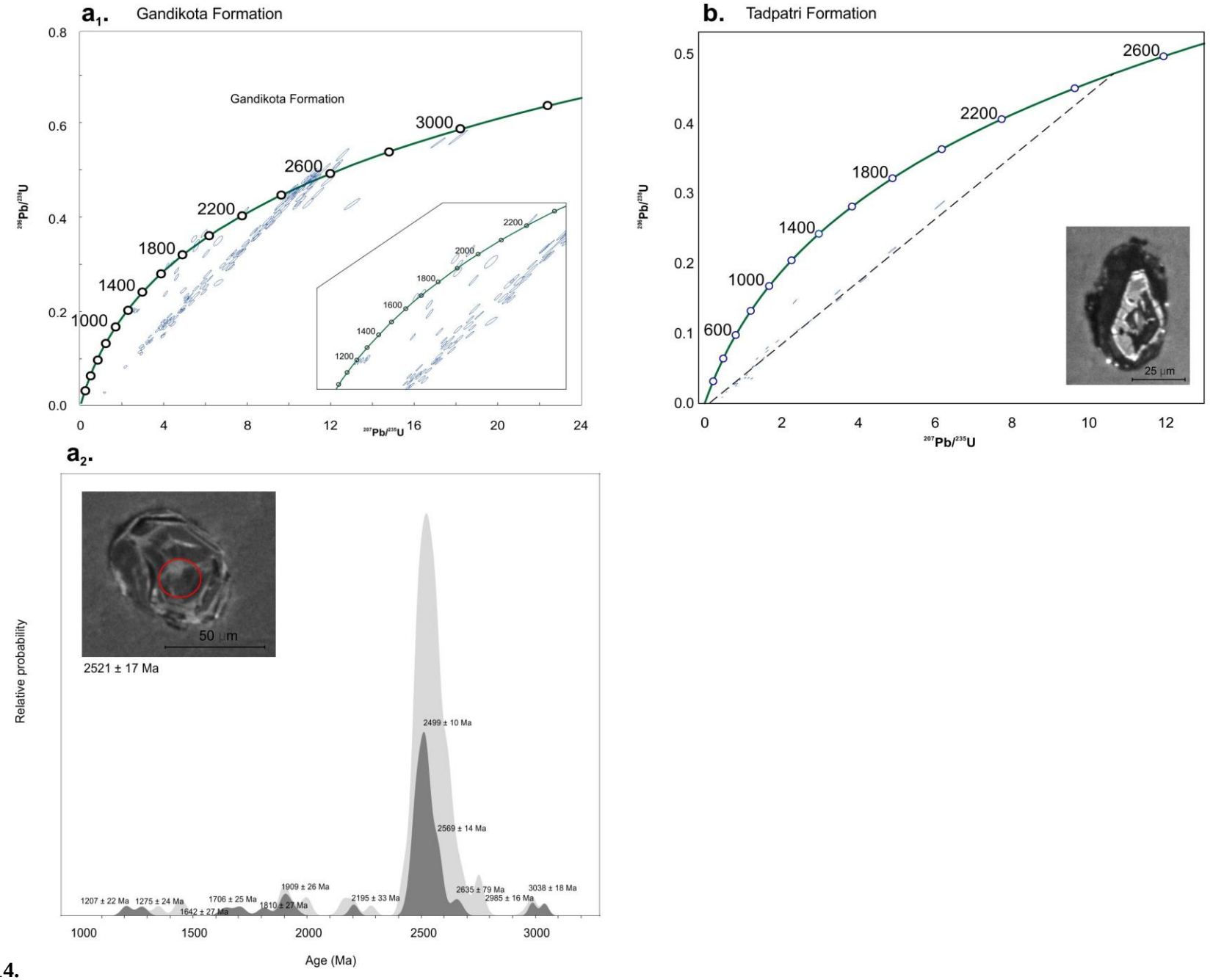
a1. Gandikota Formation
Gandikota Formation
$^{206}Pb/^{238}U$
$^{207}Pb/^{235}U$
1000
1400
1800
2200
2600
3000
a2.
50 µm
2521 ± 17 Ma
Relative probability
2499 ± 10 Ma
2569 ± 14 Ma
1207 ± 22 Ma
1275 ± 24 Ma
1642 ± 27 Ma
1706 ± 25 Ma
1810 ± 27 Ma
1909 ± 26 Ma
2195 ± 33 Ma
2635 ± 79 Ma
2985 ± 16 Ma
3038 ± 18 Ma
Age (Ma)
b. Tadpatri Formation
600
1000
1400
1800
2200
2600
25 µm

Figure 14.

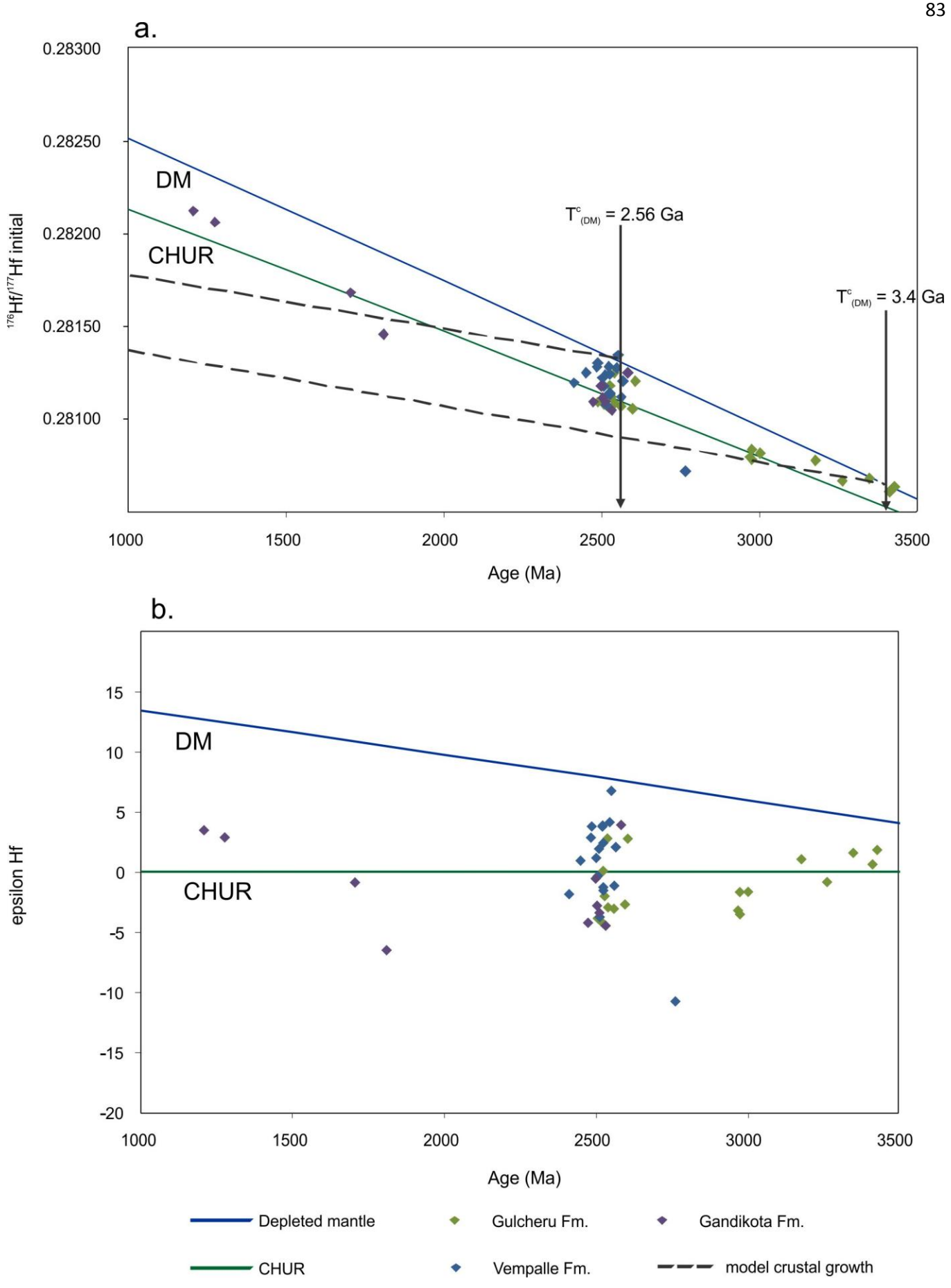
a.
0.28300
0.28250
0.28200
0.28150
0.28100
$^{176}Hf/^{177}Hf$ initial
DM
CHUR
$T^{c}_{(DM)}$ = 2.56 Ga
$T^{c}_{(DM)}$ = 3.4 Ga
1000
1500
2000
2500
3000
3500
Age (Ma)
b.
15
10
5
0
-5
-10
-15
-20
epsilon Hf
DM
CHUR
1000
1500
2000
2500
3000
3500
Age (Ma)
Depleted mantle
Gulcheru Fm.
Gandikota Fm.
CHUR
Vempalle Fm.
model crustal growth

Figure 15.

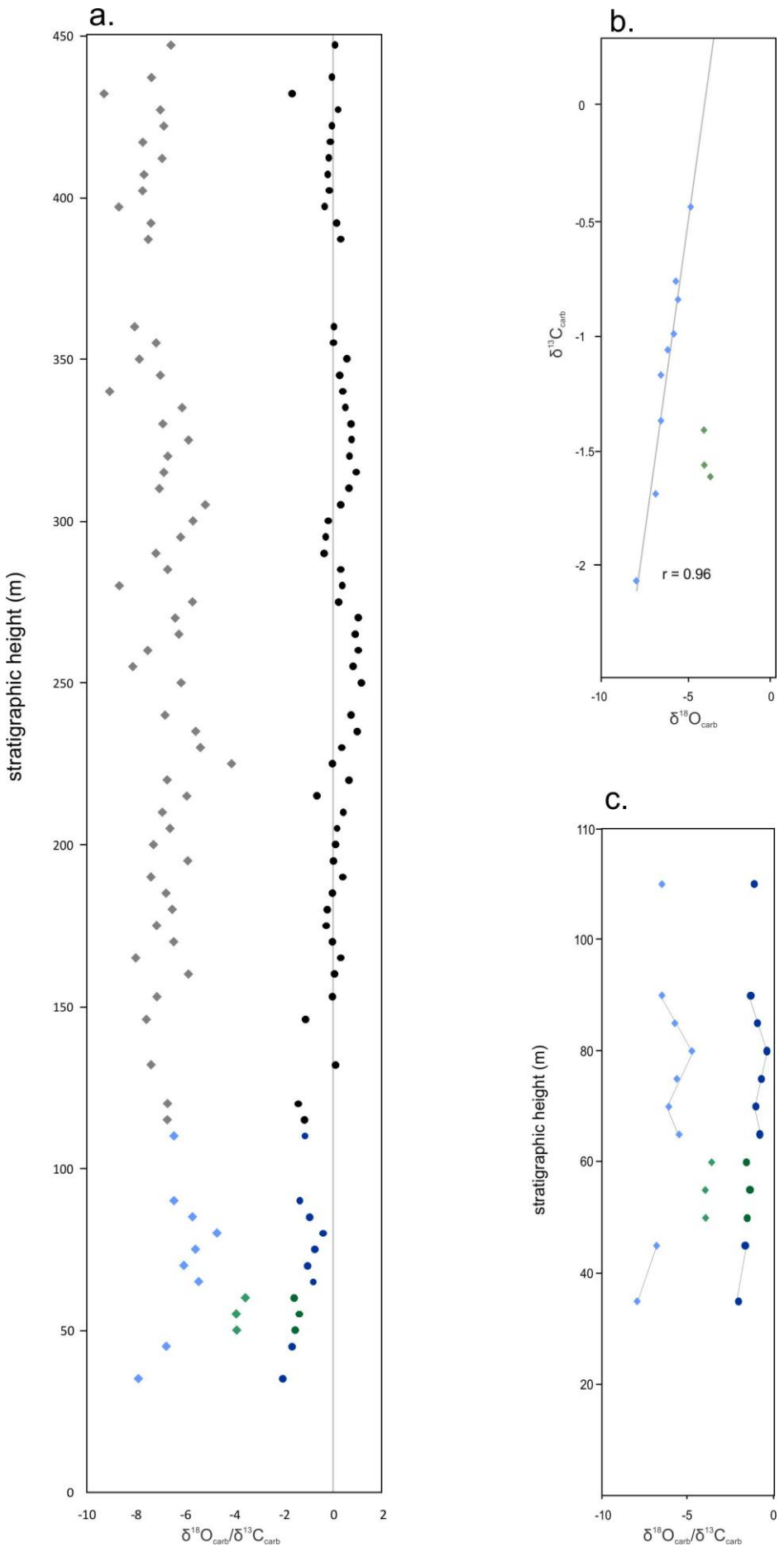
a.
stratigraphic height (m)
450
400
350
300
250
200
150
100
50
0
-10
-8
-6
-4
-2
0
2
δ18Ocarb/δ13Ccarb
b.
0
-0.5
-1
-1.5
-2
δ13Ccarb
r = 0.96
-10
-5
0
δ18Ocarb
c.
stratigraphic height (m)
110
100
80
60
40
20
-10
-5
0
δ18Ocarb/δ13Ccarb

Figure 16.

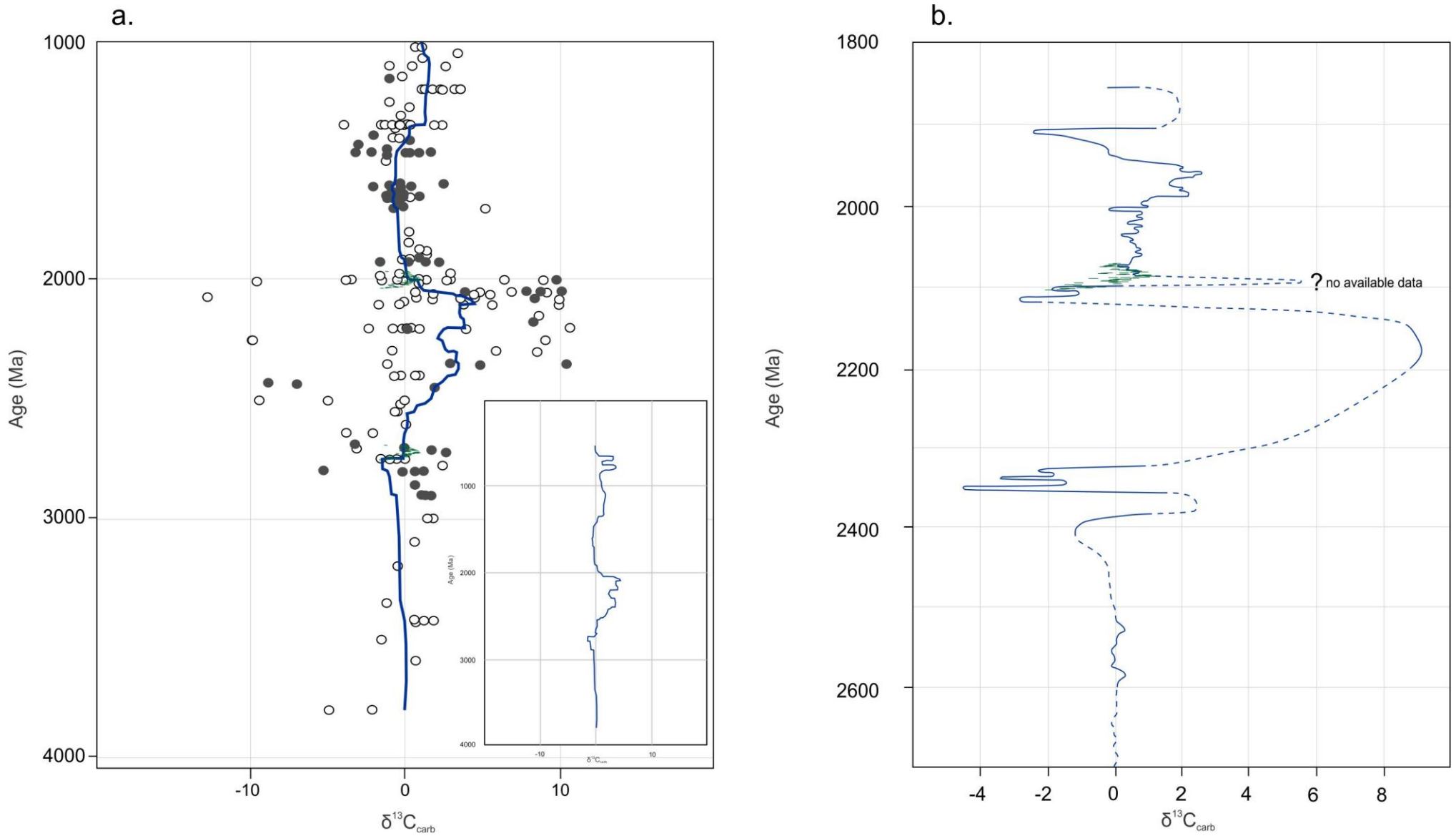
a.
1000
2000
3000
4000
Age (Ma)
-10
0
10
δ13Ccarb
b.
1800
2000
2200
2400
2600
Age (Ma)
? no available data
-4
-2
0
2
4
6
8
δ13Ccarb

Figure 17.

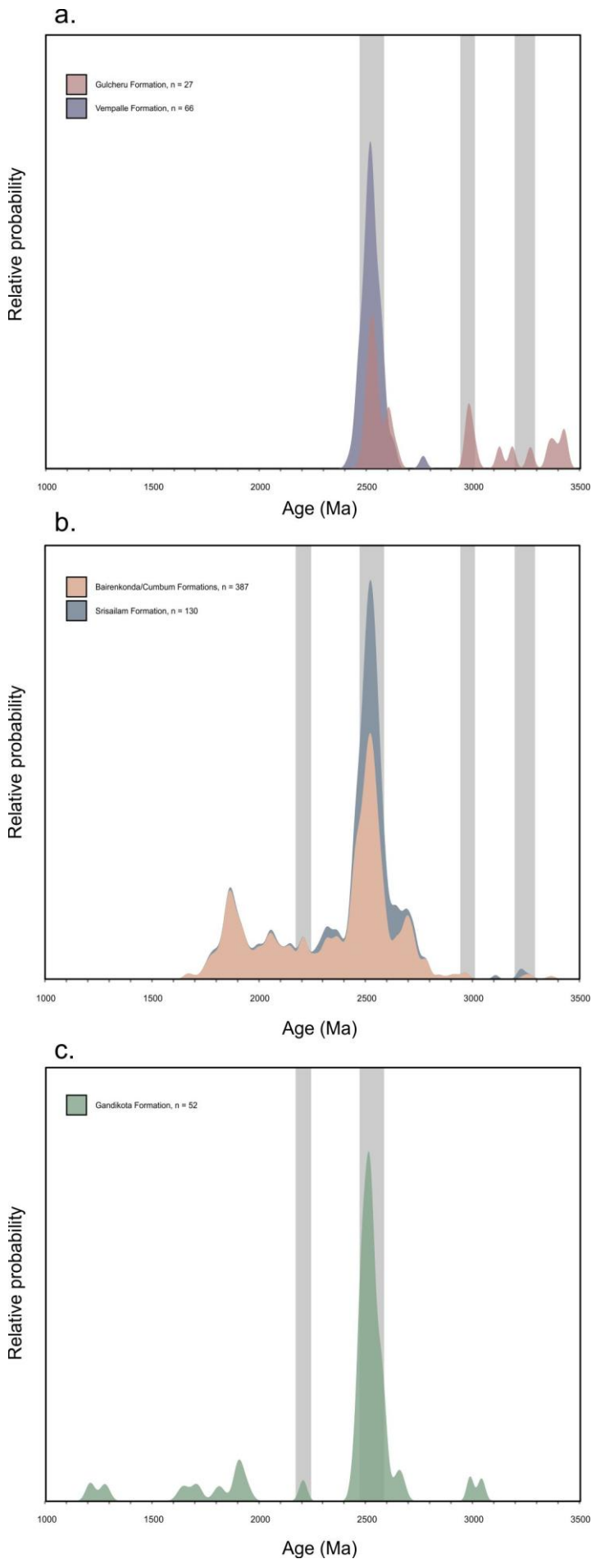
a.
Gulcheru Formation, n = 27
Vempalle Formation, n = 66
Relative probability
1000
1500
2000
2500
3000
3500
Age (Ma)
b.
Bairenkonda/Cumbum Formations, n = 387
Srisailam Formation, n = 130
Relative probability
1000
1500
2000
2500
3000
3500
Age (Ma)
c.
Gandikota Formation, n = 52
Relative probability
1000
1500
2000
2500
3000
3500
Age (Ma)

Figure 18.

Appendix I - Analytical Procedures

1 Stable isotope geochemistry

Samples were collected every five metres (where possible) along the section through the dolomitic Vempalle Formation in order to produce a record of change in isotopic composition up-section. Each sample was cut perpendicular to bedding to expose a clean face which was drilled to produce approximately five milligrams of fine powder. Discrete textures were sampled separately in order to avoid producing an average isotopic composition of different carbonate phases in the rock. Samples were sent to The Godwin Laboratory for Palaeoclimate Research at the University of Cambridge, where approximately 250 micrograms of the dried homogenised sample was transferred into exetainer vials and sealed with silicone rubber septa using a screw cap. Each sample was flushed with CP grade helium then acidified, left to react for two hours at 70^0C and then analysed using a Thermo Gas Bench preparation system attached to a Thermo MAT 253 mass spectrometer in continuous flow mode. Each run of 30 samples was accompanied by reference carbonates (Carrara Z) and two control samples (Fletton). Carrara Z has been calibrated to VPDB using the international standard NBS-19. The results are reported with reference to the international standard VPDB and the precision is better than +/- 0.08‰ for $^{12}C/^{13}C$ and +/- 0.10‰ for $^{16}O/^{18}O$. All isotopic data are provided in Appendix Table 6.

2 U-Pb zircon geochronology

Analytical techniques for U-(Th)-Pb isotopic dating of zircons follow the method outlined in Payne *et al* (2006). The isolation of zircon grains from each sample was undertaken at the University of Adelaide. Whole rock samples were crushed in a jaw crusher then milled to a medium powder in a tungsten carbide mill. The comminuted rock was passed through 75 and 125 µm mesh, then the 75-125 µm fraction was washed with water to remove residual dust and hand panned to concentrate heavy minerals. The final separate was obtained by passing the remaining grains through a Frantz magnetic barrier separator (up to 1.2 A) then methylene iodide to isolate non-magnetic grains with a density of above 3.32 g/cm^3. The resultant grains were washed with acetone then zircons were hand

picked using an optical microscope. After this stage of mineral separation, samples GF06 and GF09 yielded a small amount of and no zircons, respectively, so the remainder of the crushed rock from these two samples was sent to MinSep Laboratories in Denmark, WA to be separated.

Extracted zircon grains were mounted in epoxy resin then ground to a depth of approximately half of their thickness. The zircon mount was polished and carbon coated then imaged using a Philips XL20 scanning electron microscope with a Gatan cathodoluminescence detector in order to determine discrete domains within the zircons. A beam accelerating voltage of 15 keV and spot size of 7 were used to obtain backscattered electron and cathodoluminescence images.

LA-ICP-MS was used to determine the concentration of isotopes of uranium, lead and thorium within the zircons. Zircon grains were ablated in a helium atmosphere using a high performance New Wave Nd: Yag 213 UV laser. Ablation was performed with a spot size of 30 µm, repetition rate of 5 Hz and laser intensity of 75%. Total acquisition time was 100 seconds, with a 40 second gas blank analysis and 60 seconds of sample ablation, and the laser was fired for 10 seconds with the shutter closed prior to each ablation to allow for beam and crystal stabilisation. Dwell times for ^{204}Pb, ^{206}Pb, ^{207}Pb, ^{208}Pb, ^{232}Th and ^{238}U isotopes were 10, 15, 30, 10, 10 and 15 milliseconds respectively. Common lead was not quantitatively accounted for due to unquantifiable levels of ^{204}Hg interference on the ^{204}Pb peak. Monitoring of ^{204}Pb allowed for analyses to be disregarded if the zircon contained a substantial amount of common lead.

U-Pb fractionation was corrected for using the GEMOC GJ-1 zircon (TIMS normalisation data ^{207}Pb/^{206}Pb = 608.3 Ma, ^{206}Pb/^{238}U = 600.7 Ma and ^{207}Pb/^{235}U = 602.2 Ma; Jackson *et al.* 2004). Accuracy was monitored by repeat analyses of the in-house Plešovice zircon standard (ID-TIMS 206Pb/238U = 337.13 ± 0.37 Ma; Sláma *et al.* 2008). Over the duration of this study the reported average normalised ages for GJ-1 were 610.1 ± 2.2 Ma, 600.46 ± 0.77 Ma and 602.52 ± 0.74 Ma for the ^{207}Pb/^{206}Pb, ^{206}Pb/^{238}U and ^{207}Pb/^{235}U ages, respectively (2σ, n = 210). Reported average normalised ages for the Plešovice standard are 340.0 ± 6.7 Ma, 346.8 ± 2.9 Ma and 343.9 ± 2.6 Ma for the ^{207}Pb/^{206}Pb, ^{206}Pb/^{238}U and ^{207}Pb/^{235}U ages, respectively (2σ, n = 68). The ^{207}Pb/^{206}Pb age is

provided for all analysed grains, and concordancy was calculated by dividing the $^{206}Pb/^{238}U$ age by the $^{207}Pb/^{206}Pb$ age. A number of zircon grains were discounted due to metamictisation and above-background levels of common lead. Data reduction was completed using 'Glitter' software (Griffin *et al.* 2008) and a <10 % discordancy threshold was used to filter the data. Conventional concordia, weighted average and probability density plots were generated using Isoplot/Ex 3.00 (Ludwig 2003). Inputs to the Isoplot algorithms are the $^{207}Pb/^{235}U$ and $^{206}Pb/^{238}U$ isotopic ratios, their uncertainties at 1σ and the correlation coefficient for the construction of concordia diagrams, and the $^{207}Pb/^{206}Pb$ ages estimates and their 1σ uncertainties for the production of mean weighted ages and probability density diagrams. Where a detrital peak can be discerned from the probability density and weighted average plots, a mean weighted age of the zircons in that population has been calculated. Errors on all analysed grains are reported at 1 sigma. Isotopic data are provided in Appendix Tables 1A – 4C.

3 Hf isotope analysis

Laser spots were placed as close as possible to concordant U/Pb LA-ICP-MS spots, within the same CL zone. Zircons were ablated with a New Wave UP-193 Excimer laser (193nm) using a spot size of 50µm, frequency of 5 Hz, 4ns pulse length and an intensity of ~10 J/cm^2. Zircons were ablated in a helium atmosphere, which was then mixed with argon upstream of the ablation cell. Measurements were made using a Thermo-Scientific Neptune Multi Collector ICP-MS equipped with Faraday detectors and $10^{12}\Omega$ amplifiers. Analyses used a dynamic measurement routine with: Ten 0.524 second integrations on ^{171}Yb, ^{173}Yb, ^{175}Lu, $^{176}Hf(+Lu+Yb)$, ^{177}Hf, ^{178}Hf, ^{179}Hf and ^{180}Hf; one 0.524 second integration on ^{160}Gd, ^{163}Dy, ^{164}Dy, ^{165}Ho, ^{166}Er, ^{167}Er, ^{168}Er, ^{170}Yb and ^{171}Yb, and, one 0.524 second integration of Hf oxides with masses ranging from 187 to 196 amu. An idle time of 1.5 seconds was included between each mass change to allow for magnet settling and to negate any potential effects of signal decay. This measurement cycle is repeated 15 times to provide a total maximum measurement time of 3.75 minutes including an off-peak baseline measurement. This dynamic measurement routine is used to allow for the monitoring of oxide formation rates and REE

content of zircon and provide the option to correct for REE-oxide interferences as necessary. Hf oxide formation rates for all analytical sessions in this study were in the range 0.1-0.07%.

Hf mass bias was corrected using an exponential fractionation law with a stable $^{179}Hf/^{177}Hf$ ratio of 0.7325. Yb and Lu isobaric interferences on ^{176}Hf were corrected for following the methods of Woodhead *et al.* (2004). ^{176}Yb interference on ^{176}Hf was corrected for by direct measurement of Yb fractionation using measured $^{171}Yb/^{173}Yb$ with the Yb isotopic values of Segal *et al.* (2003). The applicability of these values were verified by analysing JMC 475 Hf solutions doped with varying levels of Yb with interferences up to $^{176}Yb/^{177}Hf$= ~0.5. Lu isobaric interference on ^{176}Hf corrected using a $^{176}Lu/^{175}Lu$ ratio of 0.02655 (Vervoort *et al.* 2004) assuming the same mass bias behaviour of as Yb.

Set-up of the system prior to ablation sessions was conducted using analysis of JMC475 Hf solution and an AMES Hf solution. Confirmation of accuracy of the technique for zircon analysis was monitored using a combination of the Plesovice, Mudtank and QGNG standards. The average value for Plesovice for the analytical session was 0.282479 (2SD = 0.000012, n = 17). This compares to the published value of 0.282482 +/- 0.000013 (2SD) by Sláma *et al.* (2008).

A number of grains were discarded due to an unacceptably high error, indicating a high level of REE and therefore a reduction in the effectiveness of the correction for Lu interference. These analyses are denoted with an asterisk in Appendix Table 5. T_{DM} and $T_{DM\ crustal}$ were calculated using ^{176}Lu decay constant after Scherer *et al.* (2001). $T_{DM\ crustal}$ was calculated using the methods of Griffin et al. (2002) with an average crustal composition of $^{176}Lu/^{177}Hf$=0.015. All isotopic data are provided in Appendix Table 5.

Appendix II - Detailed sedimentary observations, interpretations of depositional processes and assignment of facies.

1 Gulcheru Formation

1.1 Observations and interpretations

FACIES GM (CLAST-SUPPORTED POLYMICTIC CONGLOMERATE), 100-290 CM

This facies is characterised by 6 – 30 cm rounded clasts supported by a matrix of smaller (2mm – 5 cm) sub-rounded to sub-angular clasts and a dark coloured medium to coarse immature quartz sand matrix. The sediment is poorly sorted, and clasts are typically composed of microgranular quartzite (10-30 cm, ~ 40%), banded ironstone (BI) clasts (cherty and magnetic, with alternating red [5-10 mm] and black [1-5 mm] laminations – 40%) and milky white vein quartz (~20%). The proportion of BI clasts decreases up-section, as does the frequency of larger (20-30 cm) clasts. Degree of rounding of the sandy matrix increases up-section, and 5-10 cm breccia clasts with a red chert matrix and angular vein quartz clasts appear (< 5 %). This facies displays crude metre-scale bedding, and is generally conformably overlain by F2. Beds commonly fine upward slightly. Clast orientation varies from mostly random (base of the section) to strongly imbricated (higher in the section), or with only larger clasts aligned parallel to the bedding plane. Beds occasionally contain lenses of coarse sand with decimetre-scale planar cross bedding.

Depositional Processes

The very coarse, clast supported nature of facies Gm and presence of clast imbrication suggests deposition from tractional transport. The imbrication of clasts in a fairly uniform direction indicates unimodal flow to the east, where boulder sized clasts were entrained in a high energy turbulent flow. The relatively mature composition of the sandy matrix indicates that it may have been transported from a more distal source than that of the clasts, or re-worked an older quartzite or proximal aeolian environment. Both the polymictic nature of the clasts and their large size suggests that they have not

travelled far from their source. The lensoid cross-stratified coarse sand bodies fringed with strongly imbricated pebbles are likely to have been deposited as longitudinal bars.

FACIES ST (TROUGH CROSS-BEDDED GRANULAR SANDSTONE), 10-50 CM

This facies is characterised by compositionally mature decimetre-bedded medium to coarse sandstone. Grains are angular to sub-angular. The lithologies of the grains are quartz (60-80%), cherty red grains (20-40%) and occasional K-felsdpar and muscovite (<5%). Where this facies occurs immediately above F1, the contact is gradational. The sand grades from a basal granular to pebbly conglomerate comprised of sub-angular vein quartz (~2 mm-1 cm) clasts which appear near the base of the bed but fine out toward the top of the bed. Beds are massive and tabular, but often contain trough cross-bedding. Often contains small lenses of well sorted, well-rounded, more quartz-rich sand. Sedimentary structures occurring in this facies also include slump folding.

Depositional processes

The medium to coarse size of and presence of trough cross bedding in this facies indicates tractional deposition during periods of relatively high flow velocity. Slump folding may indicate current shear, or rapid deposition of sediment leading to sediment instability. The lensoid bodies of comparatively mature sand are likely to represent small (cm scale) individual channels during periods of relatively low flow velocity. The basal quartzose granular to pebbly conglomerate fining up to coarse sand suggests a waning flow velocity.

FACIES ST-GT: (CONGLOMERATIC TROUGH CROSS-STRATIFIED SAND), 130-220 CM

This facies is similar to facies St, but with multiple horizontally discontinuous cross-stratified conglomerate layers interbedded with the trough cross-stratified coarse sand. Bed thicknesses are ~20-40 cm. Sand grains are medium to coarse, and sub-rounded to sub-angular, and are compositionally mature – grain lithologies include ~60-95% quartz, 15-30% BI and lesser K-feldspar and muscovite. Conglomerate lenses are clast supported, and contain angular to sub-angular clasts of quartzite, BI and vein quartz, with clasts commonly displaying imbrication as well as centimetre to decimetre scale

cross-stratification. Occasionally, conglomerates are only one or two clasts thick, forming a pebble lag on the base of a scour. This facies typically contains small (up to ~7 cm) lenses of well sorted, well rounded more quartz-rich sand as well as fining-up layers. Sedimentary structures occurring in this facies also include scour and fill structures, and over-steepened foresets. The size of the troughs increases up-section.

Depositional processes

The pervasively cross-stratified nature of this facies and presence of interlayered imbricated conglomerate and sandstone signify tractional deposition under fluctuating flow strength conditions. Where scour-based conglomerate layers are only one or two pebbles thick, this may represent winnowing by strong currents at the erosion surface. Over-steepened foresets indicate a fluvial deposit (Wells *et al.* 1993), where a rapid aqueous current – most likely generated by a high flow event – can supply sufficient tangential shear to overturn foresets (Owen 1996). The lenses of relatively mature sand could represent small (cm-scale) individual channels. The increase in the size of the troughs may indicate a decrease in the water depth, or an increased flow velocity.

FACIES FL (LAMINATED SILTSTONE), 3-5 CM

This facies is defined by a fine grained siltstone. Beds are planar, and 0.5 – 1 cm. This facies only occurs overlying facies St, where it drapes the underlying sediments.

Depositional processes

The fine-grained nature of this facies coupled with the thin planar beds suggests deposition from suspension. This is likely to have occurred in a low-energy environment.

FACIES ST-SP: (CROSS-STRATIFIED QUARTZ ARENITE), 250-650 CM

This facies is defined by decimetre-bedded medium to coarse grained trough and (rarely) planar cross-stratified quartz sand. Grains are sub-rounded to rounded and ~ 100% quartz. Foresets are often steep (~40^0) and occasionally internally laminated, with the base of the foreset marked by small pebbles of vein quartz and BI, then fining up within the foreset lamination. Cross-bed sets vary from 5-50 cm in

thickness, increasing in thickness up-section. Pebbles also occur as lag deposits on the scour surfaces of trough cross-stratified beds (photo). The sand tends to fine up from coarse to medium sand within beds, and the size of the foresets also increases up-section. The cross-stratified beds occur in a series of stacked sand sheets.

Depositional processes

The presence of pervasive, generally steep trough cross-bedding suggests that tractional depositional processes were operating during the deposition of rocks of this facies. The appearance of occasional planar cosets suggests fluctuating current velocity, which is supported by the pebble lags seen on scour surfaces. The steep angle of the foreset s indicates that there was minimal suspended load, where the infrequency appearance of lower-angle cross-stratification indicates reduced flow velocity and an increased contribution from the suspended load (Kostaschuk & Villard 1996; Prothero & Schwab 1996). Where foresets are internally graded, this is likely to represent an alternation of deposition from avalanching particles and suspension fallout. The compositional and textural maturity of the sediment suggests that the sand was distally sourced, or came from a mature terrane. The presence of pebbles and varying bedforms represent deposition within a variable high energy environment, with fluctuations in the discharge rate.

NO EXPOSURE ZONE, 470-870 CM

Zones of no exposure are marked by silty micaceous shale interbedded with fine sandstone, as well as a reduction in the gradient of the topography.

Depositional processes

The appearance of the silty shale lag and lack of resistant outcropping rocks signifies a change in lithology, even though this lithology did not crop out in this area. The deposition of shale may have taken place under relatively low energy conditions, allowing fine-grained sediment to settle from suspension.

*1.2 **Lithological associations and environmental interpretations***

Two recurring facies successions have been identified within the Gulcheru Formation section. Facies St gradationally overlies facies Gm, reflecting a reduction in the energy of the flow resulting in an overall fining-up sequence. Facies Gm appears to show characteristics of both debris flow deposits (poor sorting, non-erosive bases) and stream flow deposits (rounded clasts, clast imbrication), and the lack of internal bounding surfaces indicates that each occurrence of facies Gm was deposited in a single event. Thus, facies Gm is interpreted here as bedload deposition from a high-magnitude stream flood on the basis of the weakly developed clast imbrication, crude stratification and common association with the occasionally cross-stratified pebbly sandstone facies, which is likely to represent a waning flow deposit from sand-laden turbulent flows (Todd 1989; Reading 1996). This is supported by the presence of the slump structures within sandy beds, which could have arisen from rapid deposition from suspension fall-out as the flood waned, or from current shear following deposition. Due to the large (up to 30 cm) size and high degree of rounding of the boulders, this association is likely to have been deposited quite close but not immediately adjacent to the source.

Additionally, facies Fl is only seen overlying facies St. In accordance with the depositional model proposed above, facies F1 is interpreted to represent deposition from the final stage of a flood event, in which suspended sediment settled out of standing water. The comparatively narrow bed width of this facies may be a product of a small suspended load due to reduced chemical weathering in the Precambrian, as a result of an absence of vegetation (Davies & Gibling 2010).

Given the imbricated gravel and pebbles, cross-stratified sand, lack of fine-grained floodplain sediment and presence of overturned foresets, facies St-Gt is interpreted as a pebbly braided stream deposit. The compositional maturity of the sediments suggests either distal deposition, or derivation from a mature or weathered source. The overturned foresets are likely to have been deposited during a high flow event, which indicates an ephemeral milieu. This is supported by the shifts between planar and trough cross bedding as well as scour-based conglomerate channels. This may have been in part due to the lack of vegetation in the Mesoproterozoic; before the advent of terrestrial plants, upstream

areas could not retain water during a storm event, so downstream fluvial areas were subject to intense flashy discharge (Davies & Gibling 2010).

Facies St-Sp is interpreted to represent a sandy braided stream of the 'South Saskatchewan' type (*sensu* Tucker 2001), which is characterised by a complex of planar and trough cross stratified sands, and a lack of fine floodplain sediment. This is likely to have arisen from fluctuating flow strength conditions, compounded by a lack of any stabilisation by terrestrial plants. The relative compositional maturity of the sediment indicates derivation from a distal source, or from exhumation of a weathered landscape. The interpretation of facies St-Gt and St-Sp as braided streams is supported by the work of Davies & Gibling (2010, and references therein) who propose that in the absence of stabilising vegetation and a large amount of fine-grained sediment, most if not all rivers adopted a braided style.

Taking into account the prevailing fluvial setting interpreted for the Gulcheru Formation section, the silts within the zone of no exposure are most likely to represent fine-grained floodplain sediment, deposited as overbank sediment, or during the waning stages of a flood, or in abandoned channels.

2 Vempalle Formation

2.1 Observations and interpretations

INTERBEDDED FINE SAND AND MUD, ~5-35 M (LU1)

This lithological unit is defined by interbedded fine grained sandstone and siltstone. The sandstone is well sorted and well rounded, and compositionally mature. Sand beds are planar and range from one to twenty centimetres, and are interbedded with shale beds of up to five centimetres. The sand often contains small symmetric ripples, or starved ripples when the sand percentage is less. The sand is also trough (and less commonly planar) cross stratified in the lowermost units of the section, with occasional herringbone cross stratification. Sand beds also occasionally contain small lenses of sub-rounded conglomerate, rip-up clasts of mud, or gritty sand. Shale beds are variably grey-green or red, and generally contain polygonal desiccation cracks. Shale also frequently drapes the troughs and crests of sandy ripples. Flaser bedding occurs within the basal ~10 m of the section, and then lenticular bedding with connected lenses (*sensu* Reineck & Wunderlich 1968) is common, and often

contains small flame structures. Where a sand bed overlies a shale bed with desiccation cracks, it occasionally contains rip-up clasts of the underlying shale, and sand beds commonly show normal grading to shale. Occasional ball and pillow type structures occur. This unit also features intermittent laterally impersistent algal laminites with black crinkly seams or small (5-10 cm in width; 4-15 cm in height) columnar or domal stromatolites exposed in cross-sectional view. In beds with a higher calcareous component, laminoid or irregular fenestrae are present, which are filled with sparry calcite or black sulphide.

Depositional processes

The planar interbedded rippled sand and shale suggests deposition by a combination of suspension fallout and tractional processes. The finest sediments are likely to have been deposited during slackwater periods, when muds could settle out of suspension, whereas the sand was deposited in a relatively active environment. The ripples within the sand are symmetric, which is indicative of bimodal flow, as is the presence of herringbone cross-stratification. Where starved ripples are present, this suggests a limited sediment supply. The dominantly trough- but occasionally planar cross stratification indicates a sporadically fairly high energy environment. The small intraformational conglomerate lenses within the sand suggest deposition within small channels. Laminoid and irregular fenestrae indicate the parting of laminae and gas entrapment resulting from desiccation, and hence are indicative of sub-aerial exposure (Tucker 2001). Further evidence for frequent sub-aerial exposure is provided by the pervasive polygonal desiccation cracks within the shale. Crinkly algal laminites suggest a moderate degree of subaerial exposure (Ginsburg *et al.* 1977). Flaser and (more commonly) lenticular bedding signify the alternate deposition of mud and rippled sand, and small flame structures within the sand beds indicate that the sand units were deposited rapidly. The basal rip-up clasts of shale within some sandy beds suggests a high energy event, where the force of the incoming sand was sufficient to rip up clasts from the underlying bed. This implies deposition during a storm event, which is supported by the presence of normally graded beds with erosive bases. These features combined suggest a high energy, storm dominated environment with bimodal flow, which was punctuated with periods of quiet, stillwater deposition and subaerial exposure.

DOLOMITE WITH INTERBEDDED SAND AND MUD, ~20 M (LU2)

This unit is defined by 10-20 cm stromatolitic dolomite beds alternating with cm-scale muddy beds, with increasing sand up-section, developing into sandy beds interspersed with cycles of carbonate and shale. Muddy beds contain polygonal desiccation cracks, and sandy dolomite beds occasionally contain a basal layer of rip-up clasts of the mud. Algal mat laminations occur in the lowermost few metres of the assemblage, and irregular fenestrae filled with black sulphides or sparry calcite occur within dolomite beds throughout the assemblage. Sand content of the dolomite beds increases up-section, until sandy beds intercalate with the dolomite. Sandy beds are occasionally wavy, with mud draped in the troughs.

Depositional Processes

The interbedded dolomite and mud (then sand) suggests alternate trapping and binding of sediment by cyanobacteria associated with chemical precipitation, with deposition from suspension. The very fresh exposure and consequent lack of visible bedforms within the dolomite beds makes it difficult to characterise the depositional processes more thoroughly. Polygonal desiccation cracks within the shale, irregular fenestrae and algal mat lamination all suggest that this environment was intermittently sub-aerially exposed, whilst the deposition of the mud and dolomite must have taken place sub-aqueously. The increase in sand within the dolomite beds reflects an increase in the energy of the depositional environment (Reading 1996), and the presence of basal rip-up clasts of shale within sandy beds supports this. The increase of sand up-section also indicates an increase in availability of sediment to the system.

THICKLY BEDDED DOLOMITE WITH MIXED SAND, 100 M (LU3)

This lithological unit is characterised by thick laterally persistent stromatolitic dolomite beds with tabular to well develop pinch and swell geometry. Dolomite beds contain sand, which occurs either mixed in with the dolomite, or as very fine beds (2-5 mm) interlayer with dolomite beds. Where sand is mixed in with the dolomite, hummocky cross-stratification is evident. Scour and fill structures also occur within the sandy dolomite. Occasionally sandy beds occur with erosional bases, which contain

intraformational clasts of the underlying dolomite, many of which are aligned with the bedding plane. Stromatolites within dolomite beds are generally columnar.

Depositional processes

The thickly bedded depositional style of this facies may signify deeper-water sub-aqueous deposition (Masse *et al.* 2003). This is supported by the lack of any sub-aerial sedimentary features, which are prevalent throughout most other assemblages within this section. The mixed sand with carbonate indicates a high-energy environment, and the presence of HCS reflects the presence of strong oscillatory flows (Reading 1996). Thin layers of sand on the base of dolomite beds are likely to be the result of discrete storm events, as are the rip-up clasts within sandy beds. The scour and fill structures indicate storm influence on deposition (Reading 1996).

STROMATOLITIC DOLOMITE, ~20-35 M (LU4)

This unit is characterised by 20-30 cm dolomite beds occasional 5-10 cm muddy intervals. The dolomite beds contain stromatolites and algal laminites as well as occasional low-angle ripples. Bed thicknesses increase up-section, and the frequency and thickness of the muddy intervals decreases. The shale layers contain desiccation cracks, and dolomite beds near the base of the unit feature large irregularly distributed fenestrae. Other features observed include prominent chert nodules, and very occasional lensoid sand bodies.

Depositional processes

The occasional occurrence of low angle ripples within dolomite beds indicates some deposition through tractional processes, and that there must have been some granular component to the dolomite. The occasional lensoid sandy bodies may represent storm events with a greater input of siliciclastic material. The algal laminates as well as stromatolites within the dolomite suggest very shallow water, with occasional sub-aerial exposure. Polygonal desiccation cracks and irregular fenestrae are also likely to have developed during these exposure periods.

SHALE WITH INTERBEDDED SAND, ~10 M (LU5)

This unit features thinly bedded red to brown shale which contains both desiccation cracks and halite pseudomorphs. Halite pseudomorphs range from 1-2 cm in size, and are generally ~square in shape, and display some internal zoning. The shale is intercalated with thin impersistent beds of fine grained quartz arenite, which occurs near the base of the section as lensoid scour and fill structures, or as lenticular bedding. Sand content increases throughout the section, and features cm-scale fining up sequences and planar cross-stratification, as well as straight crested or interference ripples. Planar cross-stratified sand beds contain basal rip-up clasts of shale.

Depositional processes

This facies assemblage appears to have been deposited through a combination of suspension fallout and tractional processes, and the decrease in mud relative to sand up-section suggests a gradual increase in the energy of the depositional setting. Desiccation cracks and halite pseudomorphs within the shale signify evaporative conditions. The intercalation of shale and arenitic sand implies periodic higher and lower energy conditions, possibly representing storm events; this is supported by the presence of basal rip-up clasts of shale in planar cross-stratified sand beds. Straight crested ripples and planar cross-bedding suggest a fairly low flow velocity, and interference ripples indicate a very shallow environment. Loading structures indicate rapid deposition of sand above unconsolidated mud. The internally zoned nature of some halite crystals suggests incorporative growth within the sediment (Erikksson *et al.* 2005).

INTERBEDDED DOLOMITE AND MUD, ~10-65 M (LU6)

This unit is defined by interbedded grey dolomite and pink to red mud in varying thicknesses. Dolomite beds are up to ~60 cm, and are stromatolitic, or contain algal laminites. The dolomites occasionally contain a small proportion of sand, and occasionally feature current scouring and small symmetric ripples on the top of beds. Spheroidal chert nodules also occur within the dolomite beds. Dolomite beds are separated by a muddy parting. The mud is thinly bedded, in planar parallel beds of

~one centimetre. Very large micritic stromatolite mounds several metres in length and > 2 metres in height occasionally occur, and these are draped with mud.

Depositional processes

The fairly cyclical depositional of planar laminated mud and dolomite may suggest an alternation between chemical precipitation of carbonates and still-water deposition of siliciclastic sediment from suspension. The presence of algal laminites as well as stromatolites indicates shallow water. The sporadic appearance of sand and occasional scour features and ripples indicate a quiet depositional setting with occasional high energy events. The large stromatolite mounds may represent extended periods of quiescence, interspersed by deposition of mud from suspension. This assemblage represents a continuously sub-aqueous shallow low-energy environment with occasional higher energy events.

INTERBEDDED SANDY DOLOMITE AND MUD, WITH OCCASIONAL SAND BEDS, >45 M (LU7)

This lithological unit is characterised by intercalated dolomite and mud, with occasional sand beds. All dolomite beds contain stromatolites and/or algal laminites, and vary in colour from light to dark grey. Beds contain varying amounts of sand, and occasionally exhibit rippled bed tops. Sand beds contain trough cross-stratification. Further internal structures were not visible due to preferential shearing along the sand beds. Mud layers are fissile, and either brown or green in colour. Lenticular bedding and flame structures were observed. This assemblage was further divided into discrete lithologies:

L1, 15-350 cm: Decimetre bedded light grey stromatolitic dolomite beds with mixed sand. Beds have rippled top surfaces.

L2, 30-500 cm: 30-100 cm bedded grey stromatolitic dolomite, with algal laminites and rippled bed tops.

L3, 15-150 cm: Thickly bedded laterally persistent tabular dark grey stromatolitic dolomite. Predominant stromatolite morphology is the ‘laterally linked’ columnar type.

L4, 10-95 cm: Decimetre bedded light grey chertified limestone, with chert nodules. The limestone appears to have been micritic.

L5, 23-80 cm: Trough cross-stratified fine grained quartz arenite, with rippled bed tops. With occasional ~1 cm fining-up sequences.

L6, 10-125 cm: Very fine-grained fissile brown or green mudstone. Occasionally with layers ~5 cm with erosive-based sand grading up into mud, with some flame structures and occasional lenticular bedding.

L7, 15-120 cm*:* Calcareous brown shale with thin pale calcareous layers. Beds are 5-10 cm, and the shale contains rare polygonal desiccation cracks.

In general, decimetre-scale beds of L4 alternate with decimetre-scale beds of L7, until nearer the top of the unit, where L6 tends to occur rather than L7. These shales and muds are interspersed (on a metre scale) with thick stromatolitic dolomite beds, with increasing sand beds appearing in association with the dolomite beds nearer the top of the section, where the dolomite beds become more frequent.

Depositional processes

This facies represents an alternation between a deposition from suspension, and precipitation of carbonate beds with the growth of stromatolites, with increasing tractional deposition of sand up-section. The laterally linked stromatolites are likely to have been deposited in shallow water with limited wave action (Logan *et al.* 1964).

2.2 Lithological associations and environmental interpretations

Two alternate depositional settings may be proposed for this succession; sediments could plausibly have been deposited in a saline lacustrine setting, or a shallow marine setting. The lacustrine model is supported by the frequent occurrence of subaerial exposure features which are present throughout the succession, and which are common in ancient lacustrine deposits (Reading 1996). However, in general, processes which operate in marginal lacustrine settings are similar to those of shallow marine

settings, so with the exception of LI (to provide an example) where such similarities exist, they are not discussed further; an outline of the proposed lacustrine depositional setting is provided following the shallow marine interpretation, but in general, depositional processes remain as described below.

The association of lithologies and sedimentary structures in LU1 could represent deposition in a muddy peritidal setting, with a restricted sediment supply and occasional high energy events, where symmetric ripples and herringbone cross-stratification suggest bi-modal flow. Rippled sand beds may have been deposited by an individual tide, with mud draping the ripples in the following slack water deposition. The association of desiccation cracks and fenestrae is likely to have developed in periods of sub-aerial exposure, and indicates deposition in the intertidal zone (Reading 1996). Lenticular bedding is also likely to have developed in the intertidal area (Reineck & Wunderlich 1968; Walker & James 1992). Flame structures within lenticular bedding and basal rip-up clasts in sand beds overlying mud indicate rapid deposition, and may have resulted from higher energy storm events. The reduction in frequency of desiccation cracks up-section, and the appearance of stromatolites indicates a slightly deeper-water setting, and may signify a transition to the upper subtidal zone. Graded bedding within this zone indicates occasional storm events, where sand scoured out the underlying mud, then progressively finer sediments were deposited as the energy of the event waned.

Alternatively, the deposition of LU1 may have occurred in a marginal lacustrine setting, as with the exception of varves, no uniquely diagnostic features occur in lake deposits, and many sedimentary structures of lacustrine deposits are similar to those of shallow marine sediments (Boggs 2001). Sand may have been supplied to the lake from a distal fan setting, and ripples and cross stratification may have originated from wave action on the lake beach during lake high-stand (Buck 1980). Mud drapes may similarly have been deposited during quiescent conditions. Fining-up sequences may represent waning sheet flood deposition as water flowed into the lake and decelerated. Storm deposits in lakes may be anomalous to those seen in shallow marine settings (Reading 1996), and hence high-energy events described above hold the same interpretation here. The frequent presence of desiccation features indicates fluctuating water levels, and periodic exposure. This unit may represent a mudflat, where graded or rippled sand beds along with sand beds with rip-up clasts were deposited due to wave

agitation during lake high-stand or during storms or periods of high sediment influx (e.g. flood events) and then muds were deposited in the following slack water stage. This is similar to the 'marginal lacustrine facies assemblage' of Elmore *et al.* (1989). Following this interpretation, all subsequent lithological changes may be due to fluctuations in the water level of the lake, as a result of the precipitation/evaporation ratio of the setting.

Shallow marine interpretation

LU1 is gradationally overlain by LU4, which represents the first occurrence of dolomite beds within the Cuddapah Supergroup. The presence of polygonal desiccation cracks, fenestrae and tepee structures within this unit indicates shallowing of the environment, which may have occurred as the rate of deposition overtook the rate of subsidence, with carbonate rocks being precipitated when the water level was higher. This lithological unit may represent deposition within the lower intertidal zone, where the surface was still occasionally sub-aerially exposed but carbonate was precipitated subaqueously when there was a limited supply of siliciclastic material.

LU4 is overlain by a relatively muddier, frequently sub-aerially exposed and variably stromatolitic succession of LU5, LU2 then again LU5. LU4 fines up into the low energy evaporative LU5. The lower part of this unit is likely to have been deposited in a coastal sabkha-like environment where extended periods of evaporation led to the desiccation of mud and the precipitation of halite crystals (in a similar manner to the lower Oaktree Formation; Erikksson *et al.* 2005). The lack of evidence of sulphates in this unit does not preclude the sabkha interpretation, as the chemical composition of seawater was not favourable to the precipitation of sulphates until ~1840 Ma, and sulphides are rare in pre-Phanerozoic deposits (Grotzinger & Kasting 1993; Pufahl *et al.* 2010). The interpretation of this unit as having been deposited in a very shallow environment is supported by the presence of interference ripples. Occasional storm events are likely to have introduced fine sand into the system – this was likely to have been rapid and relatively high energy, as evidenced by the loading structures and basal rip-up clasts of shale in sand beds. The increase of cross-stratified sand up-section suggests a slight increase of both the water depth and the energy of the system.

Alternatively, LU5 may have been deposited in small, fairly transient pools within the upper intertidal zone. The finer sediments relative to the over- and underlying strata signify a greater proportion of deposition from standing water, and the precipitation of halite may signify an increased NaCl concentration. The sandy beds indicate that this unit is still influenced by the tide, and is therefore not likely to be a sabkha deposit.

In this case, LU5 may represent relatively small, transient sabkhas which developed during periods of extended exposure, but did not develop into mature coastal sabkhas. In each case, LU5 is under- and overlain by slightly deeper water deposits, which indicates that the deposit may have been

The two observed occurrences of LU5 are separated by the ~20 m thick LU2, which is similar to LU4 in that it represents intermittent subaqueous precipitation of calcareous sediment, growth of stromatolites and deposition of sand and mud with subaerial exposure and desiccation. This suggests an interspersion of slightly deeper water, most likely to the intertidal zone. The chief difference between this unit and LU4 is that increased proportion of sand, which occurs both within dolomite beds and as discrete sandy beds. This indicates a greater input of siliciclastic material into the system, and relatively higher energy.

LU2 is overlain again by LU5, which represents a return to very shallow, probably upper intertidal conditions. This succession may represent a period in which sedimentation was of a comparable rate to subsidence, and hence the rate of deposition determined the degree of exposure; when the rate of sedimentation was slightly higher than that of subsidence, evaporative pools developed, then the reduced rate of deposition in this environment led to a slight increase in water depth. Alternatively, this could represent a period of eustatic fluctuations, where the sea level determined the depositionary environment.

This succession is in turn overlain by LU4, representing deepening water and a return to an extended period of lower intertidal conditions, with a limited input of siliciclastic material. The transgressive trend continues with the deposition of LU6, which overlies LU4. The deposition of planar laminated muds from suspension alternating with the development of stromatolites, and with occasional limited

input of siliciclastic material may have occurred within a subtidal lagoonal setting (Reading 1996). Stromatolites are likely to have accumulated whilst the water was clear, The occasional rippled sand beds with scoured bases may represent washover sand deposited during episodic storm events (Boggs 2001).

The transition from LU6 to the overlying LU3 suggests a transition to a relatively higher energy, deeper water deposition setting. Mud is absent, as is any evidence of sub-aerial exposure. Sandy layers at the base of dolomite beds are likely to have been deposited by individual storm events which increased the proportion of siliciclastic material in the system. These storm events are likely to have been of high magnitude, as occasionally dolomite clasts are found within the sandier beds. This unit is therefore likely to represent an extensive period of storm-influenced subtidal deposition.

LU3 is overlain by LU6, representing a return to a quieter depositional setting. The presence of large stromatolite mounds within this occurrence of LU6 represents extensive periods of quiet-water deposition, and suggests that the growth of large stromatolite mounds may have been at least partially responsible for the protection of the environment from the effects of wave and storm action. The absence of any mud within the stromatolite mounds, and the draped nature of the overlying mud beds suggests that the mounds may have grown in clear water conditions. This is likely to represent deposition in a relatively deep water setting with a limited, sporadic siliciclastic input (Simonson *et al.* 1993).

LU7 appears to represent a series of deepening-up cycles, where thick stromatolite beds are likely to have been deposited in fairly quiet shallow water, then shale and mud beds were deposited in deeper water. The energy of the setting appears to increase with the increase in stratigraphic height, as evidenced by the increase of sand mixed with dolomite up-section, as well as the appearance of discrete sandy beds.

Lacustrine interpretation

Where LU1 is overlain by LU4, this may represent a slight deepening of the lake, which was followed by a relative fall in water level for the deposition of LU5 and LU2. The presence of halite

pseudomorphs indicates that this would have to have been a saline lake, and the LU5-LU2-LU5 sequence represents an extended period of lake low stand, which was sporadically affected by storm events which increased the input of siliciclastic material into the lake, and left scour-based sand beds with basal rip-up clasts.

The re-appearance of F4 and transition to LU6 signifies an increase in the depth of water within the lake, along with an increase in siliciclastic input into the basin. This could be due to distal processes, with a greater amount of sand transported into the basin by fluvial processes, possibly due to storm events. This may represent a storm-influenced subtidal setting, similar to the shallow marine setting proposed above.

The deposition of LU6 may represent further deepening of the lake, and growth of stromatolites beyond the immediate influence of storm events. Conversely, the lack of sand or storm signatures in this uni may represent a change in fluvial activity around the lake, or a reduction in overall energy of the environment.

LU7 may represent cyclical fluctuations in the water level of a lake, where individual fining-up sequences occur over approximately 10 to 12 m.

3 Tadpatri Formation

3.1 Observations and interpretations

FINE SAND, 2-60 CM (F1)

This facies is characterised by a very fine to medium grained purple arkosic sandstone. It typically occurs in beds of ~2 cm which are generally planar but occasionally wavy. Beds are often planar laminated (with mm-scale alternations of fine sand and silt), or contain hummocky cross-stratification. These fine sand beds occasionally occur with a scoured contact above shale, then fine up slightly to silt-sized grains. Fining-up sequences are also seen in sand beds without an erosive contact. Fluid escape structures occur in places at the bottom of beds where the sand occurs over

shale, and some beds have loaded bases. Small (2-3 cm) ball-and-pillow structures also occur within sand beds which lie over shale.

Depositional processes

This lithology is likely to have been deposited by a combination of suspension fall-out and tractional processes. Where the sand is planar-laminated with silt, this may represent deposition from suspension (Tucker 2001). The presence of hummocky cross stratification indicates oscillatory flow conditions as well as tractional deposition processes. Where normally graded beds of L1 occur with a scoured contact above shale, this may reflect a relatively high energy event where progressively finer sediments were deposited by a flow of waning strength i.e. a turbidity current (Boggs 2001). Where normally graded beds of F1 occur *without* an erosive contact, this may suggest deposition of progressively finer sediments from suspension. Fluid escape structures and loaded bases within this unit signify rapid deposition above unconsolidated sediment. The presence of small ball-and-pillow structures also indicates a high sedimentation rate. This lithology is likely to reflect a dominantly moderately high energy setting which was occasionally affected by higher energy events.

HIGHLY CONVOLUTED FINE SAND WITH SHALE, 175 CM (F1A)

This lithology occurs in one bed only; it is nominally composed of fine sand, however it is dominated by extensive syn-sedimentary deformation. This bed is deposited over shale, and the base of the sand contains large (dm-scale) flame structures. This bed also contains well developed ball and pillow structures, where the sand which forms the balls is internally laminated, and the laminations have been curved to conform to the edge of the ball. The interior of the sand balls is relatively massive. Sand balls are ~20 cm in diameter.

Depositional processes

The internal laminations within this sand suggest that it may have initially have been deposited initially from suspension, but then was heavily disrupted when the unconsolidated or semi-consolidated underlying strata was injected into the sand. This may indicate ‘reverse density loading’,

which occurs when sand is deposited rapidly onto mud, and the sand founders, allowing the shale to intrude into the sand (Potter & Pettijohn 1977), leading to the development of the flame structures. This may occur when the underlying sediment fluidises due to a very high water content, or alternatively thixotropic processes may reduce the shear strength of the mud, promoting gravitational collapse of the sand and injection of mud (Potter & Pettijohn 1977; Rossetti 1999). This lithology represents a fairly high energy system, possibly with some tectonic disturbance.

INTERBEDDED SHALE AND FINE SAND, 2-17 CM (F2)

This facies is defined by thinly bedded to laminated very fine sand and purple shale. The shale is either purple or light grey-green. The facies typically occurs in ~3-5 cm beds that may fine upward slightly, and there is occasional wavy bedding and occasional very low angle scour structures where sand overlies shale. Flame structures occur in places at the top of beds where this facies is deposited below sand.

Depositional processes

This facies is likely to represent a combination of tractional and suspension fall-out depositional processes, where suspension fall-out is dominant. The laminated shale beds are likely to have been deposited during still-water conditions, as evidenced by the planar laminations. The presence of low-angle truncations where sand overlies shale indicates a slightly higher energy event, with deposition occurring under tractional processes, or where sand fines up to shale without an erosive base, this may suggest deposition of sediments from suspension. Where flame structures occur at the top of beds, this indicates that sediment was rapidly deposited on top of this lithology while it was still unconsolidated. This lithology may represent alternate deposition of mud from suspension, and thin sand beds or scoured sand beds during high energy events of varying magnitude.

THINLY BEDDED SHALE, 2-24 CM (F3)

This facies is characterised by light grey-green or purple shale to siltstone. It occurs in ~0.5-2 cm beds, and often has a gradational boundary with underlying sand. Bedding is generally parallel but occasionally is slightly wavy, and often contains millimetre-scale laminations.

Depositional processes

This millimetre-laminated shale is likely to have been deposited due to fall-out from suspension. The lack of any other sedimentary structures indicates that this occurred in a very low energy setting. Where this lithology is deposited with a gradational boundary from the underlying sand, this indicates deposition from a waning current. Where the shale is purple, this indicates that the sediment contains oxidised (ferric) iron, and the colour is likely to have developed post-diagenesis (Tucker 2001). The colour of the light green shale layers is due to the presence of reduced (ferrous) iron, and the reduction of the iron is likely to have occurred due to the migration of a reducing fluid (e.g. groundwater) through these beds (Tucker 2001). This may indicate that the green shale beds are more porous than those in which iron has remained in the oxidised state.

3.2 Lithological associations and environmental interpretations

Two lithological associations have been identified within the Tadpatri Formation section. Where L1 is overlain by L2, it is with a gradational contact, signifying a reduction in the energy of the depositional setting from one lithology to the next resulting in a fining-up sequence. Taking into account the planar laminated nature of the muds as well as the generally thin interbedded nature of sand and mud, this association may be interpreted as having been deposited in a sub-tidal setting, where sand layers which accumulate during storm activity alternate with very thin mud laminae formed during periods of slower accumulation (F1; Boggs 2001), then a reduction in the frequency/magnitude of storm events led to a relative increase in the periods of quiet-water deposition, but which was still affected by occasional storm events (F2).

Similarly, where F1 is gradationally overlain by F3, this reflects further reduction in the energy of the setting, but in this case without the interspersion of deposition from relatively minor storm events.

Given the alternation of sand beds of varying thickness with planar laminated shale, and occasional hummocky cross stratification, this succession is likely to have been deposited in a storm-dominated sub-tidal setting, where storms of varying magnitude sporadically affected sedimentation. Graded beds which occur without an erosive base may indicate the erosion of the beach during onshore storm events and subsequent injection of a plume of suspended fine sand into a deeper water setting, which released progressively finer sediments (Boggs 2001). Where graded beds occur with a scoured contact, this may represent small turbidity currents generated by storms of a higher magnitude (Boggs 2001). Where hummocky cross-stratification is preserved in sand beds, this indicates a storm event of sufficiently high energy that the sediment is affected by wave action generated by the storm, whereas sediments in this succession are otherwise generally not affected by wave activity. This indicates that this succession was deposited below the fair-weather wave base. The occasional presence of loaded bases and flame structures where sand overlies shale indicates that the deposition of sand beds took place rapidly, over unconsolidated sediment.

Taking into account the setting proposed for this section of the Tadpatri Formation, the presence of L1a presents an interesting problem. Whilst ball and pillow structures may be produced by the rapid deposition of sand over unconsolidated mud, it seems unlikely that this could be the cause of the convoluted bedding in this case. The development and preservation of planar laminae in the sand beds suggests that the deposition of the sand was not unusually rapid and even that the sand was semi-consolidated at the time of deformation, but the large size of the balls and flame structures indicates fairly significant disturbance. In this case, a structural cause for this convoluted bedding may be the most likely interpretation; the application of a shock to sand overlying thixotropic mud in experimental conditions has produced ball and pillow structures very similar to those seen in the field (Boggs 2001) and this may indicate that the Tadpatri Formation was affected by some seismic activity during the final stages of its deposition.

4 Gandikota Formation

4.1 Observations and interpretations

CROSS-STRATIFIED SAND

The observed lithology is characterised by sand beds of up to one metre interbedded with ~10 cm mud beds. Muddy layers are highly weathered and internal structures are not apparent. The sand is fine to coarse grained and poorly sorted, and ~100 % quartz. The sandstone features planar parallel cross-stratified beds, frequent climbing ripples and hummocky cross stratified beds. The sand also features large low-angle scour structures where finer sand has been scoured and filled by coarser sand. The sand is poorly sorted, and all foresets fine upward, resulting in prominent laminae. Bed tops feature asymmetric ripples with broken crests, and rhomboidal interference ripples. Small-scale synsedimentary detachment faulting was observed, in association with climbing ripples and flame structures.

Depositional processes

This lithology is likely to represent tractional deposition interspersed with periods of deposition from suspension. The presence of climbing ripples and synsedimentary detachment faulting is likely to reflect rapid deposition of sediment. Rhomboidal interference ripples signify deposition in a very shallow water setting, and asymmetric ripples with bifurcated crests are likely to represent formation by wave action (Tucker 2001). Scour and fill structures with relatively coarse sand are likely to event occasional relatively high energy events, and the internally graded foresets are likely al represent fluctuating flow velocity. This lithology is therefore likely to reflect deposition in a fairly high energy wave-dominated shallow water setting, with a high rate of sedimentation.

Appendix III – Restrictions on the use of zircon isotope analysis for geochronology and provenance studies

1 Detrital zircon geochronology

In addition to being a common accessory mineral in sedimentary rocks, zircon ($ZrSiO_4$) is both physically and chemically resistant, and therefore has the ability to retain substantial isotopic information, even after thermal disturbance (Finch & Hanchar 2003). Uranium and lead are strongly fractionated during the growth of zircon due to a large difference in charge and ionic radius (U^{4+} substitutes readily for Zr^{4+} within the crystal lattice whereas radiogenic Pb diffuses very slowly; Mezger & Krogstad 1997). The high U/Pb ratio of zircon makes it ideal for high-precision geochronology. Due to their durability, zircons are able to reliably preserve information about the source rocks of clastic sediments (Hay & Dempster 2009). Thus it is with reasonable confidence that the age of a detrital zircon can be assumed to represent the age of its original source, and hence to constrain the age of the sedimentary rock containing the zircon to younger than the age of the youngest grain identified within the rock (Fedo *et al.* 2003). Also, detrital zircon ages can be used to evaluate possible provenance of sediments as well as the range of sources contributing sediment to the rock. However, this is by no means an exhaustive nor representative (in terms of mass contribution) indication of sediment provenance; it merely provides an indication as to plausible sources for detrital zircons.

2 Use of detrital zircons in a provenance study

A number of considerations must be taken into account when interpreting the provenance of sediments from detrital zircon grains. Provenance studies based entirely on the age of zircon grains are highly error prone, as zircon growth may occur contemporaneously in multiple locations, or terranes of an appropriate age and location may not contain zircon-bearing lithologies (Howard *et al.* 2009), or zircon grains within key terranes may simply not yet have been dated.

Although zircon grains were sampled randomly following crushing and separation, there are several biases inherent in the methodology as well as biases of a sedimentological nature. When a rock is sampled for geochronological analysis, it is assumed that the age of zircon within the rock is representative of the age of the quartz, that detritus from all potential sources had an equal chance of reaching the basin via fluvial drainage systems, that the relative number of ages defining a detrital population reflect the contribution of a particular source to the sampled rock, and the physical and petrogenic behaviour of zircon acting as a proxy for all sediment within the rock (Moecher & Samson 2006, and references therein). In addition to this, there are a number of considerations which must be taken into account when ascribing provenance of sediments within the Cuddapah Basin: firstly, the fertility of possible contribution terranes in terms of zircon production. If potential terranes produce different proportions of zircon, then each terrane will not be represented proportionally amongst the sampled zircon grains; most notably, a dominantly mafic igneous terrane will produce significantly less zircon grains than will a felsic terrane, and hence will be significantly underrepresented in a detrital zircon study (Cookenboo *et al.* 1997).

In addition to this, it cannot be assumed that the sampling of potential populations was random and representative, or that sediment within the sample represents the quantity of sample contributed to the rock by each source. Andersen (2005) have found that detrital zircon populations are binomially rather than normally distributed, and hence that the abundance of any detrital population amounting to less than ~10% of the analysed grains will be systematically understated in any dataset of less than ~100%. Vermeesch (2004) found that the number of grains required for a statistically accurate provenance study (i.e., one in which all contributing sources comprising more than 5% of the total are represented [at the 95% confidence level]) is 117 grains. The relatively small amount of sample which could be transported from India limited the number of zircon grains which could be separated, and in all cases the number of concordant analyses fell below this recommended number. Taking the work of Andersen (2005) and Vermeesch (2004) into account, it is highly unlikely that all contributing sources are represented in the four samples, or that the detrital populations are an accurate reflection of mass balance of contributing sources.

References

ANDERSEN T. 2005. Detrital zircons as tracers of sedimentary provenance: limiting conditions from statistics and numerical simulation. *Chemical Geology* **216**, 249-270.

BOGGS S. 2001. *Principles of Sedimentology and Stratigraphy* (Third edition). Prentice Hall, New Jersey.

BUCK S., G. 1980. Stromatolite and ooid deposits within the fluvial and lacustrine sediments of the Precambrian Ventersdorp Supergroup of South Africa. *Precambrian Research* **12**, 311-330.

COOKENBOO H. O., BUSTIN R. M. & WILKS K. R. 1997. Detrital chromian spinel compositions used to reconstruct the tectonic setting of provenance: implications for orogeny in the Canadian Cordillera. *Journal of Sedimentary Research* **67**, 116-123.

DAVIES N. S. & GIBLING M. R. 2010. Cambrian to Devonian evolution of alluvial systems: The sedimentological impact of the earliest land plants. *Earth-Science Reviews* **98**, 171-200.

ELMORE R. D., MILAVEC G. J., SCOTT W. I. & ENGEL M. H. 1989. The Precambrian Nonesuch Formation of the North American Mid-Continental Rift, Sedimentology and Organic Geochemical Aspects of Lacustrine Deposition. *Precambrian Research* **43**, 191-213.

ERIKKSSON K. A., SIMPSON E. L., MASTER S. & HENRY G. 2005. Neoarchaean (*c*. 2.58 Ga) halite casts: implications for palaeoceanic chemistry. *Journal of the Geological Society of London* **162**, 789-799.

FEDO C. M., SIRCOMBE K. N. & RAINBIRD R. H. 2003. Detrital Zircon Analysis of the Sedimentary Record. *In:* Hanchar J. M. & Hoskin P. W. O. eds., *Zircon*, Vol. 53, pp 277-303, Mineralogical Society of America.

FINCH R. J. & HANCHAR J. M. 2003. Structure and Chemistry of Zircon and Zircon-Group Minerals. *In:* Hanchar J. M. & Hoskin P. W. O. eds., *Zircon*, Vol. 53, pp 1-25, Mineralogical Society of America.

GINSBURG R. N., HARDIE L. A., BRICKER O. P., GARRETT P. & WANLESS H. R. 1977. Exposure index: a quantitative approach to defining position within the tidal zone. *In:* Hardie L. A. ed.,

Sedimentation on the Modern Tidal Flats of Northwest Andros Island, Bahamas, John Hopkins University Press, Baltimore.

GRIFFIN W. L., POWELL W. J., PEARSON N. J. & O'REILLY S. Y. 2008. GLITTER: data reduction software for laser ablation ICP-MS. *In:* Sylvester P. J. ed., *Laser Ablation-ICP-MS in the Earth Sciences: Current Practices and Outstanding Issues: Mineralogical Association of Canada Short Course*, Vol. 40, pp 308-311.

GROTZINGER J. P. & KASTING J. F. 1993. New Constraints on Precambrian Ocean Composition. *The Journal of Geology* **101**, 235-243.

HAY D. C. & DEMPSTER T. J. 2009. Zircon alteration, formation and preservation in sandstones. *Sedimentology* **56**, 2175-2191.

HOWARD K. E., HAND M., BAROVICH K. A., REID A., WADE B. P. & BELOUSOVA E. 2009. Detrital zircon ages: Improving interpretation via Nd and Hf isotopic data. *Chemical Geology* **262**, 277-292.

JACKSON S. E., PEARSON N. J., GRIFFIN W. L. & BELOUSOVA E. A. 2004. The application of laser ablation-inductively coupled plasma-mass spectrometry to in-situ U/Pb zircon geochronology. *Chemical Geology* **211**, 47-69.

KOSTASCHUK R. & VILLARD P. 1996. Flow and sediment transport over large subaqueous dunes: Fraser River, Canada. *Sedimentology* **43**, 849-863.

LOGAN B. W., REZAK R. & GINSBURG R. N. 1964. Classification and environmental significance of algal stromatolites. *Journal of Geology* **72**, 68-73.

LUDWIG K. R. 2003. *User's manual for Isoplot 3.00* (Special Publication No.4.). Berkeley Geochronological Center.

MASSE J. P., FENERCI M. & PERNARCIC E. 2003. Palaeobathymetric reconstruction of peritidal carbonates Late Barremian, Urgonian, sequences of Provence (SE France). *Palaeogeography, Palaeoclimatology, Palaeoecology* **200**, 65-81.

MEZGER K. & KROGSTAD J. 1997. Interpretation of discordant U-Pb zircon ages: An evaluation. *Journal of Metamorphic Geology* **15**, 127-140.

MOECHER D. P. & SAMSON S. D. 2006. Differential zircon fertility of source terranes and natural bias in the detrital zircon record: Implications for sedimentary provenance analysis. *Earth and Planetary Science Letters* **247**, 252-266.

OWEN G. 1996. Experimental soft-sediment deformation: structures formed by the liquefaction of unconsolidated sands and some ancient examples. *Sedimentology* **43**, 279-293.

PAYNE J. L., BAROVICH K. M. & HAND M. 2006. Provenance of metasedimentary rocks in the northern Gawler Craton, Australia: Implications of palaeoproterozoic reconstractions. *Precambrian Research* **148**, 275-291.

POTTER P. E. & PETTIJOHN F. J. 1977. *Paleocurrents and Basin Analysis*. Springer Verlag, New York.

PROTHERO D. R. & SCHWAB F. 1996. *Sedimentary Geology*. W. H. Freeman and Company, New York.

PUFAHL P. K., HIATT E. E. & KURTIS KYSER T. 2010. Does the Paleoproterozoic Animikie Basin record the sulfidic ocean transition? *Geology* **38**.

READING H. G. (Editor) 1996. *Sedimentary Envrironments: Processes, Facies and Stratigraphy* (Third edition). Blackwell Publishing, Oxford.

REINECK H.-E. & WUNDERLICH F. 1968. Classification and origin of flaser and lenticular bedding. *Sedimentology* **11**, 99-104.

ROSSETTI D. D. F. 1999. Soft-sediment deformation structures in late Albian to Cenomanian deposits, São Luíi Basin, northern Brazil: evidence for palaeoseismicity. *Sedimentology* **46**, 1065-1081.

SCHERER E., MUNKER C. & MEZGER K. 2001. Calibration of the lutetium-hafnium clock. *Science* **293**, 683-687.

SEGAL I., HALICZ L. & PLATZNER I. T. 2003. Accurate isotope ratio measurements of ytterbium by multiple collcetion inductively coupled plasma mass spectrometry applying erbium and hafnium in an improved double external normalization procedure. *Journal of Analytical Atomic Spectrometry* **18**, 1217-1223.

SIMONSON B. M., SCHUBEL K. A. & HASSLER S. W. 1993. Carbonate sedimentology of the early Precambrian Hamersley Group of Western Australia. *Precambrian Research* **60**, 287-335.

SLÁMA J., KOSLER J., CONDON D. J., CROWLEY J. L., GERDES A., HANCHAR J. M., HORSTWOOD M. S. A., MORRIS G. A., NASDALA L., NORBERG N., SCHALTEGGER U., SCHOENE B., TUBRETT M. N. & WHITEHOUSE M. J. 2008. Plesovice zircon - A new natural reference material for U-Pb and Hf isotopic microanalysis. *Chemical Geology* **249**, 1-35.

TODD S. P. 1989. Stream-driven, high density gravelly traction carpets: possible deposits in the Trabeg Conglomerate Formation, SW Ireland and theoretical considerations of their origin. *Sedimentology* **36**, 513-530.

TUCKER M. E. 2001. *Sedimentary Petrology: an introduction to the origin of sedimentary rocks* (3 edition). Blackwell Publishing.

VERMEESCH P. 2004. How many grains are needed for a provenance study? *Earth and Planetary Science Letters* **224**, 441-451.

VERVOORT J. D., PATCHETT R. J., SODERLUND U. & BAKER M. 2004. Isotopic composition of Yb and the determination of Lu concentrations and Lu/Hf ratios by isotope dilution uding MC-ICPMS. *Geochemistry Geophysics Geosystems* **5**.

WALKER R. G. & JAMES N. P. (Editors) 1992. *Facies Models: Response to sea level change*. Geological Association of Canada, Canada.

WELLS N. A., RICHARDS S. S., PENG S., KEATTCH S. E., HUDSON J. A. & COPSEY C. J. 1993. Fluvial processes and recumbently folded crossbeds in the Pennsylvanian Sharon Conglomerate in Summit County, Ohio, U.S.A. *Sedimentary Geology* **85**, 63-83.

WOODHEAD J., HERGT J. & SHELLEY M. 2004. Zircon Hf-isotope analysis with an excimer laser, depth profiling, ablation of complex geometries, and concomitant age estimation. *Chemical Geology* **209**, 121-135.

Sample GF01	Isotope Ratios									Ages (Ma)								
Spot Name	Pb207/Pb206	± 1σ	Pb206/U238	± 1σ	Pb207/U235	± 1σ	Pb208/Th232	± 1σ	rho	Pb207/Pb206	± 1σ	Pb206/U238	± 1σ	Pb207/U235	± 1σ	Pb208/Th232	± 1σ	Conc. (%)
spot1	0.29007	0.00297	0.68474	0.00854	27.38681	0.33876	0.17481	0.00172	0.99178721	3418	15.83	3362.5	32.66	3397.4	12.12	3256.3	29.54	98
spot2	0.14686	0.00149	0.13821	0.00171	2.79864	0.0344	0.04931	0.00043	0.993470011	2309.6	17.28	834.5	9.67	1355.2	9.2	972.9	8.37	36
spot3	0.15987	0.00161	0.34812	0.0043	7.67379	0.09405	0.10245	0.00091	0.992223272	2454.3	16.89	1925.6	20.56	2193.5	11.01	1971.5	16.75	78
spot4	0.21986	0.0024	0.57358	0.00728	17.38795	0.22371	0.14866	0.00165	0.986507439	2979.7	17.45	2922.5	29.84	2956.5	12.35	2801.3	29.07	98
spot5	0.22359	0.00237	0.57084	0.00719	17.59853	0.22298	0.15048	0.00152	0.994088328	3006.7	16.95	2911.3	29.51	2968	12.17	2833.4	26.71	97
spot6	0.16344	0.00166	0.29529	0.00366	6.65453	0.08228	0.0875	0.00079	0.997572688	2491.6	17.03	1667.9	18.22	2066.6	10.91	1695.4	14.62	67
spot7	0.15305	0.00155	0.10704	0.00133	2.25896	0.02791	0.04851	0.00043	0.99436483	2380.3	17.19	655.6	7.72	1199.6	8.7	957.4	8.27	28
spot8	0.17445	0.00179	0.46161	0.00575	11.10309	0.13838	0.12566	0.00119	0.999454828	2600.8	17.02	2446.7	25.36	2531.8	11.61	2392.5	21.39	94
spot9	0.13724	0.00139	0.12843	0.00159	2.43019	0.03002	0.04566	0.00041	0.997791538	2192.7	17.46	778.9	9.09	1251.6	8.89	902.5	7.95	36
spot10	0.1362	0.00138	0.09406	0.00117	1.7664	0.02189	0.03598	0.00032	0.996267168	2179.4	17.56	579.5	6.88	1033.2	8.03	714.4	6.29	27
spot11	0.11838	0.00121	0.16804	0.00209	2.74283	0.03417	0.07097	0.00068	0.998360812	1932	18.19	1001.3	11.52	1340.1	9.27	1385.8	12.79	52
spot12	0.16567	0.00176	0.38268	0.00481	8.74103	0.11145	0.11568	0.00112	0.98580689	2514.3	17.77	2088.8	22.44	2311.4	11.62	2212.6	20.35	83
spot13	0.17781	0.00179	0.22619	0.00289	5.54518	0.07013	0.0229	0.00027	0.989837148	2632.6	16.68	1314.5	15.18	1907.6	10.88	457.7	5.28	50
spot14	0.1457	0.00147	0.19422	0.00248	3.90142	0.04933	0.04674	0.00046	0.990217685	2296	17.19	1144.2	13.38	1614	10.22	923.2	8.81	50
spot15	0.1626	0.00169	0.37523	0.00483	8.41216	0.10829	0.08937	0.00083	0.999928042	2482.9	17.38	2054	22.63	2276.5	11.68	1730.2	15.33	83
spot16	0.19555	0.00197	0.1612	0.00206	4.34615	0.0551	0.08063	0.00072	0.992075455	2789.4	16.4	963.4	11.46	1702.2	10.46	1567.4	13.39	35
spot17	0.1793	0.00181	0.1798	0.00231	4.44487	0.05643	0.06335	0.00056	0.988163241	2646.4	16.61	1065.9	12.6	1720.7	10.52	1241.5	10.63	40
spot18	0.16173	0.00165	0.16825	0.00216	3.75188	0.04806	0.02124	0.0002	0.997783111	2473.9	17.14	1002.4	11.95	1582.5	10.27	424.9	3.9	41
spot19	0.16365	0.00168	0.26427	0.00341	5.96299	0.0766	0.09699	0.0009	0.995538762	2493.7	17.15	1511.6	17.38	1970.5	11.17	1871.1	16.5	61
spot20	0.16273	0.0017	0.24333	0.00315	5.4598	0.07091	0.08029	0.00076	0.996745185	2484.3	17.49	1404	16.35	1894.3	11.15	1561	14.3	57
spot21	0.16582	0.00171	0.35098	0.00455	8.02472	0.10386	0.09909	0.00093	0.998365129	2515.9	17.26	1939.3	21.7	2233.8	11.69	1909.8	17.18	77
spot22	0.11503	0.00117	0.088	0.00114	1.39574	0.01795	0.0253	0.00024	0.992745092	1880.4	18.23	543.7	6.73	887.1	7.61	505	4.67	29
spot23	0.2497	0.00251	0.6092	0.00789	20.9749	0.26833	0.14408	0.00133	0.987761792	3182.9	15.81	3066.8	31.6	3137.4	12.4	2720.5	23.58	96
spot24	0.1664	0.0017	0.35393	0.00459	8.12071	0.10498	0.10947	0.00102	0.996821181	2521.8	17.07	1953.3	21.88	2244.6	11.69	2099.7	18.55	77
spot25	0.20897	0.00214	0.35867	0.00467	10.3349	0.13381	0.13261	0.00124	0.994398508	2897.6	16.52	1975.8	22.16	2465.2	11.99	2517	22.05	68
spot26	0.215	0.00219	0.4959	0.00649	14.69917	0.18989	0.08956	0.00161	0.987094412	2943.6	16.34	2596.2	27.96	2796	12.28	1733.7	29.86	88
spot27	0.1487	0.00149	0.24568	0.0032	5.03653	0.06459	0.06611	0.00058	0.984586064	2331	17.1	1416.2	16.54	1825.5	10.86	1293.9	10.99	61
spot28	0.1585	0.00159	0.2987	0.00388	6.5274	0.08359	0.08757	0.00077	0.985865332	2439.8	16.84	1684.9	19.28	2049.6	11.28	1696.7	14.39	69
spot29	0.21981	0.00235	0.55719	0.00738	16.88534	0.22362	0.13021	0.00139	0.999879777	2979.3	17.08	2855	30.57	2928.3	12.7	2474.1	24.93	96
spot30	0.15995	0.00161	0.15154	0.00197	3.34187	0.04287	0.06651	0.0006	0.986790565	2455.2	16.91	909.6	11.03	1490.9	10.03	1301.5	11.37	37

spot31	0.16462	0.00168	0.43137	0.00563	9.78997	0.12649	0.10692	0.00099	0.989957101	2503.6	17.03	2311.9	25.34	2415.2	11.9	2053.1	18.03	92
spot32	0.16836	0.00177	0.46326	0.00609	10.75309	0.14143	0.10946	0.00111	0.999503293	2541.4	17.55	2453.9	26.81	2502	12.22	2099.4	20.2	97
spot33	0.16728	0.00173	0.33617	0.00439	7.75276	0.10095	0.08155	0.00081	0.997113089	2530.6	17.28	1868.2	21.2	2202.7	11.71	1584.5	15.14	74
spot34	0.16509	0.00168	0.33288	0.00434	7.57657	0.0978	0.09054	0.00091	0.990066094	2508.5	17.03	1852.3	20.97	2182.1	11.58	1751.8	16.93	74
spot35	0.16333	0.00169	0.30539	0.00399	6.87672	0.08934	0.06699	0.00064	0.994366588	2490.4	17.28	1718	19.68	2095.7	11.52	1310.7	12.12	69
spot36	0.16686	0.00169	0.46254	0.00602	10.6407	0.13699	0.10825	0.00105	0.989171219	2526.4	16.9	2450.8	26.53	2492.3	11.95	2077.4	19.06	97
spot37	0.17086	0.00175	0.34244	0.00446	8.06662	0.10448	0.10172	0.00095	0.994468874	2566.1	17.06	1898.4	21.44	2238.5	11.7	1957.9	17.39	74
spot38	0.14	0.0014	0.05807	0.00075	1.12079	0.0143	0.00577	0.00006	0.987875814	2227.2	17.25	363.9	4.57	763.4	6.85	116.3	1.14	16
spot39	0.15132	0.00152	0.2667	0.00344	5.56385	0.07102	0.06485	0.00061	0.989623109	2360.9	17.07	1524	17.51	1910.5	10.99	1270	11.52	65
spot40	0.1652	0.00166	0.46666	0.00601	10.62826	0.13537	0.11076	0.00119	0.988977392	2509.5	16.79	2468.9	26.43	2491.2	11.82	2123.1	21.62	98
spot41	0.15662	0.00157	0.21049	0.0027	4.54507	0.05781	0.06769	0.00065	0.991585339	2419.5	16.97	1231.4	14.4	1739.3	10.59	1323.9	12.25	51
spot42	0.16005	0.00161	0.17592	0.00226	3.88162	0.04936	0.03876	0.00038	0.989848915	2456.1	16.96	1044.6	12.37	1609.9	10.27	768.5	7.46	43
spot43	0.27188	0.00277	0.49593	0.00639	18.58873	0.23727	0.13277	0.00138	0.99063264	3316.9	15.89	2596.3	27.55	3020.7	12.3	2519.8	24.56	78
spot44	0.15724	0.00157	0.15919	0.00203	3.45085	0.04359	0.03283	0.00033	0.990559419	2426.2	16.89	952.3	11.3	1516.1	9.94	652.8	6.47	39
spot45	0.14163	0.00142	0.20496	0.00261	4.00196	0.0506	0.05767	0.00057	0.992901984	2247.2	17.28	1201.9	13.98	1634.6	10.27	1133.3	10.86	53
spot46	0.29296	0.003	0.64933	0.00834	26.22478	0.33394	0.15731	0.00182	0.991416191	3433.4	15.8	3225.6	32.6	3355	12.45	2953	31.7	94
spot47	0.13183	0.00133	0.14457	0.00184	2.62737	0.03316	0.02619	0.00027	0.991639101	2122.4	17.57	870.5	10.34	1308.3	9.28	522.6	5.25	41
SPOT48	0.1623	0.00185	0.08074	0.00133	1.80544	0.02993	0.02385	0.00032	0.993663276	2479.8	19.06	500.6	7.93	1047.4	10.83	476.4	6.41	20
SPOT49	0.16696	0.00177	0.49537	0.00807	11.39592	0.18388	0.12164	0.00142	0.990469873	2527.4	17.65	2593.9	34.78	2556.1	15.06	2320.1	25.54	103
SPOT50	0.1684	0.00208	0.37253	0.00618	8.64462	0.14734	0.10483	0.00146	0.973312867	2541.8	20.55	2041.3	29.03	2301.3	15.51	2014.9	26.7	80
SPOT51	0.16568	0.00198	0.31062	0.0051	7.09268	0.11886	0.09886	0.00129	0.979750291	2514.5	19.98	1743.8	25.06	2123.1	14.91	1905.4	23.67	69
SPOT52	0.1691	0.00207	0.08759	0.00143	2.04154	0.03427	0.07217	0.00091	0.972579923	2548.8	20.34	541.3	8.48	1129.5	11.44	1408.4	17.11	21
SPOT53	0.20139	0.00212	0.4125	0.00659	11.45075	0.18125	0.085	0.00143	0.990792295	2837.5	17.02	2226.3	30.07	2560.6	14.78	1648.9	26.56	78
SPOT54	0.16945	0.00207	0.1922	0.00311	4.48943	0.07489	0.08058	0.0011	0.970005908	2552.2	20.28	1133.3	16.84	1729	13.85	1566.4	20.59	44
SPOT55	0.16328	0.00184	0.4223	0.00674	9.50583	0.15351	0.11315	0.00148	0.988307717	2489.9	18.86	2270.9	30.55	2388.1	14.84	2166.7	26.92	91
SPOT56	0.24046	0.00241	0.55893	0.00874	18.5291	0.28552	0.10346	0.00117	0.985435487	3123	15.89	2862.2	36.15	3017.6	14.84	1990	21.34	92
SPOT57	0.16899	0.00209	0.31881	0.00512	7.42825	0.12361	0.09469	0.00135	0.965096923	2547.7	20.56	1783.9	25.02	2164.4	14.89	1828.7	24.99	70
SPOT58	0.1594	0.00176	0.15037	0.00235	3.30483	0.05224	0.05965	0.00076	0.988672874	2449.3	18.54	903	13.19	1482.2	12.32	1171.1	14.59	37
SPOT59	0.28337	0.00295	0.61372	0.00954	23.97927	0.3697	0.16439	0.00192	0.991825785	3381.6	16.13	3084.9	38.12	3267.5	15.03	3076.2	33.41	91
SPOT60	0.16837	0.0018	0.52599	0.00814	12.21101	0.18972	0.13512	0.00153	0.996059744	2541.5	17.81	2724.6	34.39	2620.8	14.58	2561.7	27.28	107
SPOT61	0.17529	0.00183	0.5378	0.00827	12.99858	0.19963	0.14826	0.00181	0.998723304	2608.8	17.25	2774.3	34.68	2679.6	14.48	2794.3	31.94	106
SPOT62	0.27844	0.00285	0.74685	0.01148	28.67214	0.43704	0.18812	0.00228	0.991636665	3354.2	15.91	3595.9	42.37	3442.4	14.96	3484.1	38.77	107
SPOT63	0.16852	0.00176	0.35505	0.00545	8.24938	0.12641	0.11553	0.00131	0.998281761	2543	17.35	1958.7	25.92	2258.8	13.88	2209.8	23.71	77

SPOT64	0.26349	0.00275	0.72331	0.01115	26.27713	0.40272	0.18765	0.00219	0.994202545	3267.7	16.31	3508.4	41.7	3356.9	14.99	3476	37.23	107
SPOT65	0.12485	0.00127	0.14621	0.00223	2.51676	0.03818	0.05602	0.00063	0.994640949	2026.7	17.9	879.7	12.54	1276.9	11.02	1101.6	12.14	43
SPOT66	0.16745	0.00176	0.45106	0.00692	10.41342	0.15972	0.13663	0.00157	0.999756273	2532.3	17.5	2399.9	30.73	2472.2	14.21	2588.5	27.94	95
SPOT67	0.17859	0.00193	0.54716	0.00844	13.47213	0.20894	0.14813	0.002	0.994587004	2639.8	17.83	2813.4	35.15	2713.3	14.66	2792	35.18	107
SPOT68	0.17054	0.00176	0.52648	0.00805	12.37879	0.18843	0.142	0.00169	0.995538019	2563	17.16	2726.6	33.97	2633.6	14.3	2683.8	29.92	106
SPOT69	0.16628	0.00174	0.28755	0.00439	6.59197	0.10061	0.10426	0.00125	0.999711708	2520.6	17.42	1629.3	22	2058.3	13.46	2004.6	22.92	65
SPOT70	0.24308	0.00248	0.31395	0.00479	10.5211	0.15907	0.0377	0.0005	0.990950832	3140.3	16.14	1760.1	23.49	2481.8	14.02	747.9	9.8	56
SPOT71	0.16507	0.00167	0.46983	0.00714	10.69197	0.16124	0.12869	0.00147	0.992333357	2508.3	16.94	2482.8	31.33	2496.7	14	2446.8	26.32	99
SPOT72	0.16801	0.00171	0.3132	0.00476	7.25456	0.10943	0.09126	0.00108	0.992521956	2538	16.95	1756.4	23.36	2143.2	13.46	1765.2	20.1	69
SPOT73	0.12463	0.00128	0.29601	0.00449	5.08488	0.07679	0.10082	0.00127	0.995597967	2023.6	18.05	1671.5	22.33	1833.6	12.81	1941.5	23.38	83
SPOT74	0.17752	0.00181	0.27371	0.00416	6.69674	0.10086	0.0106	0.00015	0.990952551	2629.8	16.83	1559.6	21.03	2072.2	13.31	213	3.02	59
SPOT75	0.19187	0.00198	0.45366	0.00691	11.9965	0.18188	0.08337	0.00107	0.99536606	2758.2	16.87	2411.5	30.66	2604.1	14.21	1618.5	20.05	87
SPOT76	0.15626	0.0016	0.24603	0.00374	5.29821	0.08007	0.08049	0.00095	0.994161922	2415.5	17.27	1417.9	19.35	1868.6	12.91	1564.7	17.7	59
SPOT77	0.1187	0.00123	0.21478	0.00327	3.51363	0.05346	0.06926	0.00083	0.999353213	1936.8	18.45	1254.2	17.35	1530.3	12.03	1353.5	15.65	65
SPOT78	0.14431	0.00147	0.2532	0.00385	5.03576	0.0762	0.07651	0.00092	0.995160018	2279.6	17.49	1454.9	19.82	1825.4	12.82	1490.2	17.23	64
SPOT79	0.21721	0.00246	0.44029	0.00685	13.18011	0.20743	0.11719	0.00157	0.988551313	2960.1	18.14	2352	30.67	2692.6	14.85	2239.9	28.33	79
SPOT80	0.2538	0.00269	0.34365	0.00529	12.01963	0.18435	0.10904	0.00151	0.996351822	3208.6	16.67	1904.2	25.38	2605.9	14.38	2091.9	27.61	59
SPOT81	0.16438	0.00173	0.11181	0.00171	2.53263	0.03875	0.03404	0.00044	0.99957527	2501.2	17.56	683.2	9.92	1281.5	11.14	676.6	8.7	27
SPOT82	0.17621	0.00179	0.3108	0.00474	7.54679	0.11427	0.13	0.00163	0.992824831	2617.5	16.81	1744.6	23.33	2178.6	13.58	2470.3	29.12	67
SPOT83	0.17548	0.0018	0.38332	0.00586	9.26904	0.14083	0.11315	0.00143	0.993857882	2610.6	16.94	2091.8	27.32	2365	13.92	2166.7	25.91	80
SPOT84	0.12847	0.00135	0.28326	0.00434	5.01471	0.07712	0.09889	0.00128	0.996284287	2077.2	18.42	1607.8	21.82	1821.8	13.02	1906	23.58	77
SPOT85	0.16641	0.00174	0.1132	0.00183	2.59636	0.04152	0.03717	0.00051	0.989208347	2521.8	17.42	691.3	10.59	1299.6	11.72	737.6	9.96	27
SPOT86	0.219	0.00229	0.63419	0.01025	19.14313	0.30595	0.15913	0.00238	0.988855955	2973.3	16.77	3166.1	40.44	3049.1	15.42	2984.7	41.56	106
SPOT87	0.16613	0.00174	0.39499	0.00635	9.04536	0.14418	0.11348	0.00161	0.99149731	2519.1	17.5	2145.9	29.32	2342.6	14.57	2172.6	29.21	85
SPOT88	0.16858	0.00181	0.50863	0.00818	11.81965	0.18977	0.13237	0.00188	0.998324225	2543.6	17.92	2650.8	34.95	2590.2	15.03	2512.6	33.6	104
SPOT89	0.16685	0.00178	0.53031	0.00849	12.1973	0.19477	0.13561	0.00197	0.997425541	2526.3	17.81	2742.7	35.76	2619.7	14.99	2570.3	34.99	109
SPOT90	0.16512	0.00183	0.37991	0.00609	8.64804	0.13968	0.12703	0.00184	0.992476039	2508.8	18.56	2075.9	28.46	2301.6	14.7	2417.1	33.07	83
SPOT91	0.16314	0.00169	0.15992	0.00253	3.59678	0.05637	0.02423	0.00034	0.990641278	2488.4	17.3	956.3	14.05	1548.8	12.45	484	6.72	38
SPOT92	0.17432	0.00194	0.48449	0.00773	11.64391	0.18731	0.12907	0.00189	0.991819294	2599.5	18.44	2546.8	33.57	2576.2	15.04	2453.7	33.79	98
SPOT93	0.16512	0.00168	0.32205	0.00505	7.33151	0.11377	0.10039	0.00137	0.989614961	2508.8	17.04	1799.7	24.62	2152.7	13.87	1933.6	25.2	72
SPOT94	0.1637	0.00177	0.16317	0.00257	3.68293	0.05821	0.12471	0.00179	0.996526094	2494.2	18.13	974.4	14.23	1567.7	12.62	2375.5	32.19	39
SPOT95	0.16322	0.00167	0.36799	0.00573	8.28147	0.12789	0.10616	0.00148	0.991769046	2489.3	17.1	2020	27.01	2262.3	13.99	2039.2	27.11	81
SPOT96	0.25541	0.00258	0.36912	0.00573	12.99941	0.1993	0.04235	0.00064	0.987635319	3218.6	15.86	2025.3	26.98	2679.6	14.46	838.4	12.48	63

Sample GF14	Isotope Ratios									Ages (Ma)								
Spot Name	Pb207/Pb206	± 1σ	Pb206/U238	± 1σ	Pb207/U235	± 1σ	Pb208/Th232	± 1σ	rho	Pb207/Pb206	± 1σ	Pb206/U238	± 1σ	Pb207/U235	± 1σ	Pb208/Th232	± 1σ	Conc. (%)
spot1	0.17109	0.00174	0.52585	0.00695	12.40182	0.16256	0.12863	0.00124	0.991757151	2568.3	16.91	2724	29.36	2635.3	12.32	2445.7	22.17	106
spot2*	0.29733	0.00594	7.93587	0.33006	325.24112	13.92086	2.38402	0.07453	0.971712373	3456.4	30.63	******	238.11	5876.7	43.33	******	445.14	-
spot3	0.19248	0.0019	0.58354	0.0077	15.48121	0.20084	0.12047	0.0012	0.9831623	2763.5	16.13	2963.2	31.33	2845.3	12.37	2299	21.73	107
spot4	0.16419	0.00169	0.32844	0.00437	7.43245	0.09843	0.09238	0.00097	0.995336878	2499.3	17.18	1830.8	21.2	2164.9	11.85	1785.9	17.89	73
spot5	0.16459	0.00167	0.23126	0.00308	5.24577	0.06925	0.11154	0.00118	0.991197818	2503.4	17.01	1341.1	16.1	1860.1	11.26	2137.4	21.48	54
spot6	0.1626	0.00164	0.28064	0.00373	6.28842	0.08292	0.04952	0.00053	0.992106952	2482.9	16.92	1594.6	18.8	2016.8	11.55	977	10.3	64
spot7	0.1655	0.00167	0.42747	0.0057	9.74851	0.12902	0.1073	0.00121	0.992543573	2512.6	16.91	2294.3	25.76	2411.3	12.19	2060.1	22.11	91
spot8	0.17215	0.00174	0.45569	0.0061	10.80907	0.1434	0.11966	0.00139	0.991061226	2578.6	16.82	2420.5	26.99	2506.8	12.33	2284.5	25.16	94
spot9	0.1643	0.00168	0.48506	0.00651	10.98043	0.1468	0.13872	0.00167	0.99614184	2500.4	17.13	2549.3	28.27	2521.5	12.44	2625.7	29.55	102
spot10	0.17083	0.00175	0.51904	0.00698	12.21591	0.16352	0.13532	0.00167	0.995383551	2565.8	16.99	2695.1	29.63	2621.1	12.56	2565.2	29.77	105
spot11	0.16648	0.00173	0.50385	0.00681	11.55598	0.15627	0.14555	0.00195	0.999486698	2522.5	17.34	2630.3	29.2	2569.1	12.64	2746.6	34.36	104
spot12	0.17103	0.00191	0.49975	0.00687	11.77474	0.16538	0.15085	0.00222	0.978751122	2567.8	18.51	2612.7	29.53	2586.7	13.15	2839.8	39.01	102
spot13	0.16984	0.00171	0.1419	0.00191	3.32196	0.04426	0.04087	0.00076	0.989842368	2556.1	16.72	855.4	10.8	1486.2	10.4	809.6	14.82	33
spot14	0.16734	0.00175	0.52824	0.00718	12.18472	0.1654	0.13466	0.0026	0.998681009	2531.3	17.43	2734	30.29	2618.7	12.74	2553.5	46.35	108
spot15	0.16559	0.00167	0.48565	0.00655	11.0853	0.1474	0.11675	0.00221	0.985898318	2513.6	16.81	2551.8	28.41	2530.3	12.38	2231.9	40.08	102
spot16	0.16642	0.00168	0.51711	0.00698	11.86248	0.15793	0.12651	0.00238	0.986317312	2522	16.9	2686.9	29.65	2593.6	12.47	2407.8	42.79	107
spot17	0.1574	0.0016	0.40656	0.00548	8.82082	0.11753	0.08447	0.00161	0.98851637	2427.9	17.16	2199.2	25.14	2319.6	12.15	1639.1	29.94	91
spot18	0.16097	0.00161	0.45813	0.00616	10.16552	0.13398	0.1136	0.00217	0.980208342	2465.9	16.77	2431.3	27.22	2449.9	12.18	2174.9	39.38	99
spot19	0.15536	0.00157	0.25514	0.00343	5.46391	0.07223	0.08523	0.00167	0.983328233	2405.7	17.07	1464.9	17.62	1894.9	11.35	1653.2	31.08	61
spot20	0.16685	0.00172	0.46779	0.00632	10.75926	0.14367	0.0976	0.00187	0.988365425	2526.3	17.24	2473.8	27.77	2502.6	12.41	1882.2	34.47	98
spot21	0.16451	0.00164	0.45871	0.00615	10.40298	0.13619	0.11771	0.00224	0.976451211	2502.6	16.67	2433.9	27.19	2471.3	12.13	2249.3	40.49	97
spot22	0.16199	0.00162	0.43274	0.0058	9.66375	0.12652	0.09692	0.00185	0.976815504	2476.5	16.77	2318.1	26.12	2403.3	12.05	1869.7	34.14	94
spot23	0.15335	0.00153	0.27641	0.0037	5.84342	0.07637	0.06355	0.00121	0.97635491	2383.6	16.95	1573.2	18.7	1952.9	11.33	1245.4	22.97	66
spot24	0.1625	0.00162	0.4449	0.00596	9.96709	0.12974	0.09775	0.00187	0.971676411	2481.8	16.68	2372.5	26.57	2431.7	12.01	1885.1	34.52	96
spot25	0.16268	0.00167	0.31351	0.00428	7.02851	0.09446	0.07195	0.00164	0.984446917	2483.7	17.2	1758	21	2115	11.95	1404.3	30.85	71
spot26	0.17012	0.00188	0.51148	0.00709	11.99159	0.16713	0.11862	0.00281	0.994580492	2558.8	18.34	2662.9	30.25	2603.7	13.06	2265.8	50.74	104
spot27	0.16329	0.00166	0.46316	0.00631	10.42324	0.13935	0.09442	0.00223	0.981309315	2490	17.06	2453.5	27.79	2473.1	12.39	1823.7	41.26	99
spot28	0.16676	0.00204	0.51439	0.0073	11.8227	0.17453	0.12416	0.00311	0.961339803	2525.3	20.45	2675.3	31.07	2590.5	13.82	2365.5	55.84	106
spot29	0.16	0.00194	0.45951	0.00648	10.13399	0.14823	0.11153	0.0029	0.964105147	2455.6	20.32	2437.4	28.6	2447.1	13.52	2137.1	52.75	99
spot30	0.16013	0.00163	0.24112	0.00327	5.32227	0.07077	0.03026	0.00075	0.980477824	2457	17.07	1392.5	16.99	1872.4	11.37	602.5	14.63	57
spot31	0.16515	0.00176	0.44639	0.00612	10.16302	0.13852	0.095	0.00237	0.994151879	2509.1	17.85	2379.2	27.26	2449.7	12.6	1834.3	43.69	95

spot32	0.16163	0.00168	0.48889	0.00666	10.89381	0.14626	0.11173	0.00284	0.985559157	2472.8	17.41	2565.9	28.82	2514.1	12.49	2140.8	51.6	104
spot33	0.16209	0.00169	0.48981	0.00667	10.94597	0.14694	0.10812	0.00279	0.985797235	2477.6	17.44	2569.9	28.84	2518.5	12.49	2075.2	50.92	104
spot34	0.16334	0.00165	0.45586	0.00616	10.26689	0.13574	0.10185	0.00262	0.978407357	2490.6	16.94	2421.3	27.3	2459.1	12.23	1960.4	48.03	97
spot35	0.15631	0.00159	0.37946	0.00513	8.17867	0.10836	0.07327	0.00192	0.980020022	2416.1	17.18	2073.8	23.98	2251	11.99	1429.3	36.21	86
spot36	0.16012	0.00158	0.25551	0.00343	5.64177	0.07347	0.03352	0.00088	0.970081996	2457	16.56	1466.8	17.62	1922.5	11.23	666.5	17.3	60
spot37	0.16535	0.00174	0.33733	0.00462	7.68779	0.10404	0.0685	0.0018	0.988124853	2511.1	17.56	1873.8	22.25	2195.2	12.16	1339.1	33.98	75
spot38	0.16505	0.00165	0.5007	0.00679	11.38962	0.15062	0.10836	0.00281	0.975172006	2508	16.75	2616.8	29.16	2555.6	12.34	2079.5	51.19	104
spot39	0.16223	0.00164	0.50672	0.00687	11.32909	0.15049	0.10996	0.00285	0.979769519	2479.1	16.98	2642.6	29.41	2550.6	12.39	2108.7	51.94	107
spot40	0.15259	0.00153	0.25974	0.00351	5.46148	0.07206	0.02992	0.00078	0.976372705	2375.1	16.98	1488.5	17.95	1894.6	11.32	595.9	15.32	63
spot41	0.16486	0.00173	0.50159	0.00683	11.39453	0.15383	0.10709	0.00283	0.991454503	2506.1	17.55	2620.6	29.34	2556	12.6	2056.3	51.75	105
spot42	0.17982	0.00181	0.46329	0.00625	11.4784	0.15141	0.09378	0.00248	0.977791175	2651.2	16.56	2454	27.54	2562.8	12.32	1811.8	45.85	93
spot43	0.1665	0.00172	0.50116	0.00679	11.4959	0.15368	0.10347	0.00274	0.986690623	2522.7	17.24	2618.8	29.16	2564.2	12.49	1990.2	50.28	104
spot44	0.15346	0.00154	0.33782	0.00454	7.14201	0.09395	0.04971	0.00131	0.978826763	2384.9	16.97	1876.2	21.88	2129.3	11.72	980.6	25.17	79
spot45	0.16096	0.00161	0.35454	0.00476	7.86101	0.10326	0.04762	0.00126	0.978390123	2465.8	16.81	1956.3	22.65	2215.2	11.83	940.3	24.31	79
spot46	0.16249	0.00168	0.50143	0.00677	11.22279	0.14974	0.1077	0.00289	0.988231373	2481.8	17.33	2619.9	29.05	2541.8	12.44	2067.5	52.73	106
spot47	0.16133	0.00163	0.34394	0.00461	7.64221	0.10057	0.06345	0.00169	0.981818575	2469.6	16.93	1905.6	22.11	2189.8	11.82	1243.4	32.08	77
spot48	0.16335	0.00166	0.33022	0.00443	7.42873	0.09809	0.06287	0.00168	0.984259935	2490.7	17.04	1839.4	21.45	2164.4	11.82	1232.5	31.97	74
spot49	0.15944	0.0016	0.29236	0.00391	6.41889	0.08421	0.04318	0.00116	0.980945614	2449.7	16.92	1653.3	19.48	2034.9	11.52	854.4	22.41	67
spot50	0.16389	0.00171	0.3633	0.00487	8.19997	0.10918	0.05874	0.00403	0.993269873	2496.2	17.42	1997.8	23.02	2253.3	12.05	1153.7	76.92	80
spot51	0.16271	0.0017	0.46915	0.00629	10.51168	0.14071	0.07204	0.00501	0.998421459	2484	17.54	2479.8	27.62	2480.9	12.41	1405.9	94.49	100
spot52	0.16807	0.00181	0.50274	0.00679	11.63499	0.15844	0.10037	0.0071	0.991807788	2538.5	17.95	2625.6	29.11	2575.5	12.73	1933.1	130.34	103
SPOT53	0.16045	0.00161	0.2653	0.00388	5.86868	0.08483	0.07783	0.00079	0.988358637	2460.4	16.87	1516.9	19.79	1956.6	12.54	1515	14.79	62
SPOT54	0.166	0.00172	0.48397	0.00713	11.07632	0.16232	0.11877	0.00133	0.99473054	2517.8	17.3	2544.5	30.99	2529.6	13.65	2268.5	23.97	101
SPOT55	0.17861	0.0018	0.29414	0.00432	7.24316	0.1051	0.09647	0.00098	0.987972778	2640	16.68	1662.2	21.53	2141.8	12.95	1861.4	18.08	63
SPOT56	0.16586	0.00173	0.4706	0.00696	10.76115	0.15844	0.12594	0.0015	0.995517347	2516.3	17.43	2486.2	30.52	2502.7	13.68	2397.5	26.9	99
SPOT57	0.17126	0.00188	0.48011	0.00718	11.33593	0.17058	0.12877	0.00156	0.993831454	2570	18.21	2527.8	31.26	2551.2	14.04	2448.3	27.95	98
SPOT58	0.17677	0.0018	0.48276	0.00714	11.76568	0.17188	0.14169	0.00186	0.98773713	2622.8	16.86	2539.3	31.02	2585.9	13.67	2678.3	32.9	97
SPOT59	0.17196	0.00175	0.34936	0.00516	8.28259	0.12087	0.10096	0.00102	0.988042977	2576.8	16.87	1931.5	24.67	2262.4	13.22	1944	18.66	75
SPOT60	0.18041	0.0021	0.33085	0.00502	8.22936	0.12717	0.02905	0.00041	0.981869949	2656.6	19.16	1842.5	24.29	2256.6	13.99	578.7	8.04	69
SPOT61*	0.25824	0.00738	1.10421	0.0281	39.31402	1.15733	0.92299	0.03482	0.86445997	3236	44.36	4795.7	86.08	3753.6	29.15	******	366	148
SPOT62	0.1736	0.00215	0.45899	0.00708	10.98538	0.17574	0.13513	0.00194	0.964216361	2592.6	20.55	2435.1	31.28	2521.9	14.89	2561.9	34.52	94
SPOT63	0.17003	0.00174	0.46221	0.00688	10.83533	0.15919	0.11955	0.00122	0.987016787	2558	17.02	2449.3	30.32	2509.1	13.66	2282.4	21.96	96
SPOT64	0.16704	0.00206	0.47894	0.00739	11.02992	0.17649	0.12473	0.00166	0.964307596	2528.2	20.6	2522.7	32.22	2525.7	14.9	2375.7	29.8	100

SPOT65	0.17183	0.00187	0.52465	0.00717	12.43273	0.17425	0.13183	0.00161	0.975086613	2575.6	18.1	2718.9	30.32	2637.7	13.17	2502.9	28.79	106
SPOT66*	0.15663	0.00299	0.25279	0.00413	5.45933	0.10947	0.72265	0.01836	0.814768801	2419.6	32.01	1452.8	21.23	1894.2	17.21	******	215.37	60
SPOT67	0.16948	0.00181	0.52651	0.00726	12.30061	0.1722	0.12877	0.00144	0.984971124	2552.5	17.8	2726.7	30.67	2627.6	13.15	2448.4	25.75	107
SPOT68	0.16554	0.00188	0.50148	0.00706	11.44595	0.16561	0.12149	0.00139	0.973007911	2513.1	18.92	2620.2	30.3	2560.2	13.51	2317.4	25.04	104
SPOT69	0.16701	0.00172	0.48565	0.00671	11.18265	0.15459	0.1027	0.00113	0.999453199	2527.9	17.18	2551.8	29.13	2538.5	12.88	1976	20.73	101
SPOT70	0.15988	0.00161	0.3848	0.00532	8.48264	0.11615	0.0843	0.00082	0.990402229	2454.4	16.94	2098.7	24.77	2284.1	12.44	1635.8	15.26	86
SPOT71	0.16133	0.00186	0.12283	0.00171	2.73115	0.03971	0.04297	0.00054	0.957496785	2469.6	19.37	746.8	9.83	1337	10.81	850.4	10.45	30
SPOT72	0.16767	0.0017	0.49887	0.00694	11.53286	0.1587	0.10796	0.00103	0.989162912	2534.5	16.87	2608.9	29.86	2567.2	12.86	2072.2	18.87	103
SPOT73	0.17069	0.00182	0.50227	0.00689	11.8194	0.16588	0.14403	0.00188	0.977424874	2564.5	17.68	2623.5	29.56	2590.2	13.14	2719.7	33.28	102
SPOT74	0.16514	0.0017	0.48932	0.00681	11.1415	0.15473	0.11231	0.00118	0.997876318	2508.9	17.16	2567.7	29.5	2535	12.94	2151.4	21.47	102
SPOT75	0.12207	0.00127	0.18112	0.00248	3.04774	0.04231	0.0659	0.00091	0.986325272	1986.6	18.42	1073.1	13.53	1419.7	10.61	1290	17.23	54
SPOT76	0.13331	0.00138	0.22258	0.00307	4.09044	0.05707	0.07769	0.00111	0.988585854	2142.1	18.03	1295.5	16.19	1652.4	11.38	1512.2	20.91	60
SPOT77	0.16701	0.00178	0.49364	0.00679	11.36242	0.15755	0.12313	0.0023	0.992000433	2527.9	17.8	2586.4	29.31	2553.3	12.94	2347.1	41.37	102
SPOT78	0.16712	0.00172	0.38202	0.00522	8.79865	0.11951	0.07832	0.00133	0.994039864	2529	17.17	2085.7	24.36	2317.4	12.38	1524	24.98	82
SPOT79	0.16847	0.00174	0.50893	0.00701	11.81955	0.16216	0.12152	0.00176	0.996053871	2542.5	17.22	2652	29.93	2590.2	12.84	2318	31.65	104
SPOT80	0.16403	0.0017	0.36516	0.00507	8.25753	0.114	0.09436	0.00122	0.994328598	2497.7	17.33	2006.6	23.93	2259.7	12.5	1822.6	22.59	80
SPOT81	0.16596	0.0017	0.39972	0.00553	9.14542	0.1255	0.11296	0.00148	0.991906687	2517.3	17.11	2167.8	25.48	2352.7	12.56	2163.1	26.85	86
SPOT82	0.16607	0.00178	0.36698	0.00518	8.40177	0.11968	0.10873	0.00166	0.990915385	2518.4	17.88	2015.2	24.45	2275.4	12.92	2086.1	30.33	80
SPOT83	0.1662	0.00173	0.41818	0.00589	9.58144	0.13419	0.07643	0.00108	0.994345544	2519.8	17.35	2252.2	26.78	2395.4	12.88	1488.6	20.24	89
SPOT84	0.16467	0.0017	0.37884	0.00519	8.59897	0.11691	0.10131	0.00168	0.992415861	2504.2	17.23	2070.9	24.28	2296.4	12.37	1950.5	30.8	83
SPOT85	0.16699	0.0018	0.51368	0.0072	11.82574	0.1666	0.12336	0.00177	0.994931472	2527.7	18	2672.3	30.67	2590.7	13.19	2351.1	31.91	106
SPOT86	0.16148	0.00167	0.30166	0.00411	6.71509	0.09034	0.04908	0.00121	0.987425079	2471.2	17.36	1699.6	20.34	2074.6	11.89	968.4	23.22	69
SPOT87	0.16518	0.00189	0.52596	0.00739	11.97723	0.17244	0.13006	0.00223	0.975910739	2509.4	19.12	2724.4	31.23	2602.6	13.49	2471.4	39.92	109
SPOT88	0.16611	0.00173	0.50792	0.00705	11.63133	0.16018	0.12462	0.00185	0.992167756	2518.8	17.44	2647.7	30.12	2575.2	12.88	2373.9	33.25	105
SPOT89	0.16681	0.00171	0.49429	0.00686	11.36763	0.15571	0.11563	0.00201	0.986970754	2525.9	17.07	2589.2	29.59	2553.8	12.78	2211.6	36.39	103
SPOT90	0.16915	0.00172	0.48752	0.00673	11.36872	0.15409	0.1212	0.00236	0.981838952	2549.3	16.93	2559.9	29.17	2553.9	12.65	2312.4	42.47	100
SPOT91	0.16465	0.0017	0.40893	0.00564	9.28336	0.12672	0.11051	0.00282	0.989714289	2504	17.29	2210	25.79	2366.4	12.51	2118.6	51.27	88
SPOT92	0.16528	0.00171	0.43939	0.00615	10.01024	0.1391	0.09437	0.00192	0.992790683	2510.4	17.31	2347.9	27.53	2435.7	12.83	1822.7	35.55	94
SPOT93	0.16626	0.00166	0.52026	0.00717	11.92563	0.1605	0.12411	0.00223	0.97655113	2520.4	16.64	2700.3	30.42	2598.6	12.61	2364.7	40.09	107
SPOT94	0.14466	0.00144	0.18582	0.00256	3.70555	0.04991	0.03622	0.00063	0.977658955	2283.7	17.04	1098.7	13.91	1572.6	10.77	719.2	12.34	48
SPOT95	0.16071	0.00169	0.34017	0.00465	7.53401	0.10269	0.0815	0.00393	0.99711447	2463.1	17.63	1887.5	22.37	2177	12.22	1583.7	73.47	77
SPOT96	0.14782	0.00146	0.25723	0.00354	5.24222	0.0702	0.04516	0.0008	0.973061355	2320.9	16.89	1475.6	18.14	1859.5	11.42	892.8	15.57	64
SPOT97	0.16718	0.00173	0.52374	0.00723	12.07091	0.16426	0.12976	0.00282	0.985755601	2529.6	17.24	2715	30.57	2609.9	12.76	2466	50.4	107

SPOT98	0.14623	0.00152	0.23007	0.00313	4.63873	0.06141	0.05597	0.00337	0.973095933	2302.3	17.72	1334.9	16.41	1756.3	11.06	1100.8	64.53	58
SPOT99	0.1641	0.00167	0.50344	0.00697	11.38724	0.15526	0.13785	0.0028	0.98481816	2498.4	17.03	2628.6	29.89	2555.4	12.73	2610.1	49.71	105
SPOT100	0.15645	0.00158	0.26876	0.00373	5.79662	0.07871	0.03848	0.00078	0.97838747	2417.7	16.99	1534.5	18.93	1945.9	11.76	763.2	15.26	63
SPOT101	0.16738	0.0017	0.50124	0.00692	11.5666	0.15817	0.12039	0.00267	0.990508084	2531.7	16.91	2619.1	29.72	2570	12.78	2297.7	48.25	103
SPOT102	0.16638	0.0017	0.50226	0.00697	11.5209	0.15853	0.11406	0.00236	0.991564265	2521.6	17.09	2623.5	29.91	2566.3	12.86	2183.2	42.83	104
SPOT103	0.16104	0.00162	0.39313	0.00542	8.72917	0.11909	0.08402	0.00176	0.989553419	2466.7	16.9	2137.3	25.1	2310.1	12.43	1630.7	32.83	87
SPOT104	0.16727	0.00186	0.40464	0.00551	9.33223	0.13039	0.0995	0.00577	0.974594453	2530.5	18.56	2190.4	25.29	2371.2	12.81	1917.2	106.08	87
SPOT105	0.1697	0.00177	0.47838	0.00661	11.19063	0.15455	0.10814	0.00282	0.999507432	2554.7	17.35	2520.2	28.81	2539.1	12.87	2075.4	51.42	99
SPOT106	0.16076	0.00173	0.35993	0.00486	7.97931	0.1098	0.04891	0.00275	0.981253504	2463.7	18.05	1981.8	23.03	2228.7	12.42	965.1	53.05	80
SPOT107	0.1713	0.00189	0.5218	0.00713	12.32687	0.17279	0.12732	0.00649	0.974809306	2570.4	18.29	2706.8	30.2	2629.6	13.17	2422.3	116.3	105
SPOT108	0.15644	0.00164	0.29499	0.00399	6.36564	0.08728	0.0542	0.0022	0.98649057	2417.5	17.7	1666.4	19.86	2027.5	12.03	1066.9	42.13	69
SPOT109	0.17116	0.00183	0.50161	0.00682	11.83965	0.16355	0.1181	0.0052	0.98425245	2569	17.77	2620.7	29.3	2591.8	12.93	2256.3	94.01	102
SPOT110	0.16439	0.00176	0.29104	0.00402	6.5952	0.09216	0.06944	0.00194	0.98845949	2501.3	17.93	1646.7	20.06	2058.7	12.32	1356.9	36.62	66
SPOT111	0.16764	0.00173	0.49828	0.00686	11.51385	0.15833	0.10698	0.00289	0.998830935	2534.2	17.23	2606.4	29.53	2565.7	12.85	2054.2	52.81	103
SPOT112	0.16619	0.00182	0.45113	0.00617	10.33869	0.14501	0.12996	0.00528	0.975104176	2519.7	18.27	2400.3	27.43	2465.6	12.99	2469.6	94.49	95

Sample GF09	Isotope Ratios									Ages (Ma)								
Spot Name	Pb207/Pb206	± 1σ	Pb206/U238	± 1σ	Pb207/U235	± 1σ	Pb208/Th232	± 1σ	rho	Pb207/Pb206	± 1σ	Pb206/U238	± 1σ	Pb207/U235	± 1σ	Pb208/Th232	± 1σ	Conc. (%)
SPOT01	0.20739	0.00255	0.02786	0.00039	0.7962	0.01155	0.00275	0.00003	0.964991936	2885.2	19.8	177.2	2.42	594.7	6.53	55.6	0.63	6
SPOT02*	0.53827	0.0062	0.98534	0.01456	73.09618	1.0546	0.41622	0.00424	0.976377638	4349.6	16.77	4420.9	47.26	4371.6	14.45	7033.7	60.46	102
SPOT03*	0.50584	0.00942	0.84655	0.01665	59.02386	1.15033	0.59953	0.01062	0.990907726	4258.3	27.15	3953.7	58.13	4157.7	19.46	9493.9	134.24	93
SPOT04*	0.78399	0.05226	0.77478	0.05093	83.63683	4.7981	0.14863	0.00732	0.87272307	4892.9	91.85	3698.2	184.98	4506.6	57.56	2800.8	128.85	76
SPOT05	0.16824	0.00184	0.1048	0.00136	2.42996	0.03257	0.00773	0.00008	0.968186431	2540.2	18.27	642.5	7.96	1251.5	9.64	155.7	1.66	25
SPOT06	0.1701	0.00214	0.1486	0.00194	3.48289	0.04952	0.01056	0.00014	0.918210052	2558.6	20.92	893.1	10.9	1523.3	11.22	212.4	2.78	35
SPOT07	0.55084	0.02245	0.30566	0.01065	23.20606	0.76698	0.01768	0.0006	0.948574902	4383.4	58.33	1719.3	52.6	3235.6	32.17	354.2	11.9	39
SPOT08	0.21117	0.00262	0.0216	0.00031	0.62867	0.00936	0.00155	0.00002	0.963950716	2914.6	19.97	137.8	1.96	495.3	5.84	31.2	0.34	5
SPOT09	0.1949	0.00211	0.0408	0.00057	1.09555	0.01533	0.00336	0.00004	0.998400388	2784	17.59	257.8	3.52	751.2	7.43	67.9	0.71	9
SPOT10	0.18989	0.00203	0.0312	0.00043	0.81673	0.01121	0.00243	0.00002	0.995894291	2741.2	17.45	198.1	2.67	606.2	6.26	49.1	0.48	7
SPOT11	0.17391	0.00202	0.05238	0.00073	1.25559	0.01807	0.00294	0.00004	0.968382788	2595.6	19.21	329.1	4.47	825.9	8.13	59.4	0.73	13
SPOT12	0.20499	0.00268	0.02718	0.00038	0.76812	0.01149	0.00244	0.00003	0.934637471	2866.3	21.13	172.9	2.39	578.7	6.6	49.3	0.66	6
SPOT13	0.15491	0.00164	0.08863	0.00124	1.89237	0.02665	0.00854	0.00009	0.993458608	2400.9	17.92	547.4	7.36	1078.4	9.36	172	1.82	23
SPOT14	0.17708	0.00201	0.05042	0.00069	1.23091	0.01747	0.00463	0.00006	0.964227791	2625.7	18.77	317.1	4.23	814.8	7.95	93.4	1.14	12
SPOT15*	0.53258	0.02245	0.88399	0.03543	64.92138	2.55614	0.98675	0.04633	0.982365481	4334	60.45	4083.1	121.24	4252.9	39.37	******	471.36	94
SPOT16	0.3836	0.00486	0.00861	0.00013	0.45491	0.00673	0.00165	0.00002	0.979826948	3846	18.98	55.2	0.8	380.7	4.7	33.2	0.43	1

SPOT17*	0.81625	0.03401	1.20683	0.05543	135.80275	5.56307	0.12261	0.00404	0.891881548	4950.4	58	5102.7	161.93	4994.2	41.29	2337.7	72.81	103
SPOT18	0.2098	0.00228	0.03628	0.0005	1.0491	0.01474	0.00408	0.00005	0.980894116	2904	17.54	229.7	3.11	728.4	7.3	82.4	0.96	8
SPOT19	0.1578	0.00163	0.15888	0.00224	3.45585	0.04814	0.03398	0.00035	0.988035195	2432.3	17.43	950.5	12.43	1517.2	10.97	675.4	6.84	39
SPOT20	0.11689	0.00122	0.14553	0.00209	2.3456	0.03292	0.01062	0.00014	0.977264486	1909.2	18.61	875.9	11.74	1226.2	9.99	213.4	2.71	46
SPOT21	0.15634	0.00167	0.28383	0.00398	6.11602	0.08632	0.05936	0.00072	0.993532871	2416.5	18.02	1610.6	19.98	1992.5	12.32	1165.5	13.7	67
SPOT22	0.19737	0.00224	0.03365	0.00047	0.91524	0.01319	0.00362	0.00005	0.969176748	2804.5	18.45	213.3	2.93	659.8	6.99	73.1	0.96	8
SPOT23	0.16124	0.00187	0.21941	0.00293	4.87834	0.06841	0.02	0.00025	0.95227784	2468.7	19.5	1278.8	15.49	1798.5	11.82	400.3	4.99	52
SPOT24	0.21899	0.00233	0.02777	0.00039	0.83834	0.0118	0.00275	0.00003	0.997761882	2973.3	17.05	176.6	2.47	618.2	6.52	55.5	0.61	6
SPOT25	0.25233	0.00271	0.01632	0.00023	0.5679	0.00794	0.00246	0.00003	0.992066883	3199.4	16.86	104.4	1.44	456.7	5.14	49.7	0.57	3
SPOT26	0.1691	0.00209	0.17692	0.00255	4.12393	0.06277	0.01481	0.00023	0.946939878	2548.7	20.57	1050.1	13.98	1659.1	12.44	297.1	4.59	41
SPOT27	0.15809	0.00171	0.07425	0.00106	1.61837	0.02315	0.00272	0.00004	0.998013075	2435.3	18.24	461.7	6.38	977.4	8.98	54.8	0.72	19
SPOT28	0.19357	0.00235	0.03123	0.00044	0.8334	0.01232	0.00282	0.00004	0.953067106	2772.8	19.76	198.2	2.75	615.5	6.82	57	0.86	7
SPOT29	0.25112	0.00257	0.0353	0.00048	1.22221	0.01646	0.00743	0.00008	0.990415586	3191.9	16.09	223.6	2.98	810.8	7.52	149.5	1.62	7
SPOT30	0.14864	0.00158	0.07914	0.00106	1.62208	0.02194	0.01177	0.00015	0.990251401	2330.3	18.06	491	6.33	978.8	8.5	236.6	2.95	21
SPOT31	0.23601	0.00253	0.02487	0.00035	0.80914	0.01147	0.00288	0.00003	0.992778841	3093.2	17.03	158.3	2.22	602	6.44	58.1	0.68	5
SPOT32	0.17711	0.0023	0.05397	0.00078	1.31797	0.02032	0.00345	0.00005	0.937397964	2625.9	21.41	338.9	4.75	853.6	8.9	69.7	1.03	13
SPOT33	0.15492	0.00167	0.06388	0.00085	1.36447	0.01833	0.00626	0.00008	0.990502429	2400.9	18.2	399.2	5.13	873.8	7.87	126.2	1.69	17
SPOT34	0.17236	0.00188	0.06428	0.00089	1.52784	0.02154	0.00579	0.00008	0.982078754	2580.7	18.08	401.6	5.4	941.6	8.65	116.7	1.51	16
SPOT35	0.22794	0.0026	0.0363	0.00049	1.14099	0.01567	0.00271	0.00004	0.982884071	3037.6	18.15	229.9	3.04	773	7.43	54.8	0.78	8
SPOT36	0.16873	0.00202	0.11727	0.0016	2.7283	0.03881	0.00744	0.00011	0.959138972	2545.1	19.92	714.8	9.24	1336.2	10.57	149.7	2.3	28

Sample GF06	Isotope Ratios									Ages (Ma)								
Spot Name	Pb207/Pb206	± 1σ	Pb206/U238	± 1σ	Pb207/U235	± 1σ	Pb208/Th232	± 1σ	rho	Pb207/Pb206	± 1σ	Pb206/U238	± 1σ	Pb207/U235	± 1σ	Pb208/Th232	± 1σ	Conc. (%)
spot1	0.17087	0.00191	0.18114	0.00262	4.26638	0.06238	0.01528	0.00019	0.989238687	2566.2	18.59	1073.2	14.28	1686.9	12.03	306.5	3.76	42
spot2	0.16868	0.00202	0.3559	0.00555	8.2745	0.13104	0.04604	0.00058	0.984697581	2544.6	19.89	1962.7	26.37	2261.5	14.35	909.8	11.21	77
spot3	0.17194	0.00184	0.45873	0.00655	10.8718	0.15554	0.08858	0.00115	0.998029818	2576.6	17.78	2434	28.97	2512.2	13.3	1715.5	21.37	94
spot4	0.1638	0.00198	0.41767	0.00664	9.42775	0.15165	0.06413	0.00083	0.9883265	2495.3	20.23	2249.9	30.2	2380.5	14.77	1256.3	15.76	90
spot5	0.13775	0.00151	0.41433	0.0063	7.86433	0.11957	0.0956	0.00119	0.999922477	2199.1	18.96	2234.7	28.7	2215.6	13.7	1845.3	21.99	102
spot6	0.21479	0.00398	0.42968	0.00793	12.7232	0.25842	0.07522	0.00155	0.90865345	2942	29.61	2304.3	35.74	2659.4	19.12	1465.9	29.07	78
spot7	0.16921	0.00188	0.33001	0.00503	7.69498	0.11694	0.03244	0.00042	0.997044883	2549.9	18.5	1838.4	24.37	2196	13.66	645.3	8.3	72
spot8	0.18229	0.00314	0.26232	0.00439	6.58536	0.12522	0.02298	0.00049	0.880114019	2673.9	28.27	1501.7	22.4	2057.4	16.76	459.3	9.65	56
spot9	0.1607	0.00174	0.46204	0.00692	10.23304	0.15305	0.1088	0.00144	0.99862433	2463	18.22	2448.5	30.51	2456.1	13.83	2087.5	26.32	99
spot10	0.16246	0.00179	0.42835	0.00631	9.59194	0.14258	0.10218	0.00138	0.9910109	2481.4	18.48	2298.3	28.48	2396.4	13.67	1966.5	25.24	93
spot11	0.15844	0.00173	0.46029	0.007	10.04403	0.15159	0.10119	0.00128	0.992421242	2439.1	18.36	2440.9	30.89	2438.8	13.94	1948.3	23.41	100

spot12	0.16685	0.00183	0.43977	0.00673	10.11267	0.15494	0.08334	0.00112	0.998830392	2526.3	18.29	2349.6	30.13	2445.1	14.16	1618	20.9	93
spot13	0.16669	0.00203	0.29119	0.00465	6.68616	0.109	0.03859	0.00075	0.979550349	2524.7	20.35	1647.5	23.2	2070.8	14.4	765.4	14.54	65
spot14	0.16613	0.0018	0.27193	0.0041	6.22684	0.09425	0.0342	0.00048	0.996123261	2519.1	18.05	1550.6	20.75	2008.2	13.24	679.7	9.42	62
spot15	0.16983	0.00201	0.20937	0.00318	4.90192	0.07693	0.01876	0.0003	0.967794509	2555.9	19.64	1225.5	16.97	1802.6	13.23	375.7	5.93	48
spot16	0.11166	0.00153	0.38042	0.00582	5.85455	0.09912	0.09645	0.00154	0.903632556	1826.6	24.58	2078.3	27.2	1954.5	14.68	1861	28.34	114
spot17	0.12076	0.00156	0.26961	0.00432	4.48645	0.07633	0.03652	0.00069	0.941792701	1967.5	22.8	1538.8	21.96	1728.5	14.13	725	13.39	78
spot18	0.16835	0.00221	0.53847	0.00868	12.4947	0.21138	0.13863	0.00242	0.952840377	2541.3	21.8	2777	36.38	2642.3	15.91	2624.1	42.93	109
spot19	0.17312	0.00206	0.51084	0.0078	12.19054	0.19152	0.12768	0.00225	0.971893141	2588	19.69	2660.2	33.27	2619.2	14.74	2428.8	40.28	103
spot20	0.1714	0.00232	0.20404	0.00333	4.82053	0.08314	0.01756	0.00033	0.946266986	2571.4	22.49	1197	17.81	1788.5	14.5	351.7	6.6	47
spot21	0.13735	0.00271	0.35261	0.00632	6.67644	0.14559	0.10507	0.00239	0.821931941	2194.1	33.86	1947	30.11	2069.5	19.26	2019.4	43.67	89
spot22	0.17494	0.00195	0.14002	0.00225	3.37723	0.0547	0.01803	0.00031	0.992123546	2605.5	18.48	844.8	12.72	1499.1	12.69	361.3	6.16	32
spot23	0.18201	0.00229	0.44791	0.00761	11.24044	0.1953	0.05738	0.00229	0.977856139	2671.3	20.66	2386	33.89	2543.3	16.2	1127.7	43.84	89
spot24	0.16716	0.0018	0.5123	0.00771	11.80561	0.17789	0.12955	0.00217	0.998773289	2529.4	17.91	2666.5	32.85	2589.1	14.11	2462.2	38.75	105
spot25	0.16397	0.00178	0.49386	0.00772	11.16088	0.17422	0.12577	0.00243	0.998587493	2497	18.13	2587.4	33.29	2536.7	14.55	2394.4	43.63	104
spot26	0.17078	0.00183	0.47163	0.00711	11.10375	0.16735	0.10835	0.00175	0.999741829	2565.3	17.79	2490.7	31.13	2531.9	14.04	2079.3	31.94	97
spot27	0.16779	0.00187	0.47145	0.00721	10.90576	0.16838	0.12548	0.00226	0.99052412	2535.7	18.59	2489.9	31.58	2515.1	14.36	2389.4	40.51	98
spot28	0.17428	0.00189	0.45395	0.00664	10.91864	0.1582	0.03999	0.00051	0.990553355	2599.2	17.94	2412.8	29.43	2516.2	13.48	792.5	9.86	93
spot29	0.17977	0.00217	0.42452	0.00638	10.53046	0.16207	0.07894	0.00127	0.976488727	2650.7	19.89	2281	28.88	2482.6	14.27	1535.6	23.7	86
spot30	0.16374	0.00179	0.43369	0.00621	9.79337	0.14032	0.09282	0.00122	0.99936648	2494.6	18.3	2322.3	27.9	2415.5	13.2	1794	22.5	93
spot31	0.17715	0.00206	0.21904	0.00325	5.34566	0.08165	0.01254	0.00021	0.971415601	2626.4	19.24	1276.8	17.2	1876.2	13.07	251.9	4.24	49
spot32	0.16578	0.0018	0.47054	0.00699	10.76018	0.15912	0.07545	0.00125	0.995461816	2515.5	18.09	2485.9	30.64	2502.6	13.74	1470.3	23.5	99
spot33*	-1.28028	1.52947	-0.45126	0.48764	79.44523	61.27409	1.98992	5.13792	-1.401081634	0.1	3179.51	******		5728.71	4455.1	773.4	******	*******	#VALUE!
spot34	0.17901	0.00248	0.17732	0.0028	4.37198	0.07354	0.01264	0.00025	0.938760591	2643.7	22.8	1052.3	15.31	1707.1	13.9	253.9	5	40
spot35	0.17547	0.00212	0.29808	0.00459	7.20515	0.11415	0.02952	0.00051	0.971956792	2610.5	19.94	1681.8	22.78	2137.1	14.13	588.1	9.95	64
spot36	0.16219	0.00187	0.43044	0.00601	9.61812	0.13746	0.11027	0.00154	0.976957567	2478.6	19.29	2307.7	27.07	2398.9	13.15	2114.2	27.99	93
spot37	0.16425	0.00174	0.45367	0.00625	10.27206	0.14243	0.12416	0.00169	0.993564416	2499.9	17.74	2411.6	27.72	2459.6	12.83	2365.5	30.44	96
spot38	0.17322	0.00196	0.11273	0.00174	2.6909	0.04207	0.00813	0.00012	0.98726738	2589	18.73	688.6	10.11	1326	11.57	163.7	2.46	27
spot39	0.169	0.00209	0.18398	0.00282	4.28638	0.06894	0.01707	0.00029	0.953010937	2547.7	20.59	1088.7	15.36	1690.7	13.24	342.2	5.83	43
spot40	0.16847	0.00253	0.48276	0.00809	11.20618	0.20461	0.12719	0.00255	0.917799849	2542.5	24.96	2539.3	35.17	2540.4	17.02	2420	45.78	100
spot41	0.16759	0.0023	0.22418	0.00368	5.17648	0.09007	0.01813	0.00038	0.943420549	2533.7	22.87	1303.9	19.38	1848.8	14.81	363.2	7.52	51
spot42	0.16623	0.00177	0.49399	0.00727	11.32045	0.1678	0.11035	0.00149	0.992859939	2520	17.74	2587.9	31.36	2549.9	13.83	2115.7	27.06	103
spot43	0.16114	0.00168	0.19412	0.00285	4.31185	0.06344	0.01964	0.00026	0.997872484	2467.7	17.54	1143.7	15.4	1695.6	12.13	393.1	5.1	46
spot44	0.16617	0.00199	0.48829	0.00725	11.18745	0.17355	0.07329	0.0011	0.957120605	2519.5	20.03	2563.3	31.41	2538.9	14.46	1429.6	20.77	102

spot45	0.16972	0.00192	0.4235	0.00628	9.90707	0.15115	0.03995	0.00067	0.971948624	2554.8	18.78	2276.4	28.43	2426.2	14.07	791.8	13.1	89
SPOT46	0.19272	0.00293	0.14824	0.00219	3.94761	0.06529	0.01274	0.00022	0.893236128	2765.5	24.72	891.1	12.32	1623.5	13.4	255.9	4.35	32
SPOT47	0.17324	0.00191	0.30107	0.00398	7.19636	0.09783	0.02625	0.00033	0.972425675	2589.2	18.33	1696.6	19.74	2136.1	12.12	523.8	6.48	66
SPOT48	0.16746	0.00195	0.32386	0.00452	7.49341	0.1083	0.04621	0.00055	0.96567761	2532.5	19.42	1808.6	22.01	2172.2	12.95	913	10.67	71
SPOT49	0.1599	0.00172	0.25009	0.00342	5.5225	0.07656	0.03064	0.00039	0.986423884	2454.6	18.12	1438.9	17.64	1904.1	11.92	610.1	7.58	59
SPOT50	0.16648	0.00175	0.38263	0.0051	8.78983	0.11848	0.06875	0.00085	0.988841281	2522.6	17.56	2088.6	23.78	2316.4	12.29	1343.8	16.03	83
SPOT51	0.14424	0.00174	0.24698	0.00355	4.92637	0.07444	0.03778	0.00045	0.951233703	2278.7	20.66	1422.9	18.35	1806.8	12.75	749.5	8.75	62
SPOT52	0.16577	0.00191	0.48041	0.00679	11.00126	0.16068	0.11435	0.00133	0.967694652	2515.4	19.24	2529.1	29.57	2523.2	13.59	2188.4	24.05	101
SPOT53	0.16743	0.00177	0.17421	0.00235	4.02378	0.05492	0.02234	0.00024	0.98832204	2532.1	17.67	1035.3	12.88	1639	11.1	446.6	4.81	41
SPOT54	0.1645	0.0018	0.46015	0.00639	10.44632	0.14768	0.10128	0.00113	0.982297579	2502.5	18.27	2440.2	28.22	2475.2	13.1	1950	20.78	98
SPOT55	0.17534	0.00194	0.18886	0.00268	4.5721	0.06614	0.00882	0.0001	0.980948797	2609.3	18.29	1115.2	14.54	1744.2	12.05	177.6	2.07	43
SPOT56	0.16937	0.00183	0.36129	0.00497	8.4415	0.11838	0.02834	0.00033	0.980938402	2551.4	17.99	1988.3	23.56	2279.7	12.73	564.8	6.58	78
SPOT57	0.17641	0.00189	0.24254	0.00336	5.90226	0.08288	0.00802	0.0001	0.986562261	2619.4	17.69	1399.9	17.44	1961.6	12.19	161.5	1.94	53
SPOT58	0.17065	0.00192	0.23527	0.0033	5.53398	0.07929	0.03837	0.00054	0.978963624	2564	18.68	1362.1	17.22	1905.9	12.32	761.1	10.49	53
SPOT59	0.16561	0.00171	0.46579	0.00606	10.63438	0.13913	0.09887	0.00113	0.994429166	2513.7	17.27	2465.1	26.66	2491.7	12.14	1905.7	20.73	98
SPOT60	0.22061	0.00226	0.56301	0.00737	17.12376	0.22382	0.13214	0.00148	0.998500714	2985.2	16.41	2879	30.39	2941.8	12.54	2508.6	26.49	96
SPOT61	0.11572	0.00134	0.28811	0.00407	4.59544	0.06739	0.03929	0.00058	0.963313664	1891.2	20.68	1632.1	20.35	1748.4	12.23	779	11.31	86
SPOT62	0.12328	0.00136	0.23932	0.00318	4.06711	0.05592	0.03522	0.00046	0.966422164	2004.3	19.53	1383.2	16.52	1647.7	11.21	699.7	9.01	69
SPOT63	0.17913	0.00198	0.13689	0.00178	3.37999	0.04537	0.00715	0.0001	0.968712525	2644.8	18.2	827	10.1	1499.8	10.52	143.9	1.93	31
SPOT64	0.1659	0.00183	0.16118	0.00202	3.68668	0.04747	0.02113	0.00028	0.973321752	2516.7	18.43	963.3	11.2	1568.5	10.28	422.6	5.46	38
SPOT65	0.16667	0.00177	0.36596	0.00505	8.40904	0.11727	0.04115	0.0005	0.989503312	2524.5	17.76	2010.3	23.85	2276.2	12.66	815	9.79	80
SPOT66	0.1611	0.00164	0.48468	0.00629	10.76567	0.13953	0.12808	0.00141	0.998690652	2467.3	17.12	2547.6	27.31	2503.1	12.04	2436	25.3	103
SPOT67	0.19143	0.00202	0.08193	0.0011	2.16207	0.02934	0.00871	0.0001	0.989371445	2754.5	17.24	507.7	6.54	1168.9	9.42	175.3	2.08	18
SPOT68	0.16158	0.00174	0.43936	0.00617	9.785	0.13901	0.07839	0.00107	0.988506285	2472.3	18.1	2347.8	27.63	2414.7	13.09	1525.3	20.03	95
SPOT69	0.17056	0.00209	0.31248	0.00447	7.34569	0.11093	0.03713	0.00058	0.947259306	2563.1	20.32	1752.9	21.98	2154.4	13.5	736.8	11.25	68
SPOT70	0.17706	0.00186	0.29587	0.00378	7.22124	0.09349	0.02824	0.00035	0.986818965	2625.5	17.37	1670.8	18.82	2139.1	11.55	562.8	6.91	64
SPOT71	0.16343	0.00189	0.48701	0.00653	10.97246	0.15388	0.13452	0.00204	0.956086379	2491.5	19.32	2557.7	28.31	2520.8	13.05	2550.9	36.32	103
SPOT72	0.16189	0.00181	0.49371	0.00714	11.02016	0.16282	0.11872	0.0019	0.97882812	2475.5	18.77	2586.7	30.81	2524.8	13.75	2267.6	34.36	104
SPOT73	0.17322	0.00185	0.16398	0.00227	3.91625	0.0549	0.01944	0.00026	0.987490755	2589	17.75	978.9	12.56	1617	11.34	389.2	5.2	38
SPOT74	0.15731	0.00168	0.23403	0.00296	5.07381	0.06569	0.08358	0.00114	0.976911263	2426.9	17.98	1355.6	15.48	1831.7	10.98	1622.5	21.29	56
SPOT75	0.17576	0.00214	0.16579	0.0024	4.01869	0.06138	0.04602	0.00079	0.94778653	2613.3	20.09	988.9	13.28	1638	12.42	909.4	15.32	38
SPOT76	0.16893	0.00188	0.38743	0.00544	9.02451	0.13149	0.06168	0.00099	0.963688238	2547.1	18.55	2110.9	25.28	2340.5	13.32	1209.7	18.8	83
SPOT77	0.17735	0.00199	0.13262	0.00174	3.24249	0.04402	0.01303	0.00024	0.966426504	2628.2	18.57	802.8	9.91	1467.4	10.54	261.7	4.79	31

SPOT78	0.17084	0.00185	0.18722	0.00254	4.40963	0.06132	0.02353	0.00035	0.975621764	2565.9	17.98	1106.3	13.78	1714.2	11.51	470.1	6.85	43
SPOT79	0.1687	0.00184	0.40444	0.00569	9.40827	0.13561	0.09053	0.00129	0.976059339	2544.8	18.2	2189.4	26.12	2378.6	13.23	1751.6	23.93	86
SPOT80	0.17106	0.00209	0.20222	0.0027	4.76836	0.06807	0.02883	0.00046	0.935304327	2568	20.29	1187.3	14.45	1779.3	11.98	574.6	9.04	46
SPOT81	0.17005	0.00186	0.29706	0.00403	6.96387	0.09716	0.03115	0.00048	0.972353134	2558.1	18.16	1676.7	20.02	2106.8	12.39	620.1	9.4	66
SPOT82	0.16633	0.00173	0.48439	0.00625	11.10811	0.14532	0.12053	0.00181	0.986278648	2521.1	17.34	2546.4	27.13	2532.2	12.19	2300.2	32.74	101
SPOT83	0.08642	0.00098	0.20426	0.00264	2.43364	0.0333	0.04998	0.0008	0.944566852	1347.5	21.63	1198.2	14.12	1252.6	9.85	985.7	15.48	89
SPOT84	0.16485	0.00177	0.48809	0.00665	11.09185	0.1542	0.1016	0.00222	0.980034466	2506	17.91	2562.4	28.79	2530.9	12.95	1955.7	40.69	102
SPOT85	0.09146	0.00121	0.20773	0.00278	2.61949	0.03981	0.05644	0.00089	0.880582686	1456.2	24.86	1216.7	14.84	1306.1	11.17	1109.7	17.06	84
SPOT86	0.0905	0.00107	0.20446	0.00268	2.55112	0.03602	0.06113	0.00095	0.928354008	1436	22.3	1199.2	14.34	1286.8	10.3	1199.3	18.02	84
SPOT87	0.16962	0.00184	0.29911	0.00383	7.0079	0.0922	0.05441	0.00064	0.973250905	2553.9	18.06	1686.9	19.01	2112.4	11.69	1070.8	12.3	66
SPOT88	0.69606	0.01374	1.97425	0.04818	188.88594	4.42193	0.69959	0.01477	0.959284843	4722.6	28.08	7026.5	104.43	5327.1	23.65	******	175.67	149
SPOT89	0.16578	0.00173	0.3932	0.00511	9.00483	0.11833	0.09532	0.00104	0.98898122	2515.5	17.43	2137.7	23.63	2338.5	12.01	1840.3	19.19	85
SPOT90	0.16483	0.00184	0.2995	0.00355	6.80281	0.08438	0.04875	0.00061	0.955609254	2505.8	18.7	1688.8	17.6	2086.1	10.98	962.2	11.85	67
SPOT91	0.17642	0.00193	0.12298	0.00163	2.99289	0.04063	0.01234	0.00015	0.976330931	2619.5	18.04	747.7	9.36	1405.8	10.33	247.8	2.91	29
SPOT92	0.16962	0.00219	0.13685	0.00171	3.20854	0.04439	0.01711	0.00024	0.903178564	2553.8	21.48	826.8	9.72	1459.2	10.71	343	4.7	32
SPOT93	0.17434	0.00184	0.29484	0.0039	7.09486	0.09518	0.0248	0.00026	0.985998681	2599.8	17.52	1665.7	19.41	2123.4	11.94	495.2	5.07	64
SPOT94	0.16566	0.00179	0.41051	0.00511	9.39889	0.12016	0.08759	0.00106	0.973674523	2514.2	18.02	2217.2	23.34	2377.7	11.73	1697	19.71	88
SPOT95	0.16164	0.00171	0.14803	0.00186	3.30646	0.04229	0.034	0.00036	0.982400994	2472.9	17.7	889.9	10.44	1482.6	9.97	675.8	6.99	36
SPOT96	0.08039	0.00091	0.20179	0.00254	2.24163	0.03002	0.03621	0.00042	0.939912269	1206.5	22.08	1184.9	13.65	1194.2	9.4	718.9	8.24	98
SPOT97	0.17081	0.00187	0.4455	0.0058	10.4994	0.1414	0.08913	0.00106	0.966708099	2565.6	18.23	2375.2	25.88	2479.9	12.49	1725.8	19.58	93
SPOT98	0.16482	0.00179	0.34777	0.00484	7.90817	0.11158	0.06107	0.00068	0.986376884	2505.7	18.13	1923.9	23.14	2220.6	12.72	1198.1	12.86	77
SPOT99	0.18067	0.0025	0.1145	0.00144	2.85317	0.0403	0.01977	0.00118	0.890388635	2659	22.71	698.8	8.36	1369.6	10.62	395.8	23.45	26
SPOT100	0.16147	0.00176	0.22879	0.00297	5.08832	0.06762	0.06546	0.00276	0.976829261	2471.1	18.25	1328.1	15.59	1834.2	11.28	1281.6	52.31	54
SPOT101	0.19125	0.0023	0.11071	0.00133	2.91721	0.03718	0.01411	0.00151	0.942590587	2753	19.64	676.8	7.7	1386.4	9.64	283.2	30.1	25
SPOT102	0.11865	0.00171	0.33702	0.00469	5.50587	0.08858	0.08083	0.00383	0.864982748	1936	25.59	1872.3	22.61	1901.5	13.83	1571.1	71.64	97
SPOT103	0.1593	0.00172	0.17998	0.00237	3.94535	0.05305	0.07458	0.00334	0.979319149	2448.3	18.2	1066.9	12.96	1623	10.89	1453.9	62.78	44
SPOT104	0.17872	0.00245	0.48011	0.00697	11.82567	0.18572	0.09065	0.0072	0.924398234	2641.1	22.56	2527.7	30.35	2590.7	14.7	1753.9	133.38	96
SPOT105	0.16439	0.00169	0.4822	0.00603	10.92547	0.13649	0.11939	0.00341	0.999011756	2501.3	17.19	2536.8	26.22	2516.8	11.62	2279.5	61.57	101
SPOT106	0.1677	0.00226	0.17213	0.00245	3.97406	0.05958	0.02323	0.00282	0.949387341	2534.9	22.43	1023.8	13.47	1628.9	12.16	464.2	55.65	40
SPOT107	0.1618	0.00171	0.26512	0.00347	5.90883	0.07809	0.02792	0.00116	0.99035992	2474.6	17.68	1516	17.66	1962.5	11.48	556.7	22.88	61
SPOT108	0.16176	0.0017	0.49773	0.00631	11.09764	0.1417	0.12939	0.00392	0.992878996	2474.1	17.64	2604	27.17	2531.4	11.89	2459.5	70.07	105
SPOT109	0.1626	0.00168	0.37841	0.00482	8.47862	0.10789	0.08426	0.00245	0.999014032	2482.9	17.34	2068.8	22.52	2283.6	11.56	1635.2	45.75	83
SPOT110	0.11065	0.00165	0.35639	0.00475	5.43447	0.08676	0.08578	0.00331	0.834844811	1810.1	26.8	1965.1	22.58	1890.3	13.69	1663.4	61.57	109

SPOT111	0.16364	0.00173	0.16961	0.00225	3.8263	0.05116	0.03418	0.00123	0.992155047	2493.6	17.67	1010	12.42	1598.3	10.76	679.4	24.03	41
SPOT112	0.1756	0.00202	0.42874	0.00515	10.36992	0.13111	0.03501	0.00188	0.950063895	2611.7	19.06	2300.1	23.23	2468.4	11.71	695.5	36.62	88
SPOT113	0.16349	0.0017	0.2258	0.00282	5.08787	0.06388	0.04343	0.00128	0.994709508	2492.1	17.37	1312.5	14.81	1834.1	10.65	859.4	24.78	53
SPOT114	0.17137	0.00198	0.25335	0.00319	5.98443	0.07857	0.02646	0.00185	0.959037994	2571.1	19.18	1455.7	16.4	1973.6	11.42	527.8	36.42	57
SPOT115	0.17286	0.00191	0.5171	0.0066	12.31958	0.16117	0.1481	0.00385	0.975620897	2585.5	18.29	2686.9	28.04	2629.1	12.29	2791.5	67.76	104
SPOT116	0.10096	0.00149	0.29842	0.00395	4.15233	0.06639	0.09131	0.00245	0.827862789	1641.7	27.12	1683.4	19.63	1664.7	13.08	1766.2	45.29	103
SPOT117	0.10451	0.00141	0.30458	0.00396	4.38763	0.06557	0.09437	0.00245	0.869998727	1705.7	24.62	1714	19.58	1710	12.36	1822.7	45.17	100
SPOT118	0.16194	0.00166	0.46059	0.0057	10.28181	0.12788	0.13448	0.00339	0.995009661	2476.1	17.24	2442.2	25.17	2460.5	11.51	2550.3	60.31	99
SPOT119	0.11579	0.00142	0.34815	0.00459	5.5571	0.07898	0.1025	0.00324	0.927635517	1892.2	21.86	1925.8	21.97	1909.5	12.23	1972.2	59.47	102
SPOT120	0.16364	0.00204	0.18018	0.00236	4.06693	0.05642	0.01912	0.00197	0.944145736	2493.6	20.84	1068	12.88	1647.7	11.31	382.8	39.1	43
SPOT121	0.16209	0.0017	0.37178	0.00492	8.3069	0.10925	0.05975	0.00216	0.993810048	2477.6	17.6	2037.8	23.1	2265.1	11.92	1172.9	41.23	82
SPOT122	0.16313	0.00173	0.32688	0.00426	7.35191	0.09552	0.09022	0.0039	0.996948862	2488.4	17.73	1823.2	20.68	2155.1	11.61	1745.9	72.29	73

Sample #	Run #	Stratigraphic height (m)	Phase	Composition	$\delta^{18}O_{dol}$	$\delta^{13}C_{dol}$
1		35		DOLOMITE	-7.94	-2.08
2		41		DOLOMITE	-7.61	-1.68
3		41		DOLOMITE	-7.64	-1.69
4		41		DOLOMITE	-7.45	-1.67
5		41		DOLOMITE	-5.91	-2.96
6		41		DOLOMITE	-5.44	-3.06
7		41		DOLOMITE	-5.92	-2.45
8	2	41		DOLOMITE	-7.99	-1.74
8	1	41		DOLOMITE	-7.79	-1.86
9		41	cross-cutting vein	DOLOMITE	-7.27	-3.82
10		41		DOLOMITE	-7.7	-1.82
11		45		DOLOMITE	-6.81	-1.7
12		50		DOLOMITE	-3.96	-1.57
13		55		DOLOMITE	-3.98	-1.42
14		60		DOLOMITE	-3.61	-1.62
15		65		DOLOMITE	-5.5	-0.85
16		70		DOLOMITE	-6.1	-1.07
17		75		DOLOMITE	-5.63	-0.77
18		85		DOLOMITE	-5.75	-1
19	1	80		DOLOMITE	-4.77	-0.5
19	2	80		DOLOMITE	-4.75	-0.39
20		90		DOLOMITE	-6.5	-1.38
21		110		DOLOMITE	-6.5	-1.18
22		115		DOLOMITE	-6.77	-1.19
23		120		DOLOMITE	-6.76	-1.44
24	1	131.9		DOLOMITE	-7.47	-0.05
24	2	131.9		DOLOMITE	-7.38	0.17
25	2	145.6		DOLOMITE	-7.59	-1.05
25	1	145.6		DOLOMITE	-7.64	-1.27
26		153.1		DOLOMITE	-7.19	-0.07
27	2	160		DOLOMITE	-5.87	0.12

27	1	160		DOLOMITE	-5.96	-0.1
28	1	165		DOLOMITE	-8.08	0.15
28	2	165		DOLOMITE	-8.01	0.37
29		170		DOLOMITE	-6.51	-0.08
30		175		DOLOMITE	-7.2	-0.33
31		180		DOLOMITE	-6.57	-0.27
32		185		DOLOMITE	-6.82	-0.08
33		190		DOLOMITE	-7.43	0.35
34	2	195		DOLOMITE	-5.8	0
34	1	195		DOLOMITE	-6.08	-0.07
35		200		DOLOMITE	-7.33	0.06
36		205		DOLOMITE	-6.66	0.11
37		205	cross-cutting vein	DOLOMITE	-7.27	-0.27
38		210		DOLOMITE	-6.97	0.36
39		215		DOLOMITE	-6.57	0.64
40	1	215	cross-cutting vein	DOLOMITE	-5.45	-1.87
40	2	215		DOLOMITE	-5.39	-2.06
41	1	220		DOLOMITE	-6.75	0.49
41	2	220		DOLOMITE	-6.8	0.72
42		225		DOLOMITE	-4.17	-0.07
43		230		DOLOMITE	-5.43	0.29
44		235		DOLOMITE	-5.62	0.94
45		240		DOLOMITE	-6.86	0.67
46		250		DOLOMITE	-6.21	1.1
47		255		DOLOMITE	-6.76	0.92
48	2	255	spar	DOLOMITE	-9.61	0.69
48	1	255		DOLOMITE	-9.57	0.62
49		260		DOLOMITE	-7.56	0.97
50		265		DOLOMITE	-6.3	0.85
51		270		DOLOMITE	-6.45	0.98
52		270	spar	DOLOMITE	-6.72	0.89
53		275		DOLOMITE	-5.75	0.17
54		280		DOLOMITE	-8.71	0.32

55		280	cross-cutting vein	DOLOMITE	-9.19	0.23
56	2	285		DOLOMITE	-6.82	0.35
56	1	285		DOLOMITE	-6.69	0.17
57		285	spar	DOLOMITE	-9.66	0.14
58		285	spar	DOLOMITE	-9.51	-0.21
59		290		DOLOMITE	-7.23	-0.42
60		295		DOLOMITE	-6.23	-0.34
61		295	spar	DOLOMITE	-9.36	-0.03
62		300		DOLOMITE	-5.73	-0.24
63	1	300	spar	DOLOMITE	-8.75	-0.63
63	2	300		DOLOMITE	-9.25	-1.63
64		305		DOLOMITE	-5.23	0.25
65		310		DOLOMITE	-7.09	0.6
66	1	310	spar	DOLOMITE	-9.74	-1.02
66	2	310		DOLOMITE	-11.02	-0.23
67		315		DOLOMITE	-6.91	0.89
68		320		DOLOMITE	-6.75	0.62
69		325		DOLOMITE	-5.91	0.7
70		330		DOLOMITE	-6.95	0.67
71		335		DOLOMITE	-6.17	0.45
72	2	340		DOLOMITE	-9.06	0.38
72	1	340		DOLOMITE	-9.14	0.33
73		340	spar	DOLOMITE	-6.92	0.43
74		345		DOLOMITE	-7.05	0.23
75	1	350		DOLOMITE	-7.93	0.53
75	2	350		DOLOMITE	-7.87	0.48
76		350	spar	DOLOMITE	-7.46	0.44
77		355		DOLOMITE	-7.22	-0.04
78		360		DOLOMITE	-8.09	-0.01
79		365		DOLOMITE	-7.54	0.27
80		370		DOLOMITE	-7.43	0.09
81		375		DOLOMITE	-8.73	-0.38
82		380		DOLOMITE	-7.77	-0.2

83		385		DOLOMITE	-7.71	-0.26
84		390		DOLOMITE	-6.98	-0.22
85		395		DOLOMITE	-7.76	-0.17
86		400		DOLOMITE	-6.91	-0.09
87		405		DOLOMITE	-7.05	0.15
88	1	410		DOLOMITE	-9.47	-1.96
88	2	410		DOLOMITE	-9.19	-1.43
89	2	410	sparry vein	DOLOMITE	-10.09	-0.13
89	1	410		DOLOMITE	-10.07	-0.11
90		415		DOLOMITE	-7.41	-0.09
91		420		DOLOMITE	-6.62	0.03

Sample	U-Pb spot	Hf analysis	Hf176/Hf177	2 S.E.	Lu176/Hf177	Lu176/Hf177	U-Pb age	Hf initial	eHf	1 sigma	T(DM) Ga	T(DM) crustal	Hf chur (t)	Hf DM (t)
GF01	SPOT001	GF01_01	0.280647173	2.26929E-05	0.000628246	0.040868539	3418	0.280606	0.68	0.8	3.57	3.66	0.28059	0.280723
	SPOT004	GF01_02	0.280818812	4.3219E-05	0.000736665	0.045100333	2979.7	0.280777	-3.49	1.5	3.35	3.56	0.28087	0.281057
	SPOT005	GF01_03	0.280876416	4.09372E-05	0.001121157	0.07209233	3006.7	0.280812	-1.62	1.4	3.31	3.47	0.28086	0.281036
	SPOT023	GF01_04	0.2808019	3.27252E-05	0.000476681	0.029857625	3182.9	0.280773	1.11	1.1	3.35	3.45	0.28074	0.280903
	SPOT029	GF01_05	0.280876509	3.43998E-05	0.000827686	0.05136761	2979.3	0.280829	-1.63	1.2	3.28	3.45	0.28088	0.281057
	SPOT032	GF01_06	0.281306367	4.69662E-05	0.001356947	0.090195422	2541.4	0.281241	2.84	1.6	2.74	2.85	0.28116	0.281387
	SPOT036	GF01_07	0.281074512	3.33237E-05	0.000480506	0.026531153	2526.4	0.281051	-4.23	1.2	2.99	3.26	0.28117	0.281398
	SPOT040	GF01_08	0.281093956	2.92055E-05	0.000422798	0.024617456	2509.5	0.281074	-3.82	1.0	2.96	3.22	0.28118	0.281411
	SPOT046	GF01_09	0.280651611	4.02071E-05	0.000334409	0.018827127	3433.4	0.280629	1.89	1.4	3.54	3.60	0.28058	0.280712
	SPOT049	GF01_10	0.281192805	6.61012E-05	0.000400392	0.024346753	2527.4	0.281173	0.14	2.3	2.83	3.00	0.28117	0.281398
	SPOT055*	GF01_11	0.28121105	0.000133796	0.002626917	0.138989095	2489.9	0.281086	-3.83	4.7	2.97	3.21	0.28119	0.281426
	SPOT061	GF01_12	0.281254939	5.92994E-05	0.001179466	0.061064491	2608.8	0.281196	2.82	2.1	2.80	2.91	0.28112	0.281336
	SPOT062	GF01_13	0.280771218	4.54595E-05	0.001493206	0.08643898	3354.2	0.280675	1.64	1.6	3.49	3.56	0.28063	0.280772
	SPOT064	GF01_14	0.280715315	4.56521E-05	0.000825387	0.053265287	3267.7	0.280663	-0.80	1.6	3.50	3.63	0.28069	0.280838
	SPOT066	GF01_15	0.281166554	4.66039E-05	0.00114908	0.068849173	2532.3	0.281111	-1.97	1.6	2.92	3.13	0.28117	0.281394
	SPOT068	GF01_16	0.281082141	4.5906E-05	0.000422805	0.02278571	2563	0.281061	-3.03	1.6	2.98	3.22	0.28115	0.281371
	SPOT071	GF01_17	0.281215708	5.57734E-05	0.000906371	0.053839769	2508.3	0.281172	-0.35	2.0	2.83	3.02	0.28118	0.281412
	SPOT086	GF01_18	0.280850544	4.26736E-05	0.001063414	0.062761244	2973.3	0.280790	-3.17	1.5	3.34	3.54	0.28088	0.281061
	SPOT088	GF01_19	0.281124407	4.83916E-05	0.000971306	0.06161533	2543.6	0.281077	-2.91	1.7	2.96	3.19	0.28116	0.281385
	SPOT092	GF01_20	0.281095482	4.00616E-05	0.000958578	0.061358672	2599.5	0.281048	-2.67	1.4	3.00	3.22	0.28112	0.281343
GF06	SPOT09*	GF06_02	0.281308677	0.00026469	0.00173323	0.09675175	2502.5	0.281226	1.43	9.3	2.77	2.91	0.281186	0.281416
	SPOT14	GF06_03	0.281173714	9.77728E-05	0.001860824	0.092627059	2513.7	0.281084	-3.35	3.4	2.96	3.20	0.281179	0.281408
	SPOT15*	GF06_04	0.280969881	0.000219684	0.004945233	0.246783824	2985.2	0.280687	-6.57	7.7	3.54	3.75	0.280871	0.281052
	SPOT21*	GF06_05	0.281054179	0.000148583	0.002046189	0.11599639	2467.3	0.280958	-8.92	5.2	3.14	3.49	0.281209	0.281443
	SPOT39	GF06_08	0.281180515	6.58913E-05	0.001556764	0.078675435	2506	0.281106	-2.76	2.3	2.93	3.16	0.281184	0.281414
	SPOT51	GF06_09	0.282152839	3.80841E-05	0.001629577	0.089595847	1206.5	0.282116	3.52	1.3	1.58	1.78	0.282016	0.282377
	SPOT57*	GF06_10	0.281614519	0.000310557	0.003196401	0.172864851	1936	0.281497	-1.93	10.9	2.43	2.67	0.281551	0.281839
	SPOT60	GF06_12	0.281229555	5.85766E-05	0.001194756	0.069375243	2501.3	0.281172	-0.50	2.1	2.84	3.02	0.281187	0.281417
	SPOT65	GF06_13	0.281492331	9.14953E-05	0.001223042	0.067484977	1810.1	0.281450	-6.45	3.2	2.48	2.85	0.281632	0.281933
	SPOT70	GF06_14	0.281307288	6.43169E-05	0.001297019	0.067892451	2585.5	0.281243	3.96	2.3	2.74	2.82	0.281132	0.281354
	SPOT72	GF06_15	0.281690128	4.07501E-05	0.000448121	0.023905134	1705.7	0.281676	-0.83	1.4	2.16	2.43	0.281699	0.282010
	SPOT73	GF06_16	0.281188362	7.59577E-05	0.002177576	0.110455171	2476.1	0.281085	-4.18	2.7	2.97	3.22	0.281203	0.281436

	SPOT084	GF06_17	0.281100869	6.65588E-05	0.001239848	0.078108127	2534.4	0.281041	-4.42	2.3	3.01	3.28	0.281165	0.281392
	SPOT086*	GF06_18	0.280860259	0.000166892	0.004421532	0.189817356	3038.4	0.280602	-8.33	5.8	3.64	3.89	0.280836	0.281012
	SPOT92	GF06_19	0.282082664	7.84877E-05	0.001131566	0.082734253	1275.1	0.282055	2.92	2.7	1.65	1.87	0.281973	0.282327
	SPOT74*	GF06_20	0.281873817	0.000310811	0.003683587	0.182481096	1892.2	0.281742	5.75	10.9	2.08	2.17	0.281579	0.281872
GF14	SPOT003	GF14_01	0.280782796	5.85859E-05	0.001351341	0.078391863	2767.1	0.280711227	-10.76316911	2.050507691	3.45683801	3.823502415	0.281013687	0.281217289
	SPOT015	GF14_02	0.281255963	5.0667E-05	0.000808768	0.051620603	2504.5	0.28121729	1.166975663	1.773343492	2.77137931	2.92257536	0.281184477	0.281414828
	SPOT018	GF14_03	0.281275354	5.38095E-05	0.000655375	0.046533266	2452.5	0.281244682	0.941788308	1.883333681	2.73423033	2.895728733	0.281218197	0.28145383
	SPOT020	GF14_04	0.281208874	5.78238E-05	0.000774574	0.052718941	2510.1	0.281171751	-0.323355973	2.023834175	2.83261553	3.015166673	0.281180843	0.281410626
	SPOT021	GF14_05	0.281297012	4.47225E-05	0.000440215	0.023449305	2487	0.281276113	2.855111226	1.565286674	2.69003121	2.808825804	0.281195828	0.281427958
	SPOT031	GF14_06	0.281255268	7.65519E-05	0.000473562	0.032823714	2513.8	0.281232538	1.923888368	2.679316575	2.74843493	2.884893311	0.281178442	0.281407849
	SPOT034	GF14_07	0.281342821	9.79165E-05	0.000889684	0.056759716	2489.7	0.281300536	3.785945677	3.427078563	2.65918372	2.755587848	0.281194077	0.281425933
	SPOT051	GF14_08	0.281314817	6.36544E-05	0.000780925	0.05850811	2525.1	0.281277161	3.771805133	2.227902809	2.68965742	2.783965767	0.281171109	0.281399367
	SPOT054*	GF14_09	0.281143662	0.000111358	0.002185327	0.100347777	2517.8	0.281038598	-4.881228668	3.897538659	3.03131191	3.290072239	0.281175847	0.281404847
	SPOT056	GF14_10	0.281098485	4.96873E-05	0.000563093	0.036593712	2516.3	0.28107143	-3.748177105	1.739055799	2.96541311	3.222186526	0.28117682	0.281405973
	SPOT057	GF14_11	0.281216458	4.17653E-05	0.000335529	0.019671488	2570	0.281199984	2.064052217	1.461785453	2.79064113	2.920152914	0.281141955	0.281365647
	SPOT064	GF14_12	0.281173079	5.25838E-05	0.000978657	0.07312574	2528.2	0.281125829	-1.538848355	1.840431428	2.89627407	3.100965169	0.281169097	0.28139704
	SPOT069	GF14_13	0.281271028	5.78527E-05	0.000703211	0.05011992	2527.9	0.281237081	2.410977863	2.024845298	2.74346003	2.866932391	0.281169292	0.281397265
	SPOT073	GF14_14	0.281153735	4.03467E-05	0.000823093	0.05900044	2564.5	0.281113412	-1.142311222	1.412134704	2.9107504	3.105493761	0.281145528	0.281369779
	SPOT017	GF14_15	0.281237904	6.51999E-05	0.001022404	0.069512396	2414.6	0.28119081	-1.846916565	2.281997971	2.81140313	3.03187733	0.281242754	0.281482233
	SPOT077	GF14_16	0.281182069	6.01219E-05	0.001004794	0.067629428	2527.9	0.281133564	-1.270694219	2.104266628	2.88603066	3.084893753	0.281169292	0.281397265
	SPOT089	GF14_17	0.281318445	7.05956E-05	0.000813044	0.053796741	2525.9	0.281279227	3.863766887	2.470847511	2.6869771	2.779124003	0.28117059	0.281398766
	SPOT090	GF14_18	0.28136296	7.0856E-05	0.00187301	0.116168633	2549.3	0.281271757	4.138588978	2.479960407	2.70087564	2.78101364	0.281155399	0.281381196
	SPOT105	GF14_19	0.281390621	4.96237E-05	0.00100535	0.069557199	2554.7	0.281341561	6.746150324	1.736831006	2.60195407	2.630128653	0.281151892	0.28137714
	SPOT109	GF14_20	0.281232808	5.31797E-05	0.00065363	0.039357838	2569	0.281200729	2.06743127	1.861289475	2.79150975	2.919177204	0.281142605	0.281366398